

Review

Bio-Inspired Molecular Catalysts for Water Oxidation

Dan Xiao , Jennifer Gregg , K. V. Lakshmi * and Peter J. Bonitatibus, Jr. *

Department of Chemistry and Chemical Biology, Rensselaer Polytechnic Institute, Troy, NY 12180, USA; xiaod2@rpi.edu (D.X.); greggj31@gmail.com (J.G.)

* Correspondence: lakshk@rpi.edu (K.V.L.); bonitp2@rpi.edu (P.J.B.J.)

Abstract: The catalytic tetranuclear manganese-calcium-oxo cluster in the photosynthetic reaction center, photosystem II, provides an excellent blueprint for light-driven water oxidation in nature. The water oxidation reaction has attracted intense interest due to its potential as a renewable, clean, and environmentally benign source of energy production. Inspired by the oxygen-evolving complex of photosystem II, a large number of highly innovative synthetic bio-inspired molecular catalysts are being developed that incorporate relatively cheap and abundant metals such as Mn, Fe, Co, Ni, and Cu, as well as Ru and Ir, in their design. In this review, we briefly discuss the historic milestones that have been achieved in the development of transition metal catalysts and focus on a detailed description of recent progress in the field.

Keywords: water oxidation reaction; transition metal catalysts; ruthenium; iridium; manganese; iron; cobalt; copper; nickel



Citation: Xiao, D.; Gregg, J.; Lakshmi, K.V.; Bonitatibus, P.J., Jr. Bio-Inspired Molecular Catalysts for Water Oxidation. *Catalysts* **2021**, *11*, 1068. <https://doi.org/10.3390/catal11091068>

Academic Editor: Marius Horch

Received: 22 July 2021

Accepted: 24 August 2021

Published: 31 August 2021

Publisher's Note: MDPI stays neutral with regard to jurisdictional claims in published maps and institutional affiliations.



Copyright: © 2021 by the authors. Licensee MDPI, Basel, Switzerland. This article is an open access article distributed under the terms and conditions of the Creative Commons Attribution (CC BY) license (<https://creativecommons.org/licenses/by/4.0/>).

1. Introduction

1.1. Solar Water Oxidation in Nature

Sunlight is an abundant, green, sustainable, and renewable source of energy, however, the photochemical conversion and storage of solar energy has been a challenge [1]. Nature uses photosynthesis to convert solar energy into chemical energy through light-driven water oxidation and atmospheric CO₂ fixation [1–9]. Water oxidation, one of the most energetically demanding reactions in nature, takes place in the multi-subunit membrane protein complex, photosystem II (PSII) (Figure 1A), in plants and cyanobacteria. The structure of PSII has been determined through X-ray diffraction [10–13] and femtosecond X-ray free electron lasers (XFEL) [14–17]. Photosystem II is comprised of a core of heterodimeric polypeptides, D1 and D2, surrounded by ~20 polypeptide subunits [14], within which there are more than 1300 water molecules [10]. The waters are mostly located at the stromal and lumenal surfaces, as is commonly encountered in transmembrane proteins [10].

Photosystem II utilizes visible light to convert water into dioxygen at the catalytic tetranuclear manganese-calcium-oxo (Mn₄Ca-oxo) cluster in the oxygen-evolving complex (OEC). The Mn₄Ca-oxo cluster in the OEC has a distorted cubane-like structure with three manganese (Mn1–Mn3), one calcium, and four oxygen (O1–O3 and O5) atoms and a ‘dangling’ manganese atom (Mn4) that is linked to the cubane through di-μ-oxo linkages to the O atoms, O5 and O4 (numbering of the atoms is shown in Figure 1B) [10]. In addition to the μ-oxo-bridged oxygen atoms, the Mn₄ and Ca ions are coordinated by the water-derived ligands, W1, W2 and W3, W4 [10,14,18,19], respectively, as well as one imidazole and six carboxylate ligands that are derived from the amino acid residues in the D1 and CP43 polypeptides of PSII (Figure 1B) [10–12,14]. The Mn₄Ca-oxo cluster in the OEC is surrounded by additional amino acid residues and structured water molecules that form an extensive network of hydrogen bonds with the ligands of the Mn₄Ca-oxo cluster and are thought to facilitate substrate water delivery, electron transfer, and proton egress during the water oxidation reaction [20].

The water oxidation reaction of PSII proceeds through the formation of five charge-storage or S-states (S_0 – S_4) in the Kok S-state cycle [21], where the formation of each S-state intermediate is initiated by the absorption of a photon and the transfer of an electron (or electron and proton) [21–24]. This results in the accumulation of oxidizing equivalents at the Mn_4Ca -oxo cluster, which leads to the O–O bond formation in the transient higher-oxidation state S_4 intermediate. The conversion of two molecules of water into dioxygen entails the transfer of four electrons and the release of four protons, hence, the removal of electron(s) and the release of proton(s) proceeds in a coordinated fashion through proton-coupled electron transfer (PCET) reactions [25–27]. This prevents an overall buildup of charge through redox leveling in the OEC [28,29]. The release of protons is proposed to follow the pattern 1, 0, 1, 1, and 1 in the S_0 to S_1 , S_1 to S_2 , S_2 to S_3 , and S_3 to S_0 via transient S_4 states, respectively [30]. Photosynthetic water oxidation efficiently catalyzes the conversion of water into dioxygen with a TON of $\sim 10^6$ and a TOF of $\sim 600\text{ s}^{-1}$ [4,31]. Hence, the low over-potential and high efficiency of the OEC is a promising blueprint for the development of artificial bio-inspired catalysts for water splitting that can generate clean and renewable energy from sunlight [32–35].

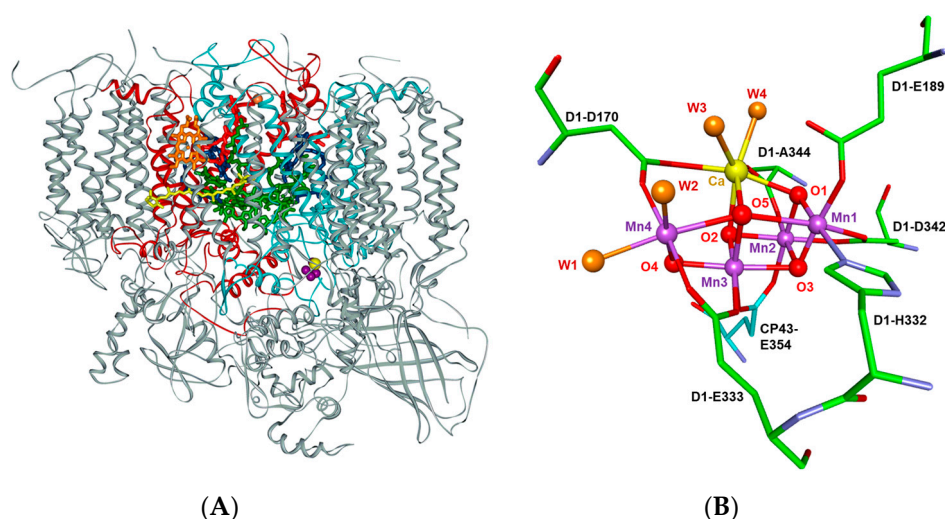


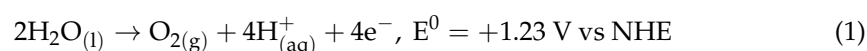
Figure 1. (A) The multi-subunit membrane protein complex, photosystem II (PSII), as observed in the 1.9 Å resolution X-ray crystal structure and (B) the tetranuclear manganese-calcium-oxo (Mn_4CaO_5) catalytic cluster in the oxygen-evolving complex (OEC) of PSII [10]. The manganese ($Mn1$ – $Mn4$), O^{2-} ($O1$ – $O5$), and Ca^{2+} ions are depicted as purple, red, and yellow spheres, respectively. The oxygen atoms of the four water-derived ligands that are coordinated to the Mn_4CaO_5 cluster, $W1$ – $W4$, are shown in orange, where $W1$ and $W2$ are coordinated to the dangling Mn ion, $Mn4$, and $W3$, and $W4$ are ligands to the Ca^{2+} ion. The amino acid residues that are coordinated to the metal ions of the Mn_4Ca -oxo cluster in the OEC are also shown.

The challenges in designing efficient artificial catalysts stem from the complexity of the water oxidation reaction, which requires the transfer of four electrons and four protons during the catalytic cycle [7,36,37]. This is a major bottleneck, as an effective catalyst would have to accommodate successive charge storage states and participate in PCET reactions during water oxidation [4,23,29,38]. Furthermore, water oxidation is energetically demanding, requiring at least 113.5 kcal/mol (equivalent to a redox potential of 1.23 V vs. normal hydrogen electrode (NHE)) to drive the reaction [39,40]. Thus, artificial water oxidation would require the presence of a strong oxidant. Finally, an efficient catalyst would need to have a mechanism for the binding of substrate water as well as egress of protons during the water oxidation reaction. The catalytic Mn_4Ca -oxo cluster of PSII is coordinated by seven amino acid residues (D1-Asp170, D1-Glu189, D1-Glu333, D1-Asp342, D1-Ala344, CP43-Glu354, and D1-Ala344) (Figure 1B) [10,12,13] that form an extensive hydrogen-bond network with other amino acid residues and structured water molecules

that facilitate the delivery of substrate water and the egress of protons in the OEC [12]. It is challenging to replicate the unique environment of the catalytic site of PSII in an artificial catalyst.

1.2. Synthetic Water Oxidation Catalysts

The water oxidation reaction of PSII has been of intense interest as it serves as a blueprint for the development of active and robust synthetic water oxidation catalysts that mimic the OEC of PSII [32–35,41,42]. The dioxygen produced is released to atmosphere, whereas the electrons and protons from water oxidation may be used to generate economically useful dihydrogen and organic molecules [1,43,44].



Synthetic catalysts for artificial water oxidation (WOC) can be classified into two groups, namely, molecular catalysts and bulk semiconductors. Although semiconductor surfaces (e.g., metals oxides) are easy to synthesize and recover and have displayed reasonable stability for the water oxidation reaction [45–47], they are generally vulnerable to harsh reaction conditions (such as low or high pH), often lack structural reproducibility, and are hard to characterize through physical and chemical methods [48]. Since the synthesis of the first well-defined molecular WOC [49], the development of such catalysts has been the subject of extensive research and the strategies that were previously employed in the field can be useful to improve the design of WOC. Amongst the current WOCs, Ru-based catalysts have received extensive attention [4,37,50–52], some of which have displayed high catalytic activity [53–55]. However, there is also an interest in developing earth-abundant, cost-effective catalysts comprised of first-row (3d) transition metals, such as manganese, iron, cobalt, copper, and nickel. In this review, we describe molecular water oxidation catalysts that are based on 3d (Mn, Fe, Co, Cu, Ni), 4d (Ru), and 5d (Ir) transition metals (Figure 2), with an emphasis on the progress in the field over the past five years. The examples discussed in this review highlight the role of ligand design in the stability, solubility, and catalytic activity of molecular WOC. We refer the reader to previous and thorough review articles [7,56–60] for catalytic systems that were developed prior to this period.

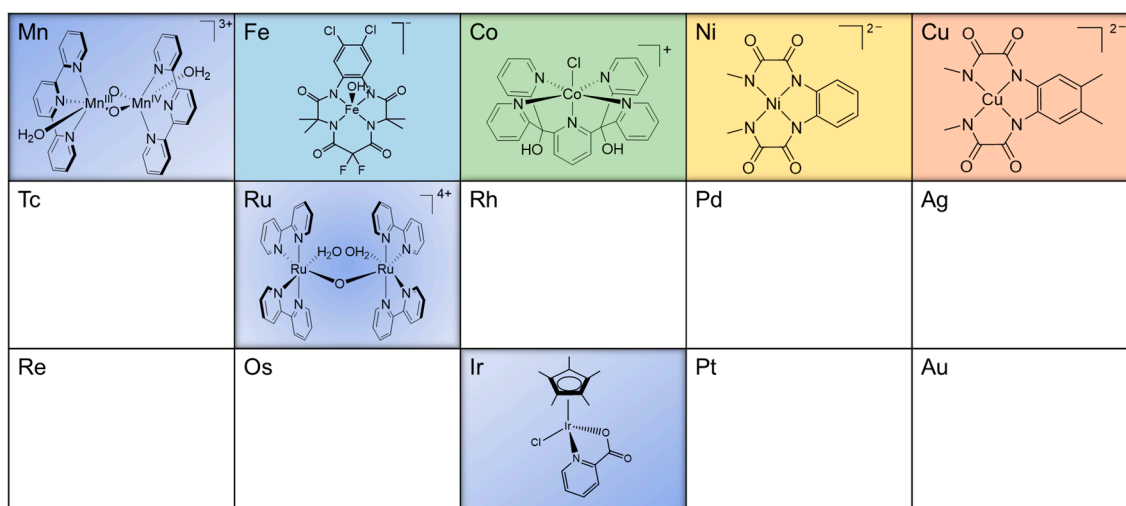


Figure 2. The 3d (Mn, Fe, Co, Ni, and Cu), 4d (Ru), and 5d (Ir) metals in the periodic table that have been incorporated in the design of synthetic bio-inspired molecular catalysts for water oxidation. Key examples of the catalysts that have been developed for each metal are also shown.

2. Ruthenium-Based Molecular Catalysts

2.1. Dinuclear Ruthenium Catalysts

The ruthenium-based dinuclear molecular catalyst for water oxidation, known as the “blue dimer”, $[(\text{H}_2\text{O})\text{Ru}^{\text{III}}(\text{bipy})_2(\mu\text{-O})\text{Ru}^{\text{III}}(\text{bipy})_2(\text{H}_2\text{O})]^{4+}$ (**1**) (Figure 3), was first reported by Meyer and coworkers in 1982 [49]. This complex is comprised of a Ru^{III} dimer, where the metal ions are linked by a μ -oxo bridge. Each Ru^{III} ion is coordinated by two bipyridine (bipy) ligands that provide an open coordination site to accommodate a water ligand. The blue dimer displayed a turnover number (TON) and turnover frequency (TOF) of 13.2 and 0.0042 s^{-1} , respectively, for the chemical oxidation of water using $[\text{Ce}(\text{NO}_3)_6][(\text{NH}_4)_2]$ (CAN) as a sacrificial oxidant (Table 1) [61,62]. CAN provides a sufficient oxidation potential to oxidize the investigated catalysts at approximately 1.75 V vs. NHE (pH 0.9) [60,63]. The mechanism of water oxidation by complex **1** was investigated by kinetic measurements in combination with isotope replacement studies to determine the kinetic isotope effect, which suggested that the reaction predominantly proceeded through a water nucleophilic attack (WNA) mechanism with the formation of a high-valent intermediate, $[(\text{O})\text{Ru}^{\text{V}}(\mu\text{-O})\text{Ru}^{\text{V}}(\text{O})]^{4+}$, where uncoordinated water molecules attack the $\text{Ru}^{\text{V}}=\text{O}$ group of the intermediate. However, the results were unable to exclude the possibility of intramolecular or bimolecular pathways in the reaction [64–67]. The moderately low catalytic performance of complex **1** was attributed to the anation of an active intermediate, in which the $[(\text{O})\text{Ru}^{\text{V}}(\mu\text{-O})\text{Ru}^{\text{V}}(\text{O})]^{4+}$ cation coordinated an anion forming the species, $[(\text{bipy})_2(\text{H}_2\text{O})\text{Ru}^{\text{IV}}(\mu\text{-O})\text{Ru}^{\text{III}}(\text{X})(\text{bipy})_2]^{4+}$ (where, $\text{X} = \text{ClO}_4^-$, CF_3SO_3^- and NO_3^-), which resulted in the deactivation of the system [68].

Studies of the blue dimer were followed by the synthesis and characterization of a series of dinuclear ruthenium complexes with a variety of ligands bridging the ruthenium ions, such as pyrazole [69,70], pyridazine [71,72], and phthalazine [73]. Tanaka et al. (2001) reported a dinuclear complex, $[\text{Ru}^{\text{II}}_2(\text{OH})_2(3,6\text{-tBu}_2\text{qui})_2(\text{btpyan})]^{2+}$ (**2**) (where 3,6-*t*Bu₂qui = 3,6-di-*tert*-butyl-1,2-benzoquinone), that featured a novel ligand, 1,8-bis(2,2':6',2''-terpyridyl)anthracene (btpyan), to bridge the two ruthenium ions [74]. Complex **2** was capable of electrochemical water oxidation with a TON of 21 in the presence of water in 1,1,1-trifluoroethanol and displayed a TON of 33,500 on the surface of an indium tin oxide (ITO) electrode [74]. Subsequently, Llobet and coworkers (2004) demonstrated that the complex $[(\text{H}_2\text{O})\text{Ru}^{\text{II}}(\text{terpy})_2(\mu\text{-bpp})\text{Ru}^{\text{II}}(\text{terpy})_2(\text{H}_2\text{O})]^{3+}$ (**3**) (where, terpy = 2,2':6',2''-terpyridine) with the bridging ligand, 3,5-bis(2-pyridyl)pyrazolate (bpp^-) displayed improved catalytic activity with a TON of 512 and a TOF of 0.014 s^{-1} for chemical water oxidation using CAN as a sacrificial oxidant [69]. The presence of the btpyan and bpp^- bridging ligands in the complexes **2** and **3**, respectively, offered alternatives to the previous strategy of μ -oxo-bridged dinuclear ruthenium complexes [4], which is unique as there are very few dinuclear ruthenium complexes that have been shown to be catalytically active in the absence of bridging μ -oxo ions.

This was followed by the development of two dinuclear ruthenium complexes $[\{\text{Ru}^{\text{II}}(\text{terpy})\text{Cl}\}_2(\mu\text{-L})]^{2+}$ (**4**) and $[\{\text{Ru}^{\text{II}}(\text{terpy})(\text{H}_2\text{O})\}_2(\mu\text{-L})]^{4+}$ (**5**) (where, L = bis[5-(5'-methyl-2,2'-bipyridinyl)]ethane) by Sakai and coworkers (2009) [75] that displayed activity for chemical water oxidation with TONs of 75 and 106, respectively, using CAN as an oxidant. It was found that the activities of complexes **4** and **5** were much higher than that of the μ -O bridged complex **1**. More importantly, an induction time of 2–3 h was observed for complex **4**. However, the initial rate of O_2 formation for complex **5**, the aqua species, did not show an induction period for oxygen formation, implying that the aqua (instead of the chloro) species was active during the catalysis of the water oxidation reaction [75]. Subsequently, Llobet and coworkers (2014) developed a powerful and oxidatively rugged complex, $[\{\text{Ru}^{\text{II}}(\text{py-SO}_3)_2(\text{H}_2\text{O})\}_2(\mu\text{-Mebbp})]^-$ (**6**) (where, HMe bbbp = 2,4-bis(bipyridin)-3-methyl-pyrazole and py-SO₃ = pyridine-3-sulfonate), with a pyrazolate-based equatorial ligand that featured a TON of 22.6 and a TOF of 0.068 s^{-1} for chemical water oxidation using CAN as an oxidant [70]. In complex **6**, Mebbp[−] is a bis(tridentate) monoanionic ligand that was designed to act as a bridging scaffold that placed the two ruthenium ions in

close proximity. The Mebbp[−] ligand appeared to induce subtle geometric variations on the relative disposition of the active Ru–OH_X groups that regulated the O–O bond formation pathway and influenced the mechanism toward WNA. This was in contrast to the intermolecular bimolecular (I2M) mechanism that was suggested for analogous complexes with 3,5-bis(2-pyridyl)pyrazolato dinucleating, Hbpp[−], ligand due to the strategic disposition and encumbrance of the terpy ligands [57,69,76,77]. This study demonstrated that subtle variations in ligand design could be used to regulate the O–O bond formation pathway of the water oxidation reaction. Additionally, the tridentate dianionic meridional pyridyl-2,6-dicarboxylato (pdc^{2−}) ligand was used to generate a dinuclear ruthenium complex **7**. Although complex **7** was not a catalyst for water oxidation, it was shown to act as a precursor for a ruthenium-aqua mononuclear complex, [Ru^{II}(pdc-κ³-N¹O²)(bipy)(H₂O)] (**31**) (where, pdc = pyridyl-2,6-dicarboxylato and bipy = 2,2'-bipyridine), that was an active water oxidation catalyst with low overpotential of 240 mV at pH 1 and a TOF of 0.2 s^{−1} [78].

Further improvements in the design of dinuclear ruthenium catalysts included the incorporation of a rigid polypyridyl equatorial ligand in [Ru^{II}₂(μ-L)(μ-Cl)(pic)₄]³⁺ (**8**) (where L = 6-di-(6'-[1'',8''-naphthyrid-2''-yl]-pyridin-2'-yl)pyrazine and pic = 4-picoline), which improved the catalytic performance for chemical water oxidation using CAN as a sacrificial oxidant at pH 1 with a TON and TOF of 538 [50,79] and 0.046 s^{−1}, respectively [50,71]. During this time, biophysical studies of PSII indicated that the presence of negatively-charged carboxylate ligands in the vicinity of the OEC likely improve the stability of the high-valent manganese intermediates by lowering the oxidation potential of the catalytic Mn₄Ca-oxo cluster [45,50,72,80]. This led to the incorporation of carboxylate ligands in the design of dinuclear ruthenium complexes [72,73]. While the dinuclear ruthenium complexes containing neutral ligands displayed high oxidation potentials, which required the use of strong chemical oxidants, such as Ce^{IV} for catalytic water oxidation, it was thought that the redox potentials of these complexes could be decreased by ligand modification. The presence of negatively-charged ligands could lower the oxidation potential of the complexes and stabilize the higher oxidation states of the metal ions [72]. In principle, this could present the possibility of driving the water oxidation reaction by a mild oxidant. Using this strategy, Sun and coworkers prepared a dinuclear ruthenium catalyst with a negatively charged dicarboxylate ligand. The complex [Ru(pic)₃(μ-cppd)Ru(pic)₃]⁺ (**9**) (where, H₂cppd = 3,6-bis-(6'-carboxypyrid-2'-yl)-pyridazine) yielded a TON and TOF of 4700 and 0.28 s^{−1}, respectively, for chemical water oxidation using CAN as an oxidant [50,73]. Moreover, the complex [Ru(pic)₂(μ-Cl)(μ-cpptz)Ru(pic)₂]⁺ (**10**) (where, H₂cpptz = 1,4-bis(6'-COOH-pyrid-2'-yl)phthalazine) displayed improved catalytic activity under identical conditions with a TON of 10,400 and a TOF of 1.2 s^{−1} [73]. Both complex **9** and **10** provided direct evidence of the benefit of introducing carboxylate functionalities in the equatorial ligand framework of dinuclear ruthenium catalysts. In 2021, Meyerstein and coworkers reported a dinuclear ruthenium carbonate complex, Na₃[Ru₂(μ-CO₃)₄], that is electrochemically active for water oxidation with a TOF of 0.10 s^{−1} under pH-neutral conditions and 1.48 s^{−1} in bicarbonate media (pH 8.3) [81].

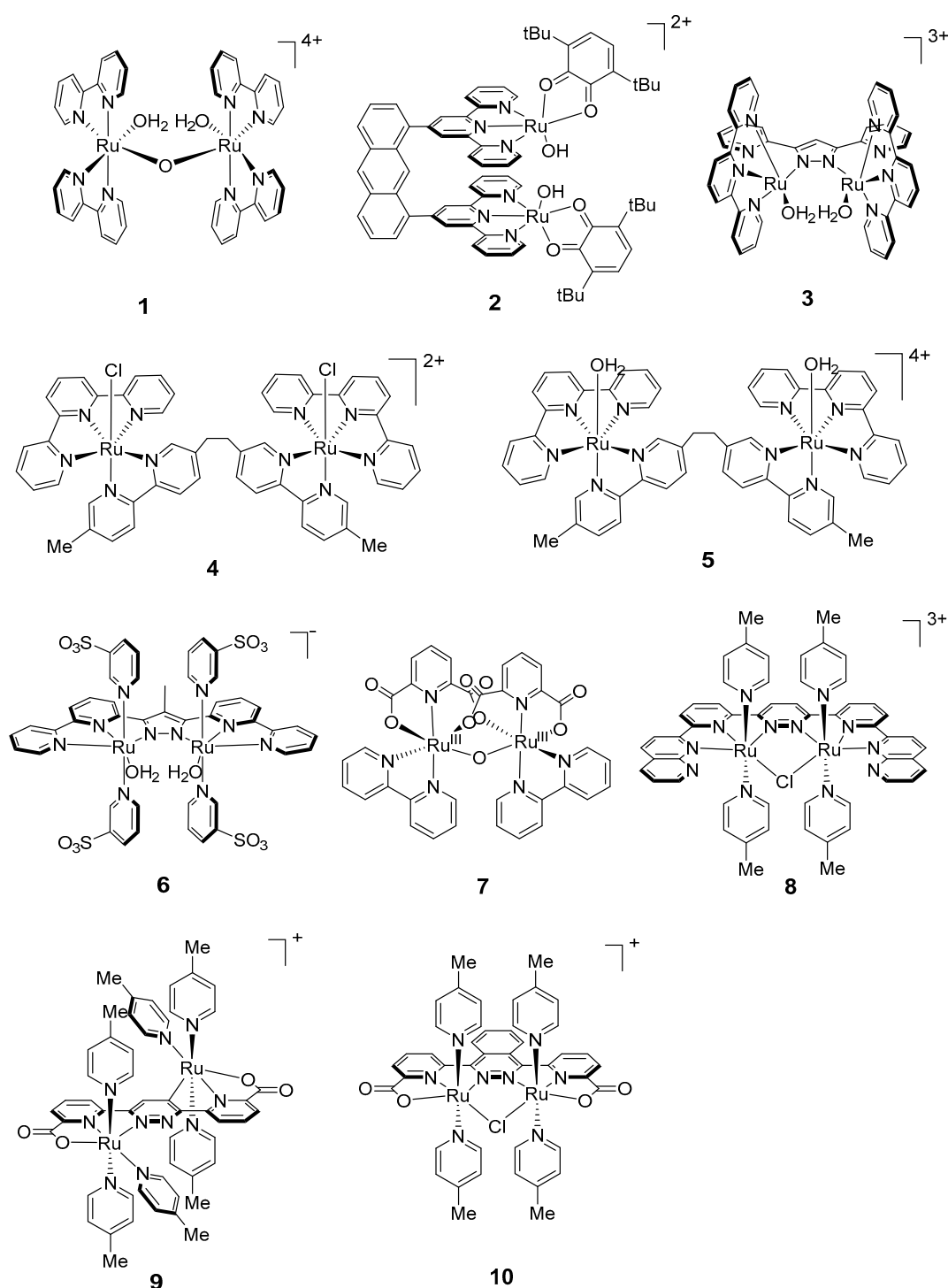


Figure 3. Chemical structures of recent dinuclear ruthenium catalysts 1–10 for water oxidation: $[(\text{H}_2\text{O})\text{Ru}^{\text{III}}(\text{bipy})_2(\mu\text{-O})\text{Ru}^{\text{III}}(\text{bipy})_2(\text{H}_2\text{O})]^{4+}$ (1, bipy = 2,2'-bipyridine) [49]; $[\text{Ru}^{\text{II}}_2(\text{OH})_2(3,6\text{-}t\text{Bu}_2\text{qui})_2(\text{btpyan})]^{2+}$ (2, btpyan = 1,8-bis(2,2':6',2''-terpyridyl)anthracene, 3,6-*t*Bu₂qui = 3,6-di-tert-butyl-1,2-benzoquinone) [74]; $[(\text{H}_2\text{O})\text{Ru}^{\text{II}}(\text{terpy})_2(\mu\text{-bpp})\text{Ru}^{\text{II}}(\text{terpy})_2(\text{H}_2\text{O})]^{3+}$ (3, bpp = 3,5-bis(2-pyridyl)pyrazolate, terpy = 2,2':6',2''-terpyridine) [69]; $[\{\text{Ru}^{\text{II}}(\text{terpy})\text{Cl}\}_2(\mu\text{-L})]^{2+}$ (4, L = bis[5-(5'-methyl-2,2'-bipyridinyl)]ethane) [75]; $[\{\text{Ru}^{\text{II}}(\text{terpy})(\text{H}_2\text{O})\}_2(\mu\text{-L})]^{4+}$ (5, L = bis[5-(5'-methyl-2,2'-bipyridinyl)]ethane) [75]; $[\{\text{Ru}^{\text{II}}(\text{py-SO}_3)_2(\text{H}_2\text{O})\}_2(\mu\text{-Mebbp})]^{-}$ (6, Mebbp = 2,4-bis(bipyridin)-3-methyl-pyrazole) [70]; $[\{\text{Ru}^{\text{III}}(\text{pdc-}\kappa^3\text{-N}^1\text{O}^2)(\text{bipy})\}_2(\mu\text{-O})]$ (7, pdc = 2,6-pyridinedicarboxylato, bipy = 2,2'-bipyridine) [78]; $[\text{Ru}^{\text{II}}_2(\mu\text{-L})(\mu\text{-Cl})(\text{pic})_4]^{3+}$ (8, L = 6-di-(6'-[1'',8''-naphthyrid-2''-yl]-pyridin-2'-yl)pyrazine, pic = 4-picoline) [71]; $[\text{Ru}(\text{pic})_3(\mu\text{-cppd})\text{Ru}(\text{pic})_3]^{+}$ (9, cppd = 3,6-bis-(6'-carboxypyrid-2'-yl)-pyridazine) [72]; $[\text{Ru}(\text{pic})_2(\mu\text{-Cl})(\mu\text{-cpptz})\text{Ru}(\text{pic})_2]^{+}$ (10, cpptz = 1,4-bis-(6'-carboxypyrid-2'-yl)-phthalazine) [73].

Table 1. Select catalytic parameters and experimental conditions for dinuclear ruthenium catalysts 1–10, which are active in water oxidation. Electrochemical and chemical water oxidation using CAN are abbreviated as ‘electrochem WO’ and ‘chem WO’, respectively. The TOF values that are not listed in this table are not available in literature.

Binuclear Ru Complex	TON	TOF (s ⁻¹)	Experimental Conditions	Reference
1	13.2	0.0042	chem WO	[49,61,62]
2	21	-	electrochem WO	[74]
3	512	0.014	chem WO	[69]
4	75	-	chem WO	[75]
5	106	-	chem WO	[75]
6	22.6	0.068	chem WO	[70]
7	inactive	inactive	electrochem WO	[78]
8	538	0.046	chem WO	[50,71,79]
9	4700	0.28	chem WO	[72,73]
10	10,400	1.2	chem WO	[73]

2.2. Mononuclear Ruthenium Catalysts

The success of the blue dimer [49] in catalyzing water oxidation and the lower catalytic activity of mononuclear ruthenium complexes in early studies [61] led to the assumption that multinuclear catalysts were required for the successful conversion of water to dioxygen. However, the design of a series of mononuclear ruthenium complexes that were catalytically active for water oxidation challenged this hypothesis [71]. The ease of the chemical syntheses led to a shift towards the design of effective mononuclear ruthenium catalysts for water oxidation. The complex [(ntp)(pic)₂Ru(H₂O)]²⁺ (**11**) (where, ntp = 2,6-di(1,8-naphthyridin-2-yl)-4-tert-butylpyridine) (Figure 4), reported by Thummel and coworkers, displayed catalytic activity for water oxidation (Table 2) and paved the way for the development of mononuclear ruthenium complexes for water oxidation. Subsequently, a study by Meyer and coworkers on the mononuclear ruthenium complexes [Ru(terpy)(bpm)(OH₂)]²⁺ (**12b**) and [Ru(terpy)(bpz)(OH₂)]²⁺ (**12c**) (where, bpm = 2,2'-bipyrimidine; bpz = 2,2'-bipyrazine) demonstrated conclusively that a single Ru site is sufficient for catalytic water oxidation [82,83]. A large number of monomeric ruthenium complexes for water oxidation have been reported since the initial findings by Thummel, Meyer and coworkers. The mononuclear ruthenium catalysts that have been reported in the literature can broadly be divided into two classes based on the equatorial and axial ligands that were employed in the respective syntheses.

Berlinguette and coworkers investigated a series of structurally related mononuclear ruthenium catalysts that were formulated as [Ru(terpy)(L)(OH₂)]²⁺ (where, L = 2,2'-bipyridine (bipy) (**12a**), 4,4'-dimethoxy-2,2'-bipyridine (bipy-OMe), and 4,4'-dicarboxy-2,2'-bipyridine (bipy-COOH)) [84]. The goal of this study was to determine the effect of the electronic density at the active site on the catalytic performance while holding the balance of the structure at parity. The effects of the systematic modification of the substituent groups on the bipy ligand of the complex indicated that while the presence of electron-withdrawing groups (EWG), such as -Cl and -COOH, suppressed the rate of the reaction, k_{obs} , and enhanced the catalytic TON, the installation of electron-donating groups (EDG), such as -OMe, accelerated the catalytic rate while decreasing the stability of the catalyst [85]. The observation of a reverse relationship between the rate of the reaction and the TON was similar to prior observations by Thummel and coworkers [86]. However, a study by Berlinguette and coworkers suggested that chemical water oxidation driven by Ce^{IV} as an oxidant led to reaction pathways that diverged from the prevailing “acid-base” mechanism for single-site catalysts. The catalysts displayed complicated pathways that involved the incorporation of O atoms from different sources [87,88].

Thummel and coworkers (2008) assessed a series of chloro-coordinated mononuclear ruthenium complexes using terpy, bipy, and related derivatives as ligands that demon-

strated high catalytic activity for water oxidation [86]. These studies demonstrated that the presence of an EDG led to an increase in the rate of the reaction with a decrease in the TON, whereas an EWG yielded a higher TON with a decrease in the rate [86]. The parent complex $[\text{Ru}^{\text{II}}(\text{terpy})(\text{bipy})(\text{Cl})]^+$ (**13a**) in this study was shown to be catalytically active for water oxidation with a TON of 390 using CAN as an oxidant, and it was suggested that the mechanism for complex **13a** involved a seven-coordinate intermediate retaining the Ru–Cl bond [86]. However, in contrast to these observations, Sakai and coworkers demonstrated that complex **13a** was inactive in the presence of NaCl in solution. This was thought to be due to a dominant shift of the substitution equilibrium, $[\text{Ru}^{\text{II}}(\text{terpy})(\text{bipy})\text{Cl}]^+ + \text{Solv} \rightleftharpoons [\text{Ru}^{\text{II}}(\text{terpy})(\text{bipy})(\text{Solv})]^{2+} + \text{Cl}^-$, towards the reactant. Moreover, since the oxygen evolution as a function of time suggested that the chloro species was inactive, the real catalyst responsible for dioxygen evolution was inferred to be the aqua species, $[\text{Ru}^{\text{II}}(\text{terpy})(\text{bipy})(\text{Solv})]^{2+}$, in solution. This suggested that the conversion of the $[\text{Ru}(\text{terpy})(\text{bipy})\text{Cl}]^+$ complex (**13a**) to the $[\text{Ru}(\text{terpy})(\text{bipy})(\text{H}_2\text{O})]^{2+}$ species (**12a**) may have been involved in the mechanism [75].

Although several studies have proposed a tentative mechanism for water oxidation involving seven-coordinate ruthenium intermediates [82,86,89], it was not possible to isolate and characterize these proposed complexes. This left an open question as to the interaction of water molecules with ruthenium in mononuclear catalysts. The use of negatively charged ligands was thought to be an appropriate means to capture high-valent ruthenium intermediates as they can stabilize higher oxidation states. Given the enhanced catalytic performance of dinuclear ruthenium complexes (**9**) and (**10**) with a dicarboxylato ligand where the introduction of negatively charged ligands dramatically lowered the oxidation potential of Ru^{II} to Ru^{III} [72,73], equatorial backbone ligands with terminating carboxylato groups were also introduced in the design of mononuclear ruthenium complexes. The synthesis of a mononuclear ruthenium complex, $[\text{Ru}(\text{bda})(\text{pic})_2]$ (**14a**) (where, $\text{bda}^{2-} = 2,2'$ -bipyridine-6,6'-dicarboxylate), was shown to stabilize a possible seven-coordinate Ru^{IV} dimeric intermediate with a proposed $[\text{HOHOH}]^-$ bridging ligand [90]. This supported the hypothesis that the O–O bond formation could arise from the coupling of two $\text{Ru}^{\text{IV}}=\text{O}$ units, termed as the “interaction between two metal oxo units” or the intermolecular bimolecular (I2M) pathway for water oxidation.

Subsequently, two mononuclear ruthenium complexes, $[\text{Ru}^{\text{II}}(\text{pdc})(\text{pic})_3]$ (**15**) and $[\text{Ru}^{\text{II}}(\text{pdc})(\text{bipy})(\text{pic})]$ (**16**) (where, $\text{H}_2\text{pdc} = 2,6$ -pyridinedicarboxylic acid), were investigated for their catalytic activity in chemical water oxidation [91]. Complex **15** displayed a TON of 553 and a TOF of 0.23 s^{-1} , which was better than complex **16**, which had a TON of 17 and a TOF of $7.2 \times 10^{-3} \text{ s}^{-1}$ at pH 1 for chemical water oxidation in the presence of Ce^{IV} ions [91]. Although both **15** and **16** employed tridentate equatorial backbone ligands containing negatively charged biscarboxylato groups, they were not as catalytically active as $[\text{Ru}(\text{bda})(\text{pic})_2]$ (**14a**) [53], which displayed a TON of 2000 and a TOF of 41 s^{-1} under similar reaction conditions. Upon closer examination, the tetradentate equatorial backbone with two axial picoline ligands in complex **14a** formed a highly distorted octahedral configuration with an “open coordination site” (O–Ru–O angle of 123°) that greatly facilitated the access of an aqua ligand [50,90]. The isolation of a Ru^{IV} dimeric intermediate with a $[\text{HOHOH}]^-$ bridging ligand from water oxidation catalyzed by complex **14a** suggested that radical coupling of $\text{Ru}=\text{O}$ units led to O–O bond formation [90]. As a result of this finding, isoquinolines were employed as axial ligands to facilitate the non-covalent attraction between them and lower the barrier of interaction for the $\text{Ru}=\text{O}$ units. This strategy succeeded as the complex $[\text{Ru}(\text{bda})(\text{isq})_2]$ (**14b**) (where, $\text{isq} = \text{isoquinoline}$) and led to a TON of 8369 and a TOF of 303 s^{-1} [53].

The studies involving mononuclear ruthenium catalysts described thus far required a powerful sacrificial oxidant, CAN, for chemical water oxidation. In principle, it should be possible to use a light-absorbing photosensitizer to conduct sustainable light-driven water oxidation. As described by Åkermark and coworkers [92], a major obstacle that is frequently encountered in light-driven water oxidation is the mismatch between the

relatively high redox potential at which a catalyst assumes its active state and the lower potential attainable with a photosensitizer. One way to decrease the redox potential of the active catalyst is to involve PCET, which is a fundamental process that is employed in nature by the OEC of PSII [25,27]. It involves the simultaneous transfer of an electron and a proton, which has a profound effect on the energetics of the water oxidation reaction. As mentioned in the Introduction section, PCET allows for redox leveling at the catalytic site, which is a prerequisite for carrying out the four-electron water oxidation reaction. Additionally, another means of altering the redox potential of the active catalyst is to coordinate electron-donating and redox-active ligands to the metal centers, which would influence the balance between efficiency and stability of the water oxidation catalysts [92]. Thus, Åkermark and coworkers demonstrated that the introduction of imidazole and phenol motifs, in combination with carboxylate groups, facilitated PCET and the formation of high-valent metal-oxo catalytic intermediates at low potentials. This strategy was implemented by the development of two mononuclear ruthenium complexes, $[\text{Ru}^{\text{III}}(\text{L})(\text{pic})_3]$ (where, L = 2-(2-hydroxyphenyl)-1H-benzimidazole-7-carboxylate (**17**) and L = 2-(2-hydroxyphenyl)-1H-benzimidazol-7-ol (**18**)), which contained negative equatorial backbone ligands comprised of imidazole and phenol motifs with a carboxylate group [92]. By using the imidazole motif, it was possible to introduce a combined redox and proton-transfer mediator, a highly active and essential element, into the mononuclear ruthenium catalysts. Complex **17**, with a single carboxylate and phenol moiety, displayed a TON of up to 4000 and a TOF of 7.4 s^{-1} with $[\text{Ru}(\text{bipy})_3]^{3+}$ as an oxidant for chemical water oxidation, and a postulated $[\text{Ru}^{\text{V}}=\text{O}]^{n+}$ intermediate of **18** was characterized by high-resolution mass spectrometry [92]. Moreover, to evaluate the possibility of performing light-driven water oxidation under homogeneous, neutral conditions at pH 7.2, the authors employed a three-component system consisting of complex **17** or **18**, a photosensitizer ($[\text{Ru}(\text{bipy})_3]^{2+}$ or $[\text{Ru}(\text{bipy})_2(\text{deeb})]^{2+}$ (where, deeb = 4,4'-di(ethoxycarbonyl)-2,2'-bipyridine)), and a sacrificial electron acceptor ($\text{Na}_2\text{S}_2\text{O}_8$). Successful evolution of dioxygen was detected upon visible-light illumination of this system. The $[\text{Ru}(\text{bipy})_3]^{2+}$ photosensitizer displayed a low TON of approx. 20, whereas, replacing $[\text{Ru}(\text{bipy})_3]^{2+}$ ($E[\text{Ru}^{\text{III}}/\text{Ru}^{\text{II}}] = 1.26 \text{ V vs. NHE}$) with the more strongly oxidizing photosensitizer $[\text{Ru}(\text{bipy})_2(\text{deeb})]^{2+}$ ($E[\text{Ru}^{\text{III}}/\text{Ru}^{\text{II}}] = 1.4 \text{ V vs. NHE}$) yielded a significantly higher TON of ~200 [92]. Similarly, $[\text{Ru}(\text{bda})(\text{pic})_2]$ (**14a**), $[\text{Ru}^{\text{II}}(\text{pdc})(\text{pic})_3]$ (**15**) and $[\text{Ru}^{\text{II}}(\text{pdc})(\text{bipy})(\text{pic})]$ (**16**) also demonstrated moderate catalytic performance for photochemical water oxidation using $[\text{Ru}(\text{bipy})_3]^{2+}$ or $[\text{Ru}(\text{bipy})_2(\text{dcb})]^{2+}$ (dcb = 4,4'-dicarboxyethyl-2,2'-bipyridine) as a photosensitizer and $[\text{Co}(\text{NH}_3)_5\text{Cl}]\text{Cl}_2$, or $\text{Na}_2\text{S}_2\text{O}_8$ as a sacrificial electron acceptor [91,93].

The design of a mononuclear ruthenium complex with a carboxylate-amide motif, $[\text{Ru}^{\text{II}}(\text{HL})(\text{pic})_3]$ (**19**) (where, L = 6-carbamoylpicolinic acid), was also shown to catalyze water oxidation (TON of 280 and TOF of 1.16 s^{-1}) at a neutral pH of 7.2 using $[\text{Ru}(\text{bipy})_3]^{3+}$ as a mild chemical oxidant [94]. This complex was similar to $[\text{Ru}^{\text{II}}(\text{pdc})(\text{pic})_3]$ (**15**), with the difference that one of the carboxylate ligands was replaced by an amide group. The crystal structure of complex **19** revealed a Ru^{III} ion due to the strong electron-donating ability of the 6-carbamoylpicolinic acid ligand. The presence of the carboxylate-amide ligand in **19** lowered the redox potential of the complex to an extent where catalytic water oxidation could take place under neutral conditions with the mild $[\text{Ru}(\text{bipy})_3]^{3+}$ oxidant [94]. In comparison with the mononuclear ruthenium complex, **19**, catalysts based on neutral nitrogen containing heterocyclic ligands were generally not compatible with the mild oxidant, $[\text{Ru}(\text{bipy})_3]^{3+}$. This study once again highlighted the importance of incorporating anionic backbone ligands to decrease the redox potential of ruthenium catalysts.

The above results led to the design of the complex $[\text{Ru}^{\text{III}}(\text{H}_2\text{pdca})(\text{pic})_3]^+$ (**20**) (where, $\text{H}_4\text{pdca} = 2,6\text{-pyridine-dicarboxamide}$), which was also shown to catalyze water oxidation at a low redox potential using $[\text{Ru}(\text{bipy})_3]^{3+}$ at pH 7.2 with a TON of 400 and a TOF of 1.6 s^{-1} [95]. The improvement of the catalytic activity in terms of TOF was attributed to the presence of a flexible equatorial backbone ligand. This was followed by the synthesis of a seven-coordinate mononuclear ruthenium complex, $[\text{Ru}^{\text{IV}}(\text{OH})(\text{tda}-\kappa\text{-N}^3\text{O})(\text{py})_2]^+$

(**21**) (where, $\text{tda}^{2-} = 2,2':6',2''\text{-terpyridine-6,6''-dicarboxylate}$) that was found to be an active and robust catalyst with a maximum TOF (TOF_{max}) of $50,000 \text{ s}^{-1}$ at pH 10 using a foot-of-wave analysis (FOWA) [54]. Based on density functional theory (DFT) calculations, it was proposed that the carboxylate moiety in the dianionic ligand, tda^{2-} , stabilized seven-coordinate intermediates in the high-valent oxidation state of the catalyst. Moreover, the dangling carboxylate group was a putative hydrogen-bonding site that could function as a proton acceptor and hence favor WNA. This could lower the free energy of the activation and lead to O–O bond formation [54]. To our best knowledge, the catalytic activity of complex **21** is the highest that has been reported in literature, albeit it uses FOWA.

The trianionic mononuclear ruthenium complex, $[\text{Ru}^{\text{V}}(\text{O})(\text{t5a-}\kappa\text{-N}^2\text{O})(\text{py})_2]$ (**22**) (where, $\text{t5a}^{3-} = 2,5\text{-bis}(6\text{-carboxylatopyridin-2-yl})\text{pyrrol-1-ide}$ and $\text{py} = \text{pyridine}$), was demonstrated to be an efficient catalyst with a TOF_{max} of 9400 s^{-1} at pH 7 via the FOWA [96]. In this case, the highly anionic nature of the backbone could reduce the redox potential of the $\text{Ru}^{\text{IV}}/\text{Ru}^{\text{V}}$ couple, and the flexibility of the carboxylate moiety could facilitate intramolecular proton transfer to facilitate O–O bond formation through WNA. However, unlike complex **21**, which required the formation of a seven-coordinate $\text{Ru}^{\text{V}}=\text{O}$ intermediate during water oxidation, complex **22** was not thought to require a seven-coordinate intermediate for O–O formation. This was due to the geometrical distortion of 12° and increased anionic nature of **22** in comparison with **21** (Table 3) [51,96]. The ligands tda^{2-} and t5a^{3-} were shown to be flexible, adaptive, multidentate, and equatorial and were thus termed as “FAME ligands” [51]. We would like to refer the readers to a recent review article that is focused on ruthenium-based molecular catalysts with the ability to achieve seven-coordinate intermediates and unprecedented activity [51].

Based on the above considerations, Llobet and coworkers developed the complex, $[\text{Ru}^{\text{II}}(\text{mcbp})(\text{py})_2]$ (**23**) (where, $\text{mcbp}^{2-} = 2,6\text{-bis}(1\text{-methyl-4-(carboxylate)-benzimidazol-2-yl})\text{pyridine}$), which also contained flexible anionic carboxylate ligands [97]. The active species, $[\text{Ru}^{\text{IV}}(\text{O})(\text{mcbp})(\text{py})_2]$ (**24**), was generated by the controlled potential electrolysis (CPE) of complex **23** and displayed improved activity for water oxidation with TOF_{max} of $40,000 \text{ s}^{-1}$ at pH 9 [97]. Additionally, the complex $[\text{Ru}(\text{bda})(\text{pic})(\text{pyC})]$ (**25**) (where, $\text{pyC} = 2\text{-pyridinecarboxylate}$), with a similar backbone as the bda family of ligands (e.g., complex **14**) but with carboxylate groups on the axial pyridine rather than equatorial backbone ligands, has also been reported in the literature. Complex **25** contained a dangling carboxylate ligand similar to complex **21**, which was suggested to facilitate a WNA pathway [98]. However, the catalytic performance of complex **25** was low with a TOF_{max} of $0.63\text{--}0.74 \text{ s}^{-1}$ measured via FOWA at pH 7, which was ascribed to its geometric features [98]. Unlike complex **14** and the parent complex **21**, $[\text{Ru}^{\text{II}}(\text{tda-}\kappa\text{-N}^3\text{O})(\text{py})_2]$, which were shown to have a distorted octahedral geometry with a large O–Ru–O angle of 123° (or an O–Ru–N angle of 125°), complex **25** displayed a near perfect octahedral geometry with an O–Ru–O angle of 93.72° [51,90,98].

Subsequently, Concepcion and coworkers incorporated phosphate ligands in a bipyridine backbone to generate complexes such as $[\text{Ru}^{\text{II}}(\text{bpaH}_2)(\text{pic})_2]^+$ (**26**) (where, $\text{bpaH}_4 = 2,2'\text{-bipyridine-6,6'-diphosphonic acid}$), $[\text{Ru}^{\text{III}}(\text{bpHc})(\text{pic})_2]^+$ (**27**), and $[\text{Ru}^{\text{II}}(\text{bpHc})(\text{isq})_2]$ (**28**) (where, $\text{bpH}_2\text{cH} = 2,2'\text{-bipyridine-6-phosphonic acid-6'-carboxylic acid}$) [99,100]. Complex **28**, with a carboxylate-phosphonate moiety, exhibited the highest activity among these complexes, with a TOF of 107 s^{-1} under acidic conditions and using CAN as an oxidant. However, the incorporation of a diphosphonate ligand in complex **26** drastically decreased the activity to 0.65 s^{-1} [100]. The complex, $[\text{Ru}^{\text{III}}(\text{tPaO-}\kappa\text{-N}^2\text{O}_\text{P}\text{OC})(\text{py})_2]^{2-}$ (**29**) (where, $\text{tPaO}^{5-} = 3\text{-(hydroxo-[2,2':6',2''-terpyridine]-6,6''-diyl})\text{bis}(\text{phosphonate})$), was derived from a seven-coordinate H_4tPa -based ruthenium complex, $[\text{Ru}^{\text{IV}}(\text{H}_2\text{tPa-}\kappa\text{-N}^3\text{O}^2)(\text{py})_2]^{2+}$ (where, $\text{H}_4\text{tPa} = 2,2':6',2''\text{-terpyridine-6,6''-diphosphonic acid}$), under neutral and basic conditions, where an exogenous OH^- ion from the solvent was coordinated to the complex $[\text{Ru}^{\text{IV}}(\text{H}_2\text{tPa-}\kappa\text{-N}^3\text{O}^2)(\text{py})_2]^{2+}$. This led to the formation of the six-coordinate complex $[\text{Ru}^{\text{IV}}(\text{OH})(\text{tPa-}\kappa\text{-N}^2\text{O})(\text{py})_2]^-$ or $[\text{Ru}^{\text{IV}}(\text{O})(\text{HtPa-}\kappa\text{-N}^2\text{O})(\text{py})_2]^-$. In this case, it was proposed that the $\text{Ru}^{\text{V}}=\text{O}$ intermediate undergoes intramolecular oxygen atom insertion into

the CH bond of a non-coordinated pyridyl ring to generate the catalytically active complex **29** with a TOF_{max} of $16,000 \text{ s}^{-1}$, measured via FOWA at pH 7.2 [101]. Most recently, there was an interesting complex, $[(\text{L}^{\text{N}5-})\text{Ru}^{\text{III}}\text{-OH}]^+$ (**30**), with a redox-active electron-rich polypyridyl ligand that was reported for electrochemical catalytic water oxidation at neutral pH [102]. Complex **30** was generated from $[(\text{L}^{\text{N}5-})\text{Ru}^{\text{III}}\text{-Cl}]$ by an oxidative-induced ligand exchange at neutral pH, and this species was electrochemically oxidized to form the active intermediate $[(\text{L}^{\text{N}5-})^+\bullet\text{Ru}^{\text{IV}}\text{=O}]^{2+}$, with a surprisingly low overpotential of 183 mV for O–O formation through a WNA pathway [102]. In this case, ligand oxidation was proposed to lower overpotential (1.0 V vs. NHE), which was supported by DFT calculations [102].

There is a family of mononuclear ruthenium complexes, $[\text{Ru}^{\text{II}}(\text{pdc-}\kappa^3\text{-N}^1\text{O}^2)(\text{bipy})(\text{H}_2\text{O})]$ (**31**) and $[\text{Ru}^{\text{II}}(\text{pdc-}\kappa^2\text{-N}^1\text{O}^1)(\text{bipy})_2]$ (**32**), containing the tridentate dianionic meridional pyridyl-2,6-dicarboxylate (pdc^{2-}) ligand that have been studied for their electrochemical activity towards water oxidation [78,103]. Complex **31** has been shown to electrochemically catalyze water oxidation with a low overpotential of 240 mV under acidic conditions (pH of 1), due to the presence of two carboxylate groups on the pdc^{2-} ligand. The complex **32** was shown to generate a Ru^{IV} intermediate, $[\text{Ru}^{\text{IV}}(\text{O})(\text{pdc-}\kappa^2\text{-N}^1\text{O}^1)(\text{bipy})_2]$, upon the addition of Ce^{IV} ions in solution and a WNA mechanism was proposed for O–O bond formation [103]. Complex **32** was studied electrochemically with a TOF of 3400 s^{-1} , and the high-valent $\text{Ru}^{\text{IV}}\text{=O}$ involved in the catalytic cycle had a seven-coordinate intermediate with a dangling carboxylate group, which could facilitate O–O bond formation by intramolecular proton transfer and thus decrease the activation energy [103]. In 2021, Ahlquist et al. reported a mononuclear catalyst, $[\text{Ru}(\text{bnda})(\text{pic})_2]$ (**33**) (where, $\text{H}_2\text{bnda} = 2,2'$ -bi(nicotinic acid)-6,6'-dicarboxylic acid), to investigate the effect of steric hindrance and hydrophilicity of the bnda backbone [104]. The comparison of the parent backbone of complex **14** and $[\text{Ru}(\text{pda})(\text{pic})_2]$ (**34**) (where, $\text{pda}^{2-} = 1,10$ -phenanthroline-2,9-dicarboxylate, $\text{pic} = 4$ -picoline) and $[\text{Ru}(\text{biqua})(\text{pic})_2]$ (**35**) (where, $\text{biqua}^{2-} = (1,1'$ -biisoquinoline)-3,3'-dicarboxylate) indicated a switching of the mechanism of O–O bond formation between the WNA and I2M pathway [104]. Based on experimental studies, catalyst **33** undergoes I2M, whereas complexes **34** and **35** follow the WNA pathway, although DFT calculations of complexes **33–35** have indicated that I2M is a more favorable pathway. This difference may be due to failure to consider solvation effects and the collision of $\text{Ru}^{\text{V}}\text{=O}$ species in the DFT calculations [104].

The modification of the axial ligands to enhance the catalytic performance of mononuclear ruthenium complexes was explored by Sun and coworkers. They designed the complexes, $[\text{Ru}(\text{bda})(\text{Im})_2]$ (**36**) (where, Im = imidazole) and $[\text{Ru}(\text{bda})(\text{Im})(\text{DMSO})]$ (**37**) (where, DMSO = dimethylsulfoxide) [105,106], which contained both imidazole and DMSO as axial ligands. Complex **36**, with two axial imidazole ligands, yielded a TON of 1150 and a TOF of 4.5 s^{-1} for chemical water oxidation [105]. In contrast, the complex $[\text{Ru}(\text{bda})(\text{Im})(\text{DMSO})]$ (**37**), which contained an imidazole and DMSO axial ligand, exhibited better stability and improved catalytic activity with a TON of 4050 and a TOF of up to 176.5 s^{-1} [105]. Detailed mechanistic investigations of the catalytic water oxidation reaction using kinetics, electrochemistry, high-resolution mass spectrometry, and density functional theory (DFT) calculations suggested the in situ formation of a Ru^{II} complex with an accessible seventh coordination site. The measured catalytic activity and kinetics revealed the influence of the axial ligands on the catalytic activity, where the increase of catalytic activity for complex **37** with an axial imidazole and DMSO ligands was attributed to the unhindered coupling between terminal oxygen atoms [105]. The catalytic activity of mononuclear ruthenium complexes was shown to be further enhanced with a TON of 6200 and TOF of 506 s^{-1} by employing two bromo substituted pyrazole-based axial ligands, $[\text{Ru}^{\text{II}}(\text{bda})(\text{L})_2]$ (**38**) (where $\text{bda}^{2-} = 2,2'$ -bypyridine-6,6'-dicarboxylate and L = 4-Br-3-methyl pyrazole). The enhanced catalytic activity of **38** was ascribed to the high hydrophobicity of the complex, which tended to favor dimerization and, hence, facilitate the I2M reaction pathway [48,106]. Complexes **36–38** presented the possibility of simultaneously observing the effects of the

axial and equatorial ligand modifications. However, the modification of the equatorial backbone ligand, bda^{2-} , used in these catalysts has not been fully explored to date. This is most likely due to the challenges that are involved in the synthesis of substituted bda^{2-} backbone ligands [50]. This is an avenue that could lead to further improvements of the catalytic performance as the introduction of substituents on the bda^{2-} backbone has been shown to influence the mechanistic pathways of mononuclear catalysts [50].

Table 2. Selected catalytic parameters and experimental conditions for Ru catalysts 11–38 in water oxidation. Electrochemical and chemical water oxidation using $[\text{Ce}(\text{NO}_3)_6][(\text{NH}_4)_2]$ (CAN) are abbreviated as ‘electrochem WO’ and ‘chem WO’, respectively. The TON or TOF values that are not listed in this table are unavailable in literature *.

Ru Complex	TON	TOF (s^{-1})	Experimental Conditions	Reference
11	260	0.014	chem WO	[50,71,86]
12a	320	0.0296	chem WO	[85]
13a	390	-	chem WO	[86]
13b	190	-	chem WO	[86]
13c	110	-	chem WO	[86]
13d	260	-	chem WO	[86]
13e	570	-	chem WO	[86]
14a	2000	41	chem WO	[53]
14b	8360	303	chem WO	[53]
15	553	0.23	chem WO	[91]
16	17	7.2×10^{-3}	chem WO	[91]
17	4000	7.4	chem WO (w/ $[\text{Ru}(\text{bipy})_3]^{3+}$)	[92]
18	180	0.3	chem WO (w/ $[\text{Ru}(\text{bipy})_3]^{3+}$)	[92]
19	280	1.16	chem WO (w/ $[\text{Ru}(\text{bipy})_3]^{3+}$)	[94]
20	400	1.6	chem WO (w/ $[\text{Ru}(\text{bipy})_3]^{3+}$)	[95]
23	n.a	-	inactive	[97]
26	5.0	0.65	chem WO	[100]
27	3.8	58	chem WO	[100]
28	3.8	107	chem WO	[100]
30	21	-	electrochem WO	[102]
31	1.2	0.2	chem WO	[78]
32	n.a	3400	electrochemWO	[103]
33	480	10	chem WO	[104]
34	310	0.102	chem WO	[107]
35	87	0.63	chem WO	[108]
36	1150	4.5	chem WO	[105]
37	4050	176.5	chem WO	[105]
38	6200	506	chem WO	[106]

* Foot of wave analysis (FOWA) was used to calculate the catalytic parameters of the following complexes: 21: TON 2.7×10^7 , TOF $50,000 \text{ s}^{-1}$ [54]; 22: TOF 9400 s^{-1} [96]; 24: TON 4×10^6 , TOF $40,000 \text{ s}^{-1}$ [97]; 25: TON 587, TOF $0.63\text{--}0.74 \text{ s}^{-1}$ [98]; 29: TON 4.2×10^7 , TOF $16,000 \text{ s}^{-1}$ [101].

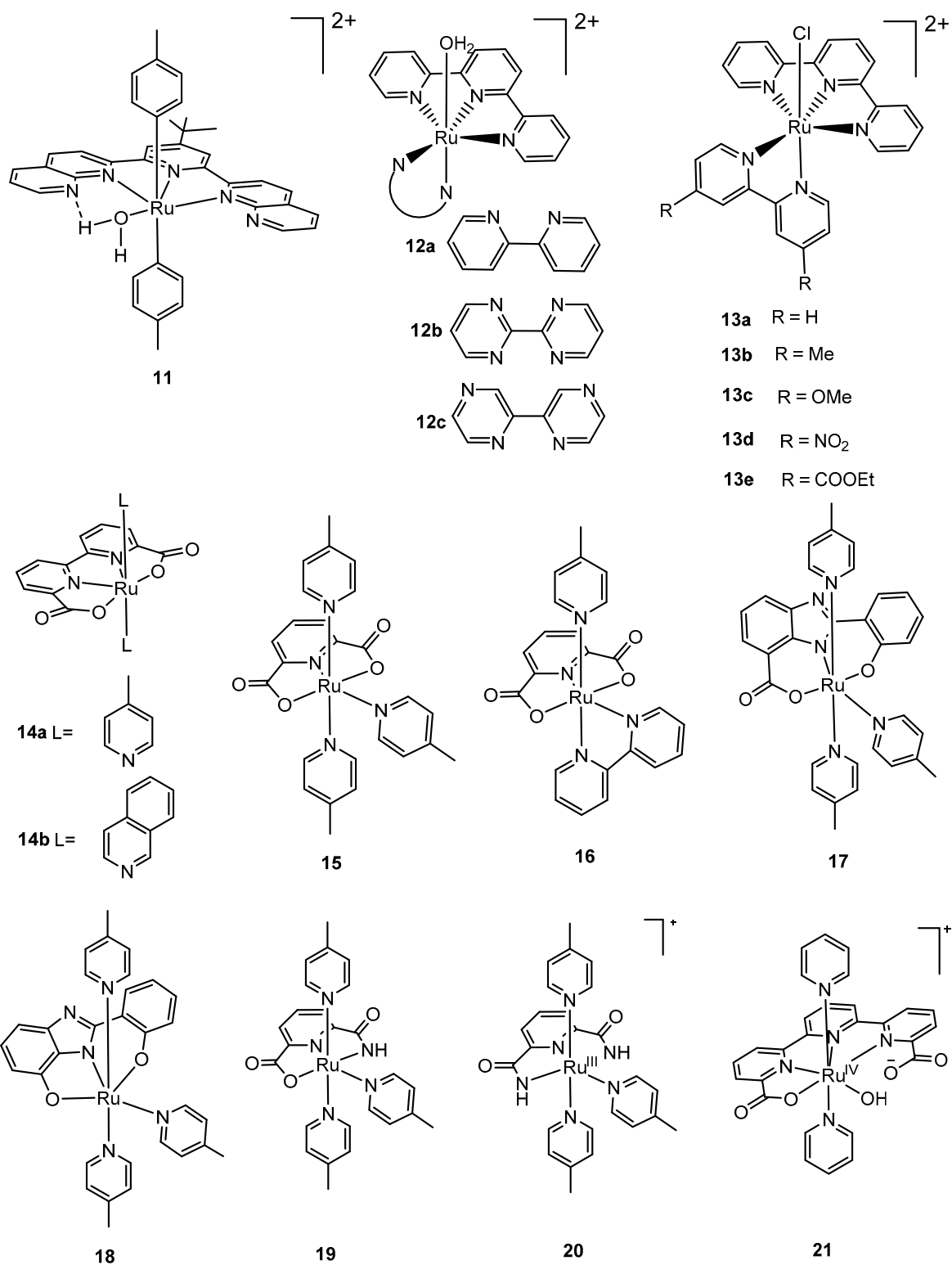


Figure 4. Cont.

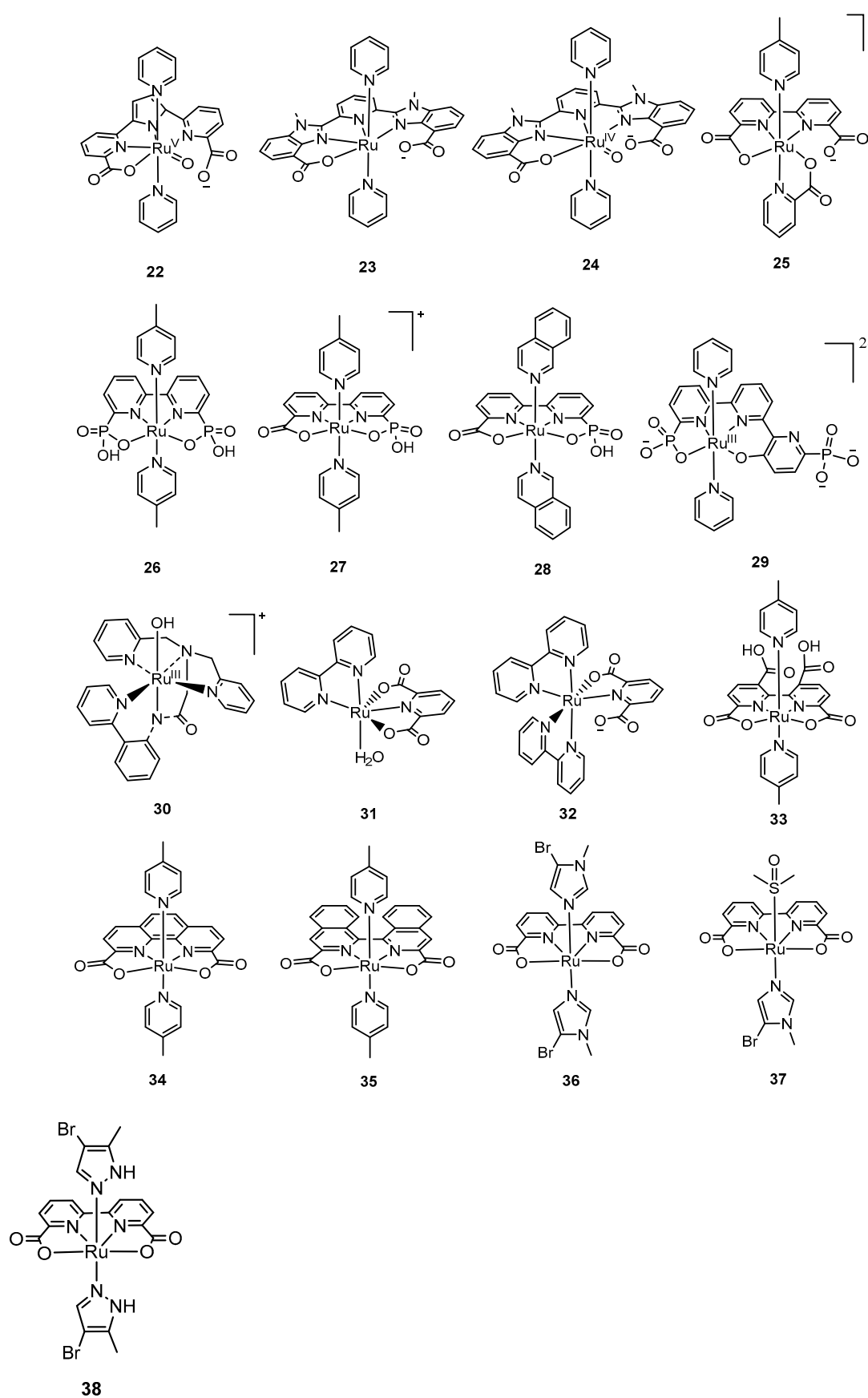


Figure 4. Selected mononuclear ruthenium complexes 11–38 for water oxidation: $[(ntp)(pic)_2Ru(H_2O)]^{2+}$ (11, ntp = 2,6-di(1,8-naphthyridin-2-yl)-4-tert-butylpyridine, pic = 4-picoline) [71,86]; $Ru(terpy)(bipy)(OH_2)]^{2+}$ (12a, bipy = 2,2'-bipyridine) [85],

[Ru(terpy)(bpm)(OH₂)]²⁺ (**12b**, terpy = 2,2':6',2''-terpyridine, bpm = 2,2'-bipyrimidine) [82]; [Ru(terpy)(bpz)(OH₂)]²⁺ (**12c**, terpy = 2,2':6',2''-terpyridine, bpz = 2,2'-bipyrazine) [82]; [Ru(terpy)(bipy)(Cl)]⁺ (**13a**, terpy = 2,2':6',2''-terpyridine, bipy = 2,2'-bipyridine); [Ru(terpy)(dmbipy)(Cl)]⁺ (**13b**, dmbipy = 4,4'-dimethyl-2,2'-bipyridine); [Ru(terpy)(dmxbipy)(Cl)]⁺ (**13c**, dmxbipy = 4,4'-dimethoxy-2,2'-bipyridine); [Ru(terpy)(dnbipy)(Cl)]⁺ (**13d**, dnbipy = 4,4'-dinitro-2,2'-bipyridine); [Ru(terpy)(dedcbipy)(Cl)]⁺ (**13e**, dedcbipy = diethyl-2,2'-bipyridine-4,4'-dicarboxylate) [86]; [Ru(bda)(pic)₂] (**14a**, bda = 2,2'-bipyridine-6,6'-dicarboxylate, pic = 4-picoline); [Ru(bda)(isq)₂] (**14b**, isq = isoquinoline) [53]; [Ru(pdc)(pic)₃] (**15**, pdc = 2,6-pyridinedicarboxylate, pic = 4-picoline) [91]; [Ru(pdc)(bipy)(pic)] (**16**, pdc = 2,6-pyridinedicarboxylate, bipy = 2,2'-bipyridine, pic = 4-picoline) [91], [Ru^{III}(L)(pic)₃] (**17**, L = 2-(2-hydroxyphenyl)-1H-benzimidazole-7-carboxylate; **18**, L = 2-(2-hydroxyphenyl)-1H-benzimidazol-7-ol) [92]; [Ru(HL)(pic)₃] (**19**, L = 6-carbamoylpicolinic acid) [94]; [Ru^{III}(H₂pdca)(pic)₃]⁺ (**20**, H₂pdca = 2,6-pyridine-dicarboxamide) [95]; [Ru^{IV}(OH)(tda-κ-N³O(py)₂)]⁺ (**21**, tda = 2,2':6',2''-terpyridine-6,6''-dicarboxylate, py = pyridine) [54]; [Ru^V(O)(t5a-κ-N²O)(py)₂] (**22**, t5a = 2,5-bis(6-carboxylatopyridin-2-yl)pyrrol-1-ide, py = pyridine) [96]; [Ru(mcbp)(py)₂] (**23**, mcbp = 2,6-bis(1-methyl-4-(carboxylate)-benzimidazol-2-yl)pyridine, py = pyridine); [Ru^{IV}(O)(mcbp)(py)₂] (**24**) [97]; [Ru(bda)(pic)(pyC)] (**25**, bda = 2,2'-bipyridine-6,6'-dicarboxylate, pic = 4-picoline, pyC = 2-pyridinecarboxylate) [98]; Ru(bpaH₂)(pic)₂] (**26**, bpaH₂ = 2,2'-bipyridine-6,6'-diphosphonate, pic = 4-picoline); [Ru^{III}(bpHc)(pic)₂]⁺ (**27**, bpH₂cH = 2,2'-bipyridine-6-phosphonic acid-6'-carboxylic acid); [Ru^{II}(bpHc)(isq)₂] (**28**, isq = isoquinoline) [100]; [Ru^{III}(tPaO-κ-N²O_PO_C)(py)₂]²⁻ (**29**, tPaO = 3-(hydroxo-[2,2':6',2''-terpyridine]-6,6''-diyl)bis(phosphonate) [101]; [(L^{N5-})Ru^{III}-OH]⁺ (**30**, L = 2-(bispyridin-2-ylmethyl-amino)-N-(2-pyridin-2-yl-phenyl)-acetamide) [102]; [Ru(pdc-κ³-N¹O²)(bipy)(H₂O)] (**31**, pdc = pyridyl-2,6-dicarboxylate, bipy = 2,2'-bipyridine) [78]; and [Ru(pdc-κ²-N¹O¹)(bipy)₂] (**32**, pdc = pyridyl-2,6-dicarboxylate, bipy = 2,2'-bipyridine) [103]; [Ru(bnda)(pic)₂] (**33**, bnda = 2,2'-bi(nicotinic acid)-6,6'-dicarboxylate) [104]; [Ru(pda)(pic)₂] (**34**, pda = 1,10-phenanthroline-2,9-dicarboxylate, pic = 4-picoline) [107]; [Ru(biqa)(pic)₂] (**35**, biqa = (1,1'-biisoquinoline)-3,3'-dicarboxylate) [108]; [Ru(bda)(Im)₂] (**36**, bda = 2,2'-bipyridine-6,6'-dicarboxylate, Im = imidazole); [Ru(bda)(Im)(DMSO)] (**37**, DMSO = dimethylsulfoxide) [105]; [Ru(bda)(L)₂] (**38**, bda = 2,2'-bipyridine-6,6'-dicarboxylate, L = 4-Br-3-methylpyrazole) [106].

Table 3. Comparison of complexes **21** and **22** that contain similar backbone ligands.

Ru Complex	CCN Angle for Free Backbone Ligand	CCN Angle for Complex (ave.) *	Coordination Number	Activation Energy	Redox Potential (Ru ^{IV} /Ru ^{III} , Ru ^V =O/Ru ^{IV} =O)
21 (tda)	120°	113.9°	7	M11-L, 19.5 kcal/mol	1.1 V, 1.43 V
22 (t5a)	126°	111.5°	6	M06-L, 14.2 kcal/mol	0.55 V, 1.41 V

* The CCN angle for complex (ave.) determined from structural data available from the Cambridge Structural Database (CSD).

3. Iridium Catalysts

Iridium-based homogeneous catalysts were not reported in the literature until 2008. Below, we briefly review the research in this area that has been summarized elsewhere through 2015 [7]. In 2008, Bernhard et al. studied bis-aqua iridium complexes (Figure 5, **40a–40e**) with cyclometalating ligands and a surrogate catalyst, [Ir^{III}(ppy)₂(bipy)]⁺ (**39**) (where, bipy = 2,2'-bipyridine, ppy = 2-phenylpyridine), without coordinated aqua ligands [109]. One of the complexes (**40d**) achieved a TON of 2760 after a week in Ce^{IV} solution (Table 4), while the investigation of catalytic activity of the surrogate catalyst displayed no oxygen evolution. This finding suggested that open coordination sites (for water ligands) were necessary for catalysis [109]. In 2009, Crabtree and coworkers developed precatalysts based on iridium with pentamethylcyclopentadienyl (Cp*) and 2-phenylpyrimidine (or ppy) ligands [110]. The precursor, [Ir^{III}(Cp*)(ppy)(Cl)] (**41a**), catalyzed water oxidation driven by Ce^{IV} with a TOF of 54 min⁻¹, which was considered the most active catalyst at that time [110]. The [Ir^V(Cp*)(O)(ppy)]⁺ species was proposed as a possible intermediate in agreement with electronic structure calculations by DFT [110]. The following year, Crabtree and coworkers developed iridium half-sandwich complexes, such as Cp*Ir(N-C)X, [Cp*Ir(N-N)X]X, and [CpIr(N-N)X]X (where, X = Cl, I or NO₃⁻), as precatalysts for water oxidation, which have been reviewed in the literature [7].

In this review, we highlight that the tris-aqua [Cp*Ir(H₂O)₃]SO₄ (**42a**) and dimeric [(Cp*Ir)(μ-OH)₃(IrCp*)]OH (**43**) complexes exhibited TOFs of up to 20 min⁻¹ and 25 min⁻¹

on a per-iridium basis, respectively, with Ce^{IV} as the primary oxidant at pH 0.89 [111]. DFT calculations indicated that an O–O bond was formed by the intermolecular attack of water to an iridium oxo ligand, and proton transfer to the oxo group was assisted by an additional water molecule [111]. A parallel study on a tris-aqua complex, $[\text{Cp}^*\text{Ir}(\text{H}_2\text{O})_3](\text{NO}_3)_2$ (**42b**), was conducted by MacChioni and coworkers, which highlighted that both the synthetic ease to the tris-aqua complex, $[\text{Cp}^*\text{Ir}(\text{H}_2\text{O})_3](\text{NO}_3)_2$ (**42b**), as well as the high activity with TOFs up to 15.7 min^{-1} with long-term activity [112]. Another complex, $[\text{Cp}^*\text{Ir}(\text{bzpy})\text{NO}_3]$ (**44**) (where, bzpy = 2-benzoylpyridine), with NO_3^- as a ligand to impart water solubility, was examined with a TON of 1250 and a TOF of 8.46 min^{-1} , as measured by UV-Vis under CAN [112,113]. The value increased to 12.7 min^{-1} when the oxygen evolution was measured by a Clark electrode [113] and up to 31 min^{-1} by probing different catalyst concentrations [114].

Iridium complexes with a carbene-type ligand were developed by Bernhard and coworkers in 2010 and two resulting complexes, **45** and **46**, exhibited excellent stability with TONs of 10,000 and 8350 within 5 days, respectively [115]. In 2011, Crabtree and coworkers incorporated an N-heterocyclic carbene (NHC) ligand and Cp^* to form the complex $[\text{Cp}^*\text{Ir}(\text{NHC})\text{Cl}]$ (**47**) as a precatalyst that displayed moderate activity with a TOF of 8 min^{-1} driven by CAN and a TOF of $12\text{--}16 \text{ min}^{-1}$ with sodium periodate (at pH 5); deactivation of the precatalyst was ascribed to the low pH in Ce^{IV} solution under the former conditions [116]. As incorporation of a carboxylate moiety into ligands on ruthenium proved to be an effective strategy to improve catalytic activity (*vide supra*), MacChioni and coworkers developed a series of iridium complexes, **48a–48d** and **49**, as precatalysts for water oxidation [114]. The complexes **48a** and **48b** exhibited impressive performances with TOFs of 287 min^{-1} and 277 min^{-1} under optimized conditions with Ce^{IV} as sacrificial oxidant, respectively, whereas complex **49**, bearing a dicarboxylate moiety, turned out to be the least active [114]. Complex **48d**, with a pendant $-\text{COOH}$ moiety, featured the lowest potential and exhibited a TOF of 17 min^{-1} [114]. In 2012, MacChioni and coworkers developed the precatalyst $[\text{IrCl}(\text{Hedta})]\text{Na}$ (**50**) with monoprotonated ethylenediaminetetraacetic acid (edta) with a goal to replace Cp^* as it slowly degraded in harsh acidic oxidative conditions [117]. The Hedta ligand is easy to synthesize and can stabilize metal ions in high oxidation states [117]. The complex (**50**) exhibited excellent stability with a TON up to 12,000, whereas it showed only moderate TOFs of 5.4 to 7.3 min^{-1} [117]. An interesting finding was the neutral complex $[\text{Ir}(\text{H}_2\text{O})(\text{Hedta})]$, which catalyzed water oxidation with a TOF of 2.6 min^{-1} . It was suggested that the complex $[\text{IrCl}(\text{Hedta})]^-$ underwent ligand exchange with water to generate $[\text{Ir}(\text{H}_2\text{O})(\text{Hedta})]$ for water oxidation [117]. In 2014, MacChioni et al. developed Cp^* -based precatalysts **41b**, **51a**, **51b**, **52**, **53**, **54**, and **55**, some with strongly electron-donating amido ligands. These complexes showed stabilities through TONs > 500 for all the precatalysts examined. The complexes $[\text{Cp}^*\text{Ir}(\text{bimH}_2)\text{Cl}]\text{Cl}$ (**54**) (where, bimH₂ = 2,2'-bismidazole) and $[\text{Cp}^*\text{IrCl}(\mu^2-\kappa^2-\kappa^1\text{-bimH})\text{IrCl}_2\text{Cp}^*]$ (**55**) displayed high catalytic activities with TOFs of 26 min^{-1} and 58 min^{-1} , respectively, as measured by a Clark electrode. Complex **52**, bearing an NHC ligand, showed a TOF of 7 min^{-1} from UV-Vis data [118], which agreed well with analogous complex $[\text{Cp}^*\text{Ir}(\text{NHC})\text{Cl}]$ (**47**) with a TOF of 8 min^{-1} reported by Crabtree et al. [116]. Although an NHC ligand can effectively stabilize high-valent iridium (IV), as evidenced by the EPR observations [116], Cp^*Ir precatalysts incorporating the NHC ligand did not display high catalytic activity.

Molecular iridium catalysts experienced noteworthy progress in 2015 when Brudvig, Crabtree, Schmuttenmaer and coworkers developed an inactive molecular iridium catalyst, $[\text{Cp}^*\text{Ir}(\text{pyalc})\text{OH}]$ (**56**), that dimerized in NaIO_4 solution to generate a highly active system once bound to an oxide surface. The so-called het-WOC (**56-het**) can electrochemically catalyze water oxidation with low overpotential ($\eta = 14 \text{ mV}$) and a high TOF (7.9 s^{-1}) and stability, with a TON of 10^6 [119]. This het-WOC is different from a benchmark IrO_2 nanomaterial (60–100 nm) that required 580 mV to reach an oxygen evolution rate of 6.6 s^{-1} per electroactive iridium atom [119].

Bernhard and coworkers developed a series of iridium(III) complexes in 2016 [120,121] and 2017 [120,121] with tetradentate bis(pyridine-2-sulfonamide) (bpsa) chelates (57–59) to form resilient wrap-around ligand environments; this structure provides a strong electron-donating environment to stabilize positively-charged iridium intermediates. These catalysts (57–59) exhibited good stability with TONs up to 3540, whereas the best initial TOF of these catalysts was $7.5 \times 10^{-3} \text{ s}^{-1}$ [120]. Through the modification of the linker moiety to tune the electronic structures of complexes 60 and 61a–61d, complex 60 exhibited good catalytic activity with a TON of 13,840 and a TOF of $1.38 \times 10^{-2} \text{ s}^{-1}$; the complex $[\text{Ir}^{\text{III}}(\text{bpsa-Ph})(\text{Cl})_2]^-$ (61a) achieved an even higher TON of 16200 and a TOF $3.90 \times 10^{-2} \text{ s}^{-1}$ with Ce^{IV} as oxidant at pH 1 [121]. (Please note that complex 59 and 61a are the same; due to different experimental conditions reported, the TON and TOF data reported in reference [121] is larger than that reported in reference [120]). Electrochemical quartz-crystal microbalance studies were employed to distinguish the heterogeneous WOCs from homogeneous catalysts; dynamic light scattering (DLS) experiments ruled out IrOx particles for catalytic activity in Ce^{IV} -driven water oxidation [120,121]. More recently, Bonchio et al. [122] reported the first light-driven water oxidation catalyst, an $\text{Ir}^{\text{IV,IV}}_2(\text{pyalc})_2$ μ -oxo-dimer (where, $\text{pyalc} = 2\text{-(2'-pyridyl)-2-propanoate}$) called ‘Ir-blue’, synthesized by reacting inactive complex $[\text{Cp}^*\text{Ir}(\text{pyalc})\text{OH}]$ (56) with excess sodium periodate [123]. The catalytic activity of the dimer depended on the light intensity and can reach up to a TON of 32 and TOF of $9.7 \times 10^{-2} \text{ s}^{-1}$ per iridium center under standard photochemical water oxidation conditions, e.g., $\text{Ru}(\text{bipy})_3^{2+}$ as a photosensitizer and $\text{Na}_2\text{S}_2\text{O}_8$ as sacrificial electron acceptor [122].

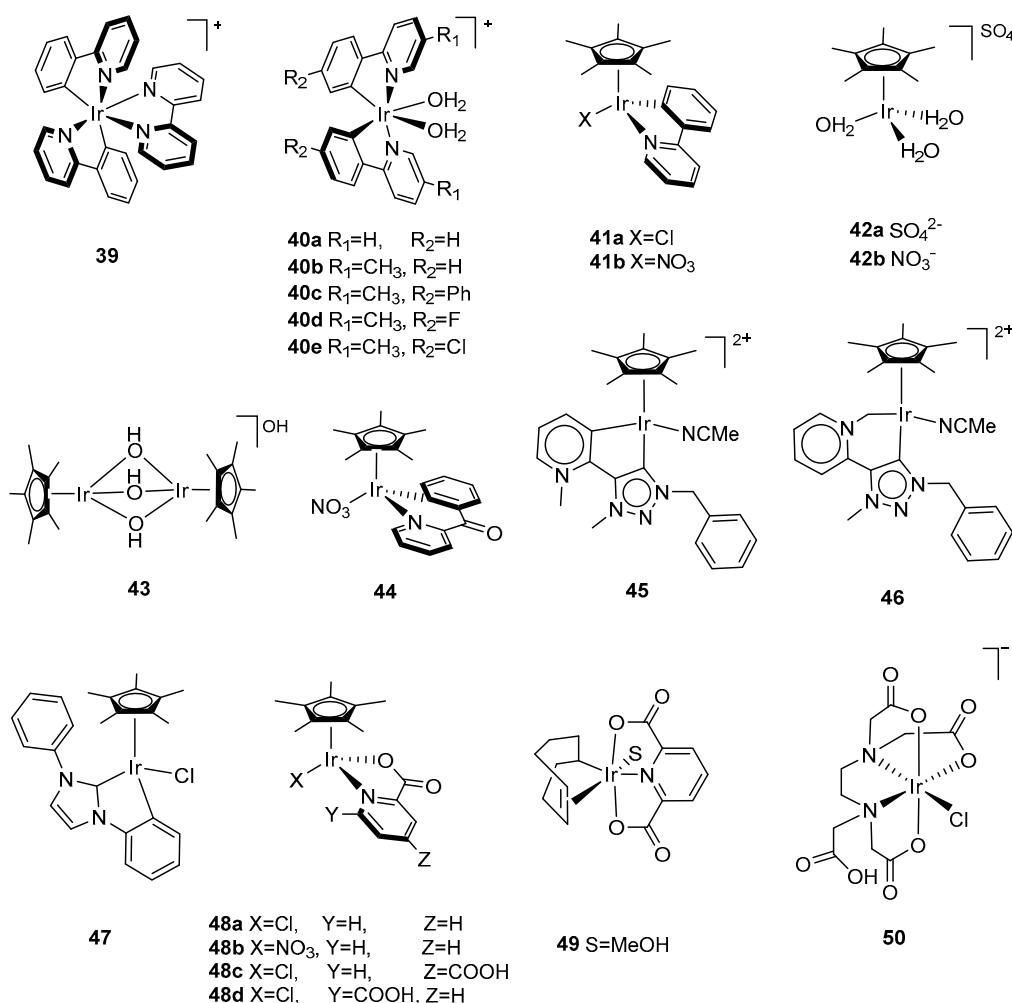


Figure 5. Cont.

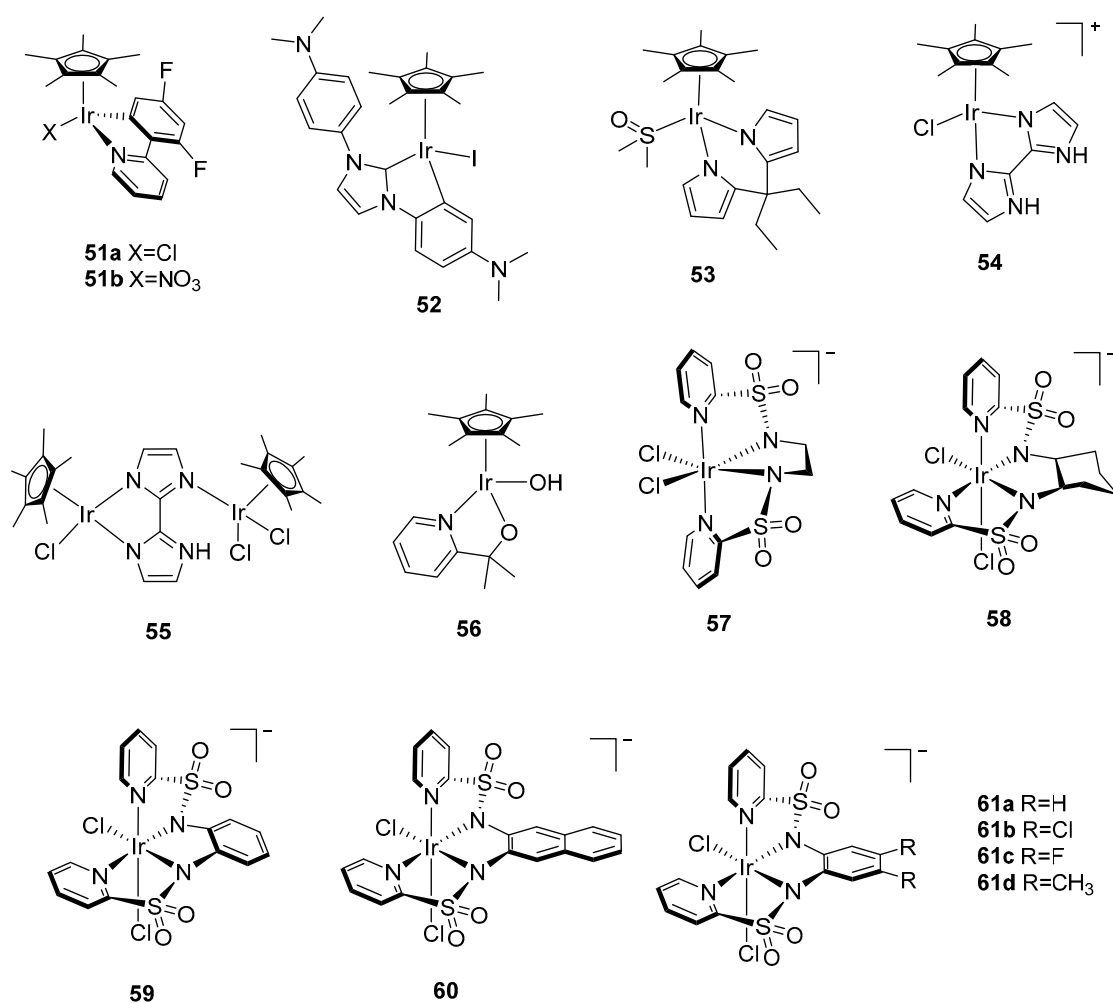


Figure 5. Chemical structures of iridium catalysts 39–61 for water oxidation: $[\text{Ir}^{\text{III}}(\text{ppy})_2(\text{bipy})]^+$ (39, ppy = 2-phenylpyridine, bipy = 2,2'-bipyridine) [109]; $[\text{Ir}(\text{ppy})_2(\text{H}_2\text{O})_2]^+$ (40a, ppy = 2-phenylpyridine); $[\text{Ir}(5\text{-R}_1,4'\text{-R}_2\text{-2-phenylpyridine})_2(\text{H}_2\text{O})_2]^+$ (40b, $\text{R}_1 = \text{CH}_3$, $\text{R}_2 = \text{H}$; 40c, $\text{R}_1 = \text{CH}_3$, $\text{R}_2 = \text{Ph}$; 40d, $\text{R}_1 = \text{CH}_3$, $\text{R}_2 = \text{F}$; 40e, $\text{R}_1 = \text{CH}_3$, $\text{R}_2 = \text{Cl}$) [109]; $[\text{Ir}^{\text{III}}(\text{Cp}^*)(\text{ppy})(\text{Cl})]$ (41a, Cp^* = pentamethylcyclopentadienyl, ppy = 2-phenylpyridine); $[\text{Ir}^{\text{III}}(\text{Cp}^*)(\text{ppy})(\text{NO}_3)]$ (41b, Cp^* = pentamethylcyclopentadienyl, ppy = 2-phenylpyridine) [110]; $[\text{Cp}^*\text{Ir}(\text{H}_2\text{O})_3]\text{SO}_4$ (42a, Cp^* = pentamethylcyclopentadienyl) [111]; $[\text{Cp}^*\text{Ir}(\text{H}_2\text{O})_3](\text{NO}_3)_2$ (42b, Cp^* = pentamethylcyclopentadienyl) [112]; $[(\text{Cp}^*\text{Ir}(\mu\text{-OH})_3(\text{IrCp}^*))\text{OH}]$ (43, Cp^* = pentamethylcyclopentadienyl) [111]; $[\text{Cp}^*\text{Ir}(\text{bzpy})\text{NO}_3]$ (44, bzpy = 2-benzoylpyridine) [112]; $[\text{Cp}^*\text{Ir}(\text{MeCN})(\text{L})]^{2+}$ (45, L = 2-(1-benzyl-1H-1,2,3-triazol-4-yl)pyridine, carbon-bound); (46, L = 2-(1-benzyl-1H-1,2,3-triazol-4-yl)pyridine, nitrogen-bound) [115]; $[\text{Cp}^*\text{Ir}(\kappa^2\text{-C}^2, \text{C}^{2'}\text{-NHC})\text{Cl}]$ (47, $\kappa^2\text{-C}^2, \text{C}^{2'}\text{-NHC} = \kappa^2\text{-C}^2, \text{C}^{2'}\text{-1,3-diphenylimidazol-2-ylidene}$) [116]; $[\text{Cp}^*\text{Ir}(\kappa^2\text{-N,O})\text{X}]$ (48a, $\kappa^2\text{-N,O} = 2\text{-pyridinecarboxylate}$, X = Cl; 48b, $\kappa^2\text{-N,O} = 2\text{-pyridinecarboxylate}$, X = NO₃; 48c, $\kappa^2\text{-N,O} = 4\text{-carboxy-2-pyridinecarboxylate}$, X = Cl; 48d, $\kappa^2\text{-N,O} = 6\text{-carboxy-2-pyridinecarboxylate}$, X = Cl); $[\text{Ir}(\kappa^3\text{-N,O,O})(1\text{-}\kappa\text{-4,5-}\eta^2\text{-C}_8\text{H}_{13})(\text{MeOH})]$ (49, $\kappa^3\text{-N,O,O} = 2,6\text{-pyridinedicarboxylate}$) [114]; $[\text{IrCl}(\text{Hedta})]^-$ (50, Hedta = monoprotonated ethylenediaminetetraacetic acid) [117]; $[\text{Cp}^*\text{Ir}(2',4'\text{-F}_2\text{-ppy})\text{Cl}]$ (51a, 2',4'-F₂-ppy = 2',4'-difluoro-2-phenylpyridine); $[\text{Cp}^*\text{Ir}(2',4'\text{-F}_2\text{-ppy})(\text{NO}_3)]$ (51b, 2',4'-F₂-ppy = 2',4'-difluoro-2-phenylpyridine); $[\text{Cp}^*\text{Ir}(\kappa^2\text{-C}^2, \text{C}^{2'}\text{-NHC})\text{I}]$ (52, $\kappa^2\text{-C}^2, \text{C}^{2'}\text{-NHC} = \kappa^2\text{-C}^2, \text{C}^{2'}\text{-1,3-bis(4-(N,N-dimethylamino)phenyl)-imidazol-2-ylidene}$); $[\text{Cp}^*\text{Ir}(\text{bpyr})(\text{DMSO})]$ (53, bpyr = bis-diethyl-pyrrole, DMSO = dimethylsulfoxide); $[\text{Cp}^*\text{Ir}(\text{bimH}_2)\text{Cl}]\text{Cl}$ (54, bimH₂ = 2,2'-bisimidazole); $[\text{Cp}^*\text{IrCl}(\mu^2\text{-}\kappa^2\text{-}\kappa^1\text{-bimH})\text{IrCl}_2\text{Cp}^*]$ (55, bimH = 2,2'-bisimidazole) [118]; $[\text{Cp}^*\text{Ir}(\text{pyalc})\text{OH}]$ (56, pyalc = 2-(2'-pyridyl)-2-propanolate) [119]; $[\text{Ir}(\text{bpsa-en})\text{Cl}_2]^-$ (57, bpsa-en = *N,N'*-(ethane-1,2-diyl)bis(pyridine-2-sulfonamide)); $[\text{Ir}(\text{bpsa-Cy})\text{Cl}_2]^-$ (58, bpsa-Cy = *N,N'*-(1*R*,2*R*)-cyclohexane-1,2-diyl)bis(pyridine-2-sulfonamide)); $[\text{Ir}(\text{bpsa-Ph})\text{Cl}_2]^-$ (59, bpsa-Ph = *N,N'*-(phenylene-1,2-diyl)bis(pyridine-2-sulfonamide)) [120]; $[\text{Ir}(\text{bpsa-NPTH})\text{Cl}_2]^-$ (60, bpsa-NPTH = *N,N'*-(naphthalene-2,3-diyl)bis(pyridine-2-sulfonamide)) [121]; $[\text{Ir}(\text{bpsa-Ph})\text{Cl}_2]^-$ (61a, bpsa-Ph = *N,N'*-(phenylene-1,2-diyl)bis(pyridine-2-sulfonamide)); $[\text{Ir}(\text{bpsa-PhdCl})\text{Cl}_2]^-$ (61b, bpsa-PhdCl = *N,N'*-(4,5-dichloro-phenylene-1,2-diyl)bis(pyridine-2-sulfonamide)); $[\text{Ir}(\text{bpsa-PhdF})\text{Cl}_2]^-$ (61c, bpsa-PhdF = *N,N'*-(4,5-difluoro-phenylene-1,2-diyl)bis(pyridine-2-sulfonamide)); $[\text{Ir}(\text{bpsa-PhdMe})\text{Cl}_2]^-$ (61d, bpsa-PhdMe = *N,N'*-(4,5-dimethyl-phenylene-1,2-diyl)bis(pyridine-2-sulfonamide)) [121].

Table 4. Selected catalytic parameters and experimental conditions for Ir catalysts 39–61 for water oxidation. Electrochemical and chemical water oxidation using CAN are abbreviated as ‘electrochem WO’ and ‘chem WO’, respectively. The TON or TOF values that are not listed in this table are unavailable in literature.

Ir Complex	TON	TOF	Condition	References
39	0	0 s ⁻¹	chem WO	[109]
40a	2490	-	chem WO	[109]
40b	2270	-	chem WO	[109]
40d	2760	-	chem WO	[109]
41a	n.a	54, 4.68 min ⁻¹	chem WO	[110,112]
41b	>500	14 min ⁻¹	chem WO	[118]
42a	-	20 min ⁻¹	chem WO	[111]
42b	-	15.7 min ⁻¹	chem WO	[112]
43	-	25 min ⁻¹	chem WO	[111]
44	1250	8.4, 8.46, 12.7, 31 min ⁻¹	chem WO	[112–114]
45	10,000	314 h ⁻¹	chem WO	[115]
46	8350	-	chem WO	[115]
47	-	8 min ⁻¹	chem WO	[116]
48a	1200	287 min ⁻¹	chem WO	[114]
48b	2000	277 min ⁻¹	chem WO	[114]
48c	750	23 min ⁻¹	chem WO	[114]
48d	1300	17 min ⁻¹	chem WO	[114]
49	500	5 min ⁻¹	chem WO	[114]
50	12,000	5.4–7.3 min ⁻¹	chem WO	[117]
51b	500	11 min ⁻¹	chem WO	[118]
52	n.a	7 min ⁻¹	chem WO	[118]
53	500	11 min ⁻¹	chem WO	[118]
54	500	26 min ⁻¹	chem WO	[118]
55	500	58 min ⁻¹	chem WO	[118]
56 het *	10 ⁶	7.9 s ⁻¹	electrochem WO	[119]
57	245	9.07 × 10 ⁻⁴ s ⁻¹	chem WO	[120]
58	2000	3.55 × 10 ⁻³ s ⁻¹	chem WO	[120]
59	3540	3.55 × 10 ⁻³ s ⁻¹	chem WO	[120]
60	13,840	1.38 × 10 ⁻² s ⁻¹	chem WO	[121]
61a	16,200	3.90 × 10 ⁻² s ⁻¹	chem WO	[121]
61b	15,860	3.24 × 10 ⁻² s ⁻¹	chem WO	[121]
61c	13,210	1.69 × 10 ⁻² s ⁻¹	chem WO	[121]
61d	14,700	2.13 × 10 ⁻² s ⁻¹	chem WO	[121]

* 56 het is abbreviated from ‘56-heterogenous catalyst’, generated from a dimer of 56 bound to the surface of nanoITO suspended on a fluorine-doped tin oxide (FTO) coated glass slide.

4. Catalysts Based on First Row Transition Metals

First-row transition metals have been attracting research attention in the design of efficient molecular catalysts for water oxidation due to their abundance and low cost. However, the development of water oxidation catalysts based on first-row transition metals is relatively limited by virtue of being substitutionally labile, which indicates that ligands coordinated to these metals can exchange with water and/or solvents [4]. In many cases, initial precursor complexes decompose to catalytically active metal oxide particle precipitates. Therefore, studies on water oxidation catalysts based on first-row transition metals should be carefully evaluated to rule out the formation of corresponding metal oxide particles responsible for catalyzing water oxidation. To overcome these challenges, ligands need to be structurally engineered with high metal ion affinity (even in aqueous media) to permit access to and stabilize elevated oxidation states.

4.1. Manganese Catalysts

With manganese present in the natural OEC, synthetic complexes based on manganese have attracted significant scientific interest over the years. In early studies, Brudvig,

Crabtree and coworkers had proposed that the dimanganese di- μ -oxo complex, $[\text{Mn}^{\text{III,IV}}_2(\mu\text{-O})_2(\text{bipy})_4][\text{ClO}_4]_3$, was active in chemical water oxidation [124,125]. Although numerous synthetic models containing Mn have been constructed in the past 30 years [126], only a few of the complexes have demonstrated catalytic activity for water oxidation [127,128]. The first synthetic functional Mn cubane model, $\text{Mn}_4\text{O}_4(\text{O}_2\text{P}(\text{Ph})_2)_6$, was synthesized in 1997 [129]. This complex, as well as the $\text{Mn}_4\text{O}_4((\text{MePh})_2\text{PO}_2)_6$ catalyst reported by Disimukes and coworkers [130,131], can release dioxygen with UV light absorption in the gas phase as shown in Equation (2):



These two functional cuboidal clusters release dioxygen (concomitant with ligand dissociation) when excited under photochemical conditions. It has been proposed that an intramolecular two-electron charge transfer weakened Mn–O bonds and considerable distortion of the complex resulted in loss of the phosphinate bridge [130,131]. The distortion of core bonds allowed for the oxygen atoms to move in close proximity to form a peroxy intermediate, thereby lowering the activation barrier for dioxygen formation [130,131]. Subsequently, a synthetic Mn_4Ca cluster featuring high structural resemblance to the natural OEC was found to be inactive in water oxidation [132].

In 1994, a chelating bis-porphyrin model was used to form stable catalytic complexes, **62**, **63**, and **64** (Figure 6). Complex **64** showed the highest activity at high potentials (1.8–2.0 V vs. Ag/Ag^+) with a TON of up to 9.2 in acetonitrile containing $[\text{nBu}_4\text{N}][\text{OH}]$ [133] (Table 5). The key intermediate involved in water oxidation, a dinuclear $\text{Mn}^{\text{V}}=\text{O}$ (**65**) (Figure 6), was characterized by spectroscopic methods; however, the mechanism of O–O bond formation was inconclusive as there were two pathways to form an O–O bond: either by the attack of external water on the $\text{H}_2\text{O}-\text{Mn}^{\text{V}}=\text{O}$ group or by the coupling two $\text{Mn}^{\text{V}}=\text{O}$ units in the dimer [134].

The earliest Mn complexes that were found to be active in light-driven water oxidation were coordinated to a dianionic tetradentate N_2O_2 Schiff base ligand, of which the complex $[\text{Mn}^{\text{III}}(\text{salpd})(\text{H}_2\text{O})_2][\text{ClO}_4]_2$ (where, *salpd* = propane-1,3-diylbis(salicylideneimine)) was found to be the most active [128]. The rate of dioxygen evolution was independent of solvent, however, it depended on the concentration of the manganese complex (and quinone) as well as the pH of the reaction mixture [128]. The modification of the electronic properties of the ligand generated an active complex under irradiation and in the presence of *p*-benzoquinone, although the activity was not as good as the parent complex, $[\text{Mn}^{\text{III}}(\text{salpd})(\text{H}_2\text{O})_2](\text{ClO}_4)_2$ [135]. Water photolysis occurred when an aqueous solution of a salen-based dimer, $[\text{Mn}^{\text{III}}(3,5\text{-Cl-salen})(\text{H}_2\text{O})_2](\text{ClO}_4)_2$ (where, 3,5-Cl-salen = *N,N'*-3,5-dichloro(salicylidene)-1,2-diaminoethane), was irradiated under visible light together with bulk *p*-benzoquinone [136]. X-ray diffraction presented the possibility of hydrogen bonding interactions in the system [136]. Another functional model in this context employed the negatively charged pentadentate ligand, *N*-methyl-*N'*-carboxymethyl-*N,N'*-bis(2-pyridylmethyl)ethane-1,2-diamine (*mcbpen*[−]), which can catalyze water oxidation driven by *tert*-butylhydrogenperoxide (TBHP) or Ce^{IV} [137]. The evolution of dioxygen using Ce^{IV} (pH 1) was in lower yields compared to TBHP (pH 4.75), as the pH of Ce^{IV} is very low and does not favor the formation of high-valent oxo-bridged Mn intermediates [137]. Unlike the case of $[\text{Mn}^{\text{III,IV}}_2(\mu\text{-O})_2(\text{terpy})_2(\text{H}_2\text{O})_2](\text{NO}_3)_3 \cdot 6\text{H}_2\text{O}$, which generated dioxygen under sodium hypochlorite and oxone (with ultimate decomposition to permanganate) [138,139], the complex $[\text{Mn}^{\text{II}}_2(\text{mcbpen})_2(\text{H}_2\text{O})_2](\text{ClO}_4)_2$ was not shown to produce permanganate as a product of water oxidation catalysis with either TBHP or Ce^{IV} as oxidant [137].

In 1999, Brudvig and coworkers synthesized a functional model, $[\text{Mn}^{\text{III,IV}}_2(\mu\text{-O})_2(\text{terpy})_2(\text{H}_2\text{O})_2](\text{NO}_3)_3$ (**66**), for water oxidation with a TOF of 0.67 s^{-1} [138,139]. The success of the model encouraged the group to develop a series of complexes with the general formula, $[\text{Mn}^{\text{III,IV}}_2(\mu\text{-O})_2(\text{L})_2(\text{X})_2]^{3+}$ (L = terpy, terpy derivatives and X = labile ligand), with their catalytic performance assayed in situ and in pure solution with ox-

one as the oxidant [140]. The parent catalyst with terpy, **66**, exhibited the best catalytic performance and the in situ solution showed relatively higher catalytic rate than that of corresponding pure complex, which was ascribed to additional oxone solution [140]. An ^{18}O isotope labeling experiment was carried out to study the mechanism of water oxidation by the complex with oxone as an oxidant due to the fast exchange of oxygen in hypochlorite. It was proposed that O–O bond formation involved the attack of water (or oxone) on a $\text{Mn}^{\text{V}}=\text{O}$ intermediate. Other functional μ -oxo-bridged dinuclear models included $[\text{Mn}(\text{PaPy}_3)(\mu\text{-O})(\text{PaPy}_3)\text{Mn}]^{2+}$ (**67**), reported by Brudvig and coworkers in 2013 with a TOF of $13.9 \times 10^{-3} \text{ s}^{-1}$ using oxone as an oxidant [141], and the recent complex, $[\text{Mn}(\text{bipyalk})(\text{H}_2\text{O})(\mu\text{-O})_2(\text{OTf})_2]$ (**68**), reported by Crabtree, Brudvig and coworkers that achieved a TOF of $5.5 \times 10^{-3} \text{ s}^{-1}$ with oxone as an oxidant [142]. Additionally, three functional mononuclear manganese complexes, **69–71**, were developed by Brudvig and coworkers in 2013 [141]. The catalytic performance of these complexes was examined with oxone as an oxidant. Complex **69** did not show evolution of dioxygen, however, complexes **70** and **71** displayed a TOF of $9.9 \times 10^{-3} \text{ s}^{-1}$ and $3.4 \times 10^{-3} \text{ s}^{-1}$, respectively, under the same conditions, highlighting the role that the anionic N-donor carboxamido ligand in complex **70** played in stabilizing high-valent intermediate(s) [141].

Table 5. Selected catalytic parameters and experimental conditions for Mn catalysts **62–71** for water oxidation. Electrochemical and chemical water oxidation are abbreviated as ‘electrochem WO’ and ‘chem WO’, respectively. The TON or TOF values that are not listed in this table are unavailable in literature.

Mn complex	TON	TOF	Condition	References
62	-	0.04 min^{-1}	electrochem WO	[133]
63	-	0.05 min^{-1}	electrochem WO	[133]
64	9.2	0.11 min^{-1}	electrochem WO	[133]
65	-	-	chem WO w/m-CPBA	[134]
66	>50	0.67 s^{-1}	chem WO w/oxone	[139,143]
67	-	$13.9 \times 10^{-3} \text{ s}^{-1}$	chem WO w/oxone	[141]
68	-	$5.5 \times 10^{-3} \text{ s}^{-1}$	chem WO w/oxone	[142]
69	inactive	inactive	chem WO w/oxone	[141]
70	-	$9.9 \times 10^{-3} \text{ s}^{-1}$	chem WO w/oxone	[141]
71	-	$3.4 \times 10^{-3} \text{ s}^{-1}$	chem WO w/oxone	[141]

4.2. Iron Catalysts

The development of iron-based complexes for water oxidation started in 2010 when Bernhard and Collins and coworkers employed tetraanionic tetraamido macrocyclic ligands (TAML), given this ligand type was known to effectively stabilize high oxidation states of transition metals and were robust against oxidation [144]. Fe-TAMLs will catalyze the evolution of dioxygen from water; complex **72e** (Figure 7) exhibited the best catalytic activity with a TOF of 1.3 s^{-1} and a TON of 16 using CAN as an oxidant at pH 0.7 [144,145]. The catalytic activity of Fe-TAMLs increase from **72a** to **72e** (Figure 7), with complex **72a** the least stable showing no dioxygen evolution [145]. Another Fe-TAML complex (**73a**) with a methylamino bridging group (—NMe) was reported in 2014 by Dhar and coworkers with an improved TON of 220, whereas the TOF of the complex decreased to 0.67 s^{-1} with the photosensitizer $[\text{Ru}(\text{bipy})_3]^{2+}$ and $\text{Na}_2\text{S}_2\text{O}_8$ as the sacrificial oxidant [146]. This complex, **73a**, was found to catalyze WO driven under chemical conditions by CAN with a TON of 10 and a TOF of 0.03 s^{-1} ; the lower performance was ascribed to demetalation at pH 1. To improve the stability of Fe-TAMLs in acidic solution, a nitro group (—NO₂) was introduced to further optimize catalytic performance [146]. This modification to **73b** showed a slight improvement with a TON of 17 and a TOF of 0.06 s^{-1} compared to complex **73a** under chemical WO with Ce^{IV} as an oxidant. Under photochemical WO conditions, **73a** exhibited better activity than **73b** with a TON of 60 and a TOF of 0.21 s^{-1} . Supported by characterization data from techniques such as electron paramagnetic resonance (EPR),

ultraviolet–visible spectroscopy (UV-Vis), and high-resolution mass spectrometry (HRMS), it was proposed that a high-valent $\text{Fe}^{\text{V}}=\text{O}$ intermediate was generated during photochemical irradiation. Likewise, O–O bond formation was said to involve a nucleophilic attack by water at $\text{Fe}^{\text{V}}=\text{O}$ to generate a Fe^{III} -hydroperoxo intermediate, which then oxidized to release dioxygen and regenerate the original Fe^{III} -TAML aqua complex [146].

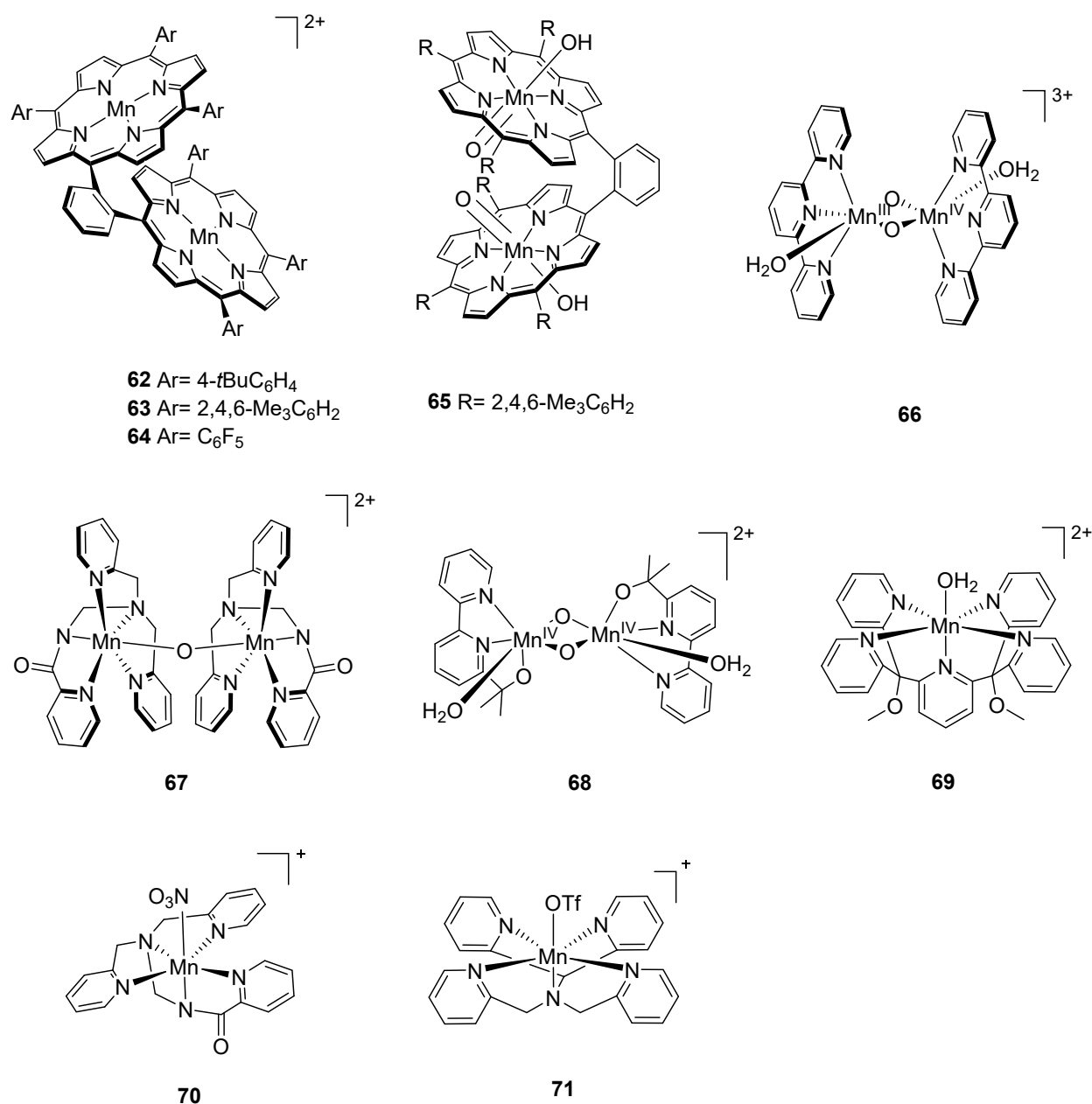


Figure 6. Chemical structures of selected manganese catalysts **62–71** for water oxidation: $[\text{Mn}_2(\mu\text{-}o\text{-xyl})(t\text{BuPP})_2]^{2+}$ (**62**, *t*BuPP = 5,10,15,20-tetrakis(4-*tert*-butylphenyl)-21*H*,23*H*-porphin) [133]; $[\text{Mn}_2(\mu\text{-}o\text{-xyl})(\text{TMP})_2]^{2+}$ (**63**, TMP = 5,10,15,20-tetrakis(2,4,6-trimethylphenyl)-21*H*,23*H*-porphin) [133]; $[\text{Mn}_2(\mu\text{-}o\text{-xyl})(\text{PFPP})_2]^{2+}$ (**64**, PFPP = 5,10,15,20-tetrakis(pentafluorophenyl)-21*H*,23*H*-porphin) [133]; $[\text{Mn}^{\text{V}}_2(\mu\text{-}o\text{-xyl})(\text{TMP})_2(\text{OH})_2(\text{O})_2]^{2+}$ (**65**, TMP = 5,10,15,20-tetrakis(2,4,6-trimethylphenyl)-21*H*,23*H*-porphin) [134]; $[\text{Mn}^{\text{III/IV}}_2(\mu\text{-O})_2(\text{terpy})_2(\text{H}_2\text{O})_2]^{3+}$ (**66**, terpy = 2,2':6',2''-terpyridine) [138,139]; $[\text{Mn}(\text{PaPy}_3)(\mu\text{-O})(\text{PaPy}_3)\text{Mn}]^{2+}$ (**67**, PaPy₃H = *N,N*-bis(2-pyridylmethyl)-amine-*N*-ethyl-2-pyridine-2-carboxamide) [141]; $[\text{Mn}^{\text{IV}}(\text{bipyalk})_2(\text{H}_2\text{O})_2(\mu\text{-O})_2]^{2+}$ (**68**, bipyalk = 2-([2,2'-bipyridin]-6-yl)propan-2-olate) [142]; $[\text{Mn}(\text{PY5})(\text{OH}_2)]^{2+}$ (**69**, PY5 = 2,6-bis(bis(2-pyridyl)methoxymethane)-pyridine) [141]; $[\text{Mn}(\text{PaPy}_3)(\text{NO}_3)]^+$ (**70**, PaPy₃H = *N,N*-bis(2-pyridylmethyl)-amine-*N*-ethyl-2-pyridine-2-carboxamide) [141]; $[\text{Mn}(\text{N4Py})\text{OTf}]^+$ (**71**, N4Py = *N,N*-bis(2-pyridyl-methyl)-*N*-bis(2-pyridyl)methylamine) [141].

A systematic study of iron complexes for water oxidation was reported by Lloret-Fillol and Costas et al. in 2011 [147]. Neutral tetradentate organic ligands were employed to form complexes **74–80** (Figure 7), and their catalytic performances are listed in Table 6. To compare other metals with the same Me₂Pytacn ligand (where, Me₂Pytacn = 1-(2'-pyridylmethyl)-4,7-dimethyl-1,4,7-triazacyclononane), complexes [M(OTf)₂(Me₂Pytacn)] (M = Ni, Co, Mn) were synthesized and it was found that these metal complexes were inactive for water oxidation, whereas complex **74**, featuring Fe, was highly active with a TON of 70 and a TOF of 0.12 s⁻¹ using CAN as the oxidant [147]. A structural feature shared among complexes **74–78** is that they exhibit two *cis* labile coordination sites, which could serve as a rationale in the design of iron-based catalysts for WO. In support of this, amongst complexes **74–80**, the latter two (**79** and **80**) are inactive; **79** features two *trans* labile ligands, and complex **80** has only one available (solvated) coordination site. An isotope labeling experiment involving complex **74** confirmed water (as opposed to NaIO₄) as the oxygen source for dioxygen and a kinetic study showed Fe^{IV}=O to be an intermediate (resting state) as characterized by UV-Vis and electrospray ionization mass spectrometry (ESI-MS). The mechanism was suggested to involve the oxidation of Fe^{IV}=O to form Fe^V=O, which undergoes attack by water to form Fe^{III}-hydroperoxide required for O–O bond formation. Fe^{III}-hydroperoxide will then undergo further oxidation by Ce^{IV} to form Fe^{IV}-hydroperoxide, which catalyzes the release of dioxygen [147]. DFT and time-dependent DFT calculations [148] were employed to study the catalytic cycle driven by Ce^{IV}. A more energetically favorable pathway was suggested by evoking the +IV oxidation state for all on-cycle intermediates. In 2014, Sun and coworkers explored 11 iron-based complexes, all of which featured 2 *cis* labile coordination sites. In addition, carboxylate or ethanolate moieties were incorporated into the design of iron-based catalysts although these modifications were not found to be as effective as similar designs for ruthenium-based catalysts for WO [149]. Dinuclear complexes structurally mimicking the 'blue dimer' (*vide supra*) were found to be inactive toward WO [149]. Only 2 complexes out of the 11 that were examined, **81** and **82**, catalyzed WO to generate dioxygen with a moderate catalytic performance, with a TOF of 0.1 s⁻¹ for complex **82** [149]. This study also ruled out the presence of nanoparticulate iron oxide in the system, which can be responsible for WO [149].

In 2015, two other aminopyridyl iron complexes, **83** and **84**, were reported by Costas and Lloret-Fillol and coworkers to be topological isomers that achieved TONs of 160 and 380, respectively, and TOFs of 0.16 s⁻¹ and 0.28 s⁻¹, respectively [150]. The mechanism of dioxygen evolution was proposed to involve an iron-oxo-cerium intermediate, O=Fe^{IV}–O–Ce^{IV}, which was characterized by UV-Vis, cryospray high-resolution mass spectrometry (CSI-HRMS), and resonance Raman spectroscopy [150]. A different mechanism based on the formation of an iron–oxo–cerium adduct was proposed for complex **83** in water oxidation, and this heteronuclear dinuclear species was experimentally characterized [150]. Two iron-based complexes, **85** and **86**, with different tetraazadentate ligands were reported by Thapper and coworkers in 2016 [151]. These two complexes leveraged a design wherein labile ligands are oriented in a *cis* conformation. Complexes **85** and **86** catalyze WO with TONs of 14 and 2 and TOFs of 0.18 s⁻¹ and 2 × 10⁻³ s⁻¹, respectively, using Ce^{IV} as oxidant [151].

Thummel et al. reported an interesting Fe^{III}(dpa) complex, **87**, with a square planar tetradentate polypyridyl ligand featuring two labile *trans* ligands that evolves dioxygen with a TOF of 0.23 s⁻¹ driven by Ce^{IV} [152]. Another two mononuclear polypyridyl iron-based complexes with the pyridine-2,6-diylbis[di(pyridin-2-yl)methanol] (Py5OH) ligand were developed by Thapper and coworkers in 2016 [153]. The only difference between complexes **88** and **89** is that the axial chloride ligand in **88** was replaced by a methanol ligand in **89**; both are catalytically active under acidic Ce^{IV}/[Ru(bipy)₃]³⁺-driven chemistry, however, their activity depends on specific conditions for WO. For instance, complex **88** exhibited better catalytic performance than complex **89** under *neutral* pH with [Ru(bipy)₃]³⁺ as an oxidant for WO (TOF of 2.2 s⁻¹ vs. 0.9 s⁻¹); however, the opposite results

were observed when *acidic* conditions were employed. Additionally, the axial chloride ligand played a role in stabilizing catalyst **88** relative to **89**, which degraded at a higher pH (10.5 vs. 9.5) [153]. Dynamic light scattering experiments were employed to examine the integrity of the complexes; no iron oxide (nano)particles were found in these systems, yet these particles were detected when the pH achieved ≥ 9 [153].

Complexes **79**, **81**, **90**, and **91** are representatives of iron catalysts containing secondary or tertiary amino ligands. The first two complexes were discussed earlier in this section. In 2015, Lau et al. reported that complex **90** with a cyclam ligand exhibited catalytic activity toward WO when NaIO_4 was used as oxidant, with TONs up to 1030 [154]. In the same year, Zhan and coworkers reported the first water-soluble iron-cyclen complex (**91**) for electrochemical WO with a TOF up to 65 s^{-1} [155]. However, the result from this study was proven to be incorrect due to the formation of iron oxide particulates, which were shown by Najafpour et al. to be responsible for WO [156].

Impressive progress in iron-based catalysts for water oxidation was made in 2016 when Kawata and Masaoka and coworkers reported that a penta-nuclear iron catalyst achieved a TON of 10^7 and a TOF of 1900 s^{-1} under electrochemical water oxidation [157]. Intramolecular O–O bond formation was proposed as the mechanism that involved two iron-oxo moieties [157]. The dinuclear iron complexes, **92–95**, have also been developed and examined. Complex **92**, reported in 2014 by Najafpour and coworkers, can catalyze water oxidation with a TOF of 0.72 s^{-1} in the presence of Ce^{IV} , whereas the catalytic activity of complex **93**, reported by Ding and Ma and coworkers, exhibited a TON of 2380 and a TOF of 2.2 s^{-1} using oxone as an oxidant [158,159]. Related bis(μ -O) complexes, **94** and **95**, were investigated for water oxidation. In the presence of Ce^{IV} , **94** showed reasonable activity with a TOF of 2.2 s^{-1} [152], while electrocatalytic water oxidation was achieved with complex **95** with a TOF of 1.2 s^{-1} [160].

4.3. Cobalt Catalysts

The study of cobalt-based catalysts for water oxidation started approximately a decade ago. The design of such catalysts has been challenging given that the (pre-)catalyst complexes are prone to degradation under harsh (oxidative) conditions and the substitutional lability of cobalt, particularly as Co^{3+} . When a cobalt-based complex degrades, the $\text{Co}^{2+}/^{3+}$ ion forms as the corresponding hydroxide (and/or oxide), which can efficiently catalyze water oxidation to release dioxygen. Numerous studies have claimed new cobalt-based molecular catalysts with impressive catalytic performances [161,162], but upon further investigation, cobalt oxide nanoparticles were shown to be the catalytically active species responsible for WO [163,164].

In 2010, Hill and coworkers reported a cobalt-based molecular catalyst, $[\text{Co}_4(\text{H}_2\text{O})_2(\text{PW}_9\text{O}_{34})_2]^{10-}$, with a polyoxometalate (POM) ligand (polytungstophosphate) for water oxidation with a TOF of >5 using $[\text{Ru}(\text{bipy})_3]^{3+}$ as an oxidant in sodium phosphate buffer at pH 8 [161]. In 2011, Hill and coworkers reported that the cobalt-POM, $[\text{Co}_4(\text{H}_2\text{O})_2(\text{PW}_9\text{O}_{34})_2]^{10-}$, was an efficient catalyst for photon-driven water oxidation with a TON of 224 using the photosensitizer $[\text{Ru}(\text{bipy})_3]^{2+}$, $\text{Na}_2\text{S}_2\text{O}_8$ as the sacrificial electron acceptor, and light [165]. However, a study on the cobalt-POM, $[\text{Co}_4(\text{H}_2\text{O})_2(\text{PW}_9\text{O}_{34})_2]^{10-}$, under electrochemical conditions revealed that degradation of the catalyst resulted in the formation of CoO_x , which was determined to be the real catalyst for WO [163]. The absorbance at 580 nm measured by UV-Vis spectroscopy decreased over a period of 3 h, which corresponded to the degradation of the catalyst and formation of CoO_x films (identified by UV-Vis, scanning electron microscopy (SEM), and energy-dispersive X-ray (EDX)). The activity of CoO_x was confirmed by observing similar catalytic activity from an electrode with deposited CoO_x films as compared to cobalt-POM. The film deposited on an electrode was rinsed prior to insertion into a solution of sodium phosphate buffer at pH 8 (without the cobalt-POM), and the catalytic performance by the controlled-potential electrolysis was similar to the cobalt-POM system [163].

Table 6. Selected catalytic parameters and experimental conditions for Fe catalysts 72–95 in water oxidation. Photochemical, electrochemical and chemical water oxidation are abbreviated as ‘photochem WO’, ‘electrochem WO’ and ‘chem WO’, respectively. Unless otherwise mentioned, chemical WO was carried out with CAN. The TON or TOF values that are not listed in this table are unavailable in literature. The irradiation wavelength for photochemical WO is in parentheses.

Fe Complex	TON	TOF (s ⁻¹)	Condition	References
72e	16	1.3	chem WO	[145]
73a	220	0.67	photochem WO (440 nm)	[146]
73b	60	0.21	photochem WO (440 nm)	[146]
74	70	0.12	chem WO	[147]
75a	360/1050	0.23/0.062	chem WO w CAN/NaIO ₄	[147]
75b	320	0.14	chem WO	[147]
76	63	0.046	chem WO	[147]
77	145	0.14	chem WO	[147]
78	40	0.015	chem WO	[147]
79	Inactive	Inactive	chem WO	[147]
80	Inactive	Inactive	chem WO	[147]
81	1.6	-	chem WO	[149]
82	65	0.1	chem WO	[149]
83	380	0.28	chem WO	[150]
84	5	6.9 × 10 ⁻³	chem WO	[150]
85	14	0.18	chem WO	[151]
86	2	2 × 10 ⁻³	chem WO	[151]
87	-	0.23	chem WO	[152]
88	5/26.5	0.53/2.2	chem WO w/CAN/[Ru(bipy) ₃] ³⁺	[153]
89	16/7	0.75/0.9	chem WO w/CAN/[Ru(bipy) ₃] ³⁺	[153]
90	1030	0.028	chem WO w/NaIO ₄	[154]
91	-	65	electrochem WO	[155]
92	<1	0.72	chem WO	[158]
93	2380	2.2	chem WO w/oxone	[159]
94	-	2.2	chem WO	[152]
95	-	1.2	electrochem WO	[160]

Inspired by the topology of the OEC of PSII (i.e., a tetranuclear manganese-calcium-oxo cluster, Mn₄CaO₅), several tetranuclear cobalt complexes for WO have been developed [143,166–168]. In 2011, Dismukes and coworkers reported a tetra-cobalt complex, [Co₄O₄(μ-OAc)₄(py)₄] (96), featuring a cuboidal Co₄O₄ core that was found to catalyze water oxidation by a light-driven process using [Ru(bipy)₃]²⁺ as the photosensitizer and Na₂S₂O₈ as the sacrificial electron acceptor (TON > 40 and TOF of 0.02 s⁻¹) [143] (Table 7). Scandola and coworkers also studied the photocatalytic activity of [Co₄O₄(μ-OAc)₄(py)₄] (96) and reported a quantum yield of 0.3 [167]. Following this work (in 2012), Sartorel and coworkers developed a series of isostructural tetra-cobalt complexes with *para*-substituted pyridine ligands [166]. Six complexes were generated (97a–97f) and screened under photochemical conditions, as described above, e.g., components of light, [Ru(bipy)₃]²⁺, and Na₂S₂O₈ [166]. These complexes have TONs of approximately 140, and amongst them, 97a has the largest electron transfer rate (2.51 × 10⁸ M⁻¹ s⁻¹) and the highest quantum efficiency (80%) [166]. The overpotential of these complexes varies in a narrow range of 0.50–0.57 V, indicating no apparent effect from the substitution on the pyridine [166]. Nocera and coworkers questioned the catalytic activity of these complexes with a report identifying a Co(II) impurity in Co₄O₄(OAc)₄(py-X)₄ as being responsible for the activity in water oxidation [169]. The study qualitatively and quantitatively suggested the presence of Co(II) by EPR, nuclear magnetic resonance (NMR) line broadening analysis, and electrochemical titration. The EPR spectrum of Co₄O₄(OAc)₄(py-COOMe)₄ that was purified by column chromatography does not show a broad line feature over the g = 10 to 2 range, whereas the spectrum of the crude material showed a broad signal over the same range [169] that was suggestive of Co(II) [170]. To quantitatively confirm the presence of a Co(II) species, a ³¹P

NMR line broadening analysis was employed to determine the concentration of Co^{2+} ions, which was on average 0.16 mM for a crude sample of 852 ppm [169]. Moreover, EDTA was used to titrate solutions of crude and purified $\text{Co}_4\text{O}_4(\text{OAc})_4(\text{py}-\text{COOMe})_4$; CV showed almost complete catalytic suppression of crude sample with EDTA, whereas the purified sample with EDTA exhibited CV wave reversibility [169].

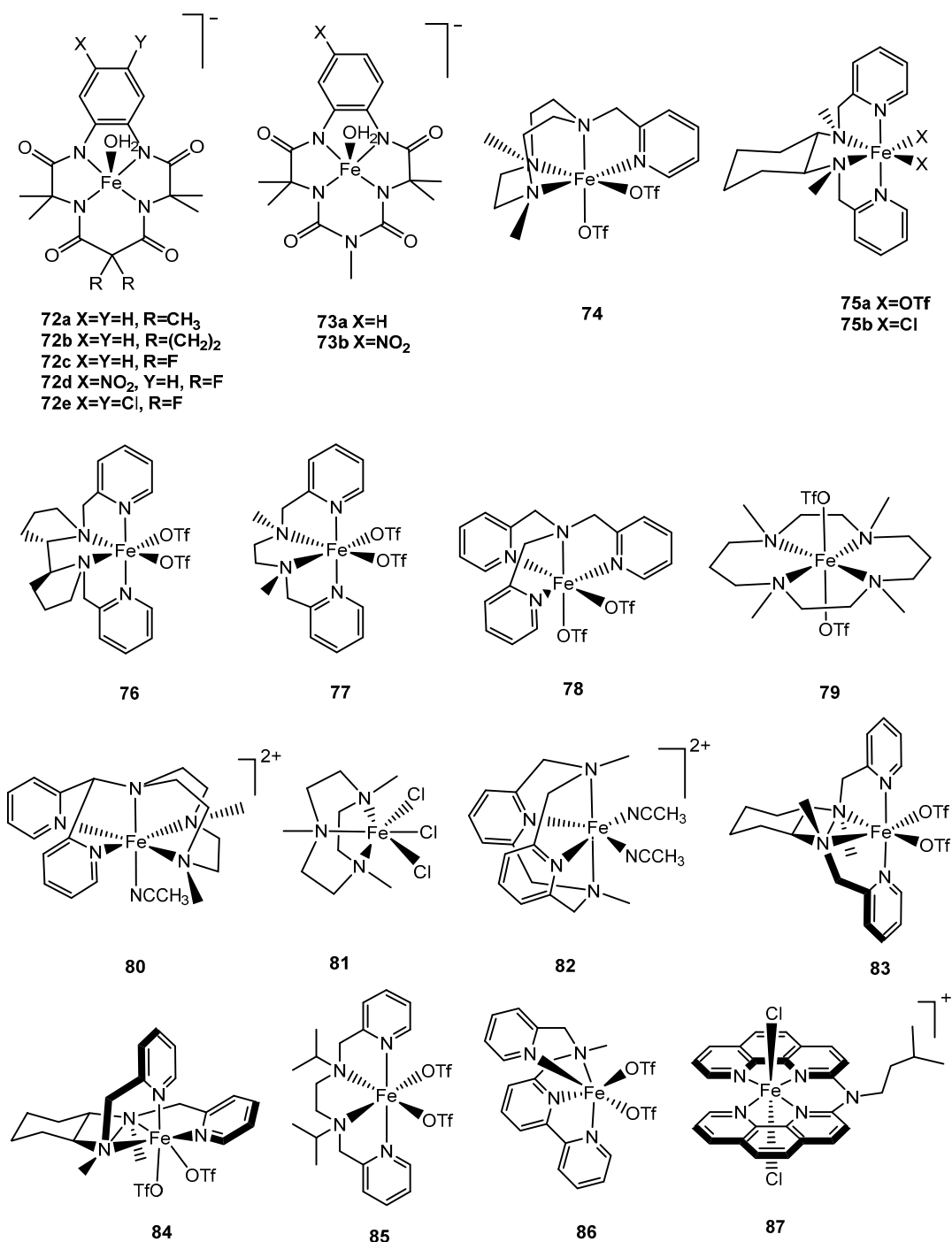


Figure 7. Cont.

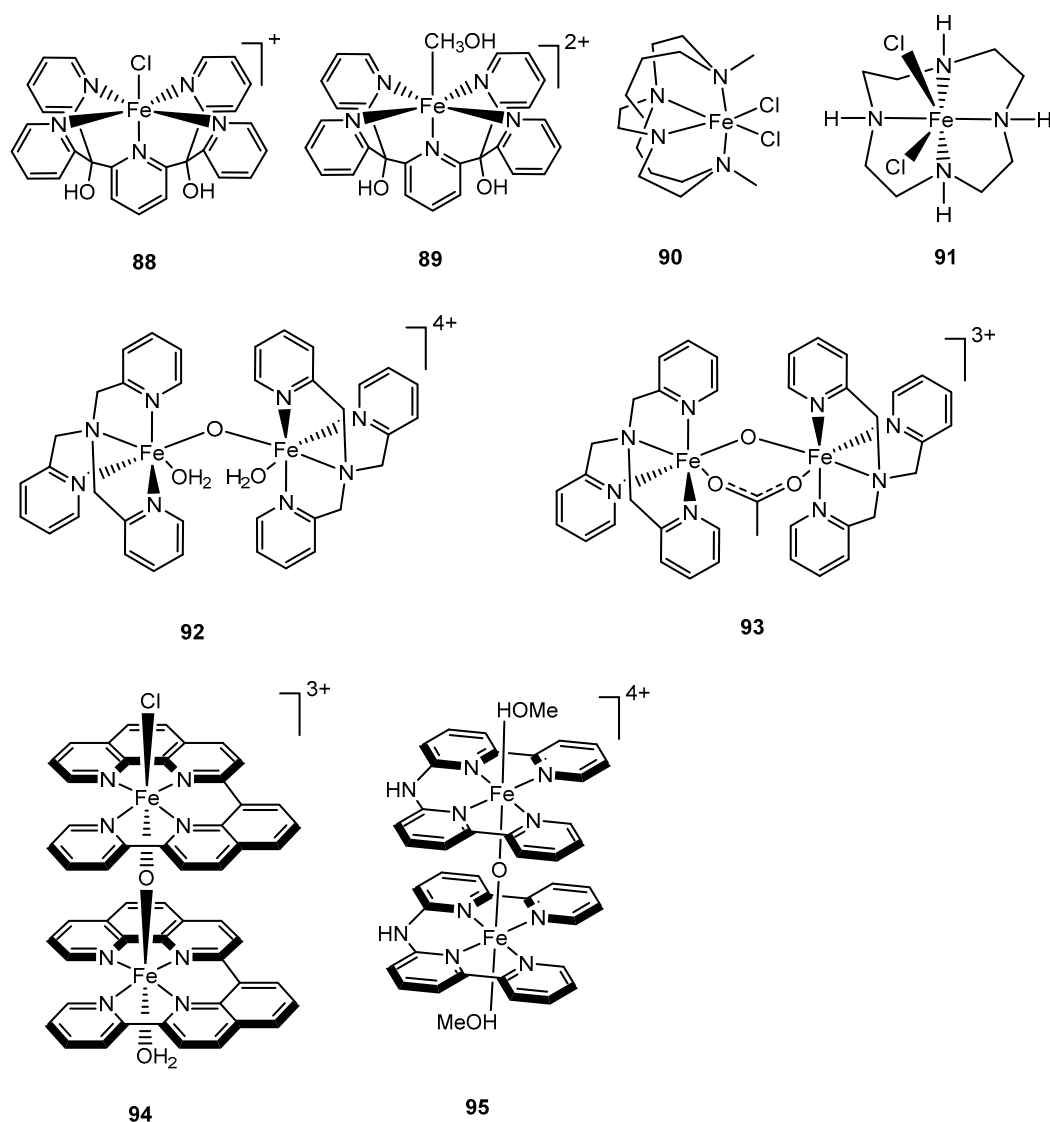


Figure 7. Selected iron complexes 72–95 for water oxidation: Fe-TAMLs (72a–72e, TAML = tetraanionic tetraamido macrocyclic ligands) [145]; Biuret-modified Fe-TAMLs (73a–73b, TAML = tetraanionic tetraamido macrocyclic ligands) [146]; [Fe(OTf)₂(Me₂Pytacn)] (74, Me₂Pytacn = 1-(2'-pyridylmethyl)-4,7-dimethyl-1,4,7-triazacyclononane) [147]; [Fe(OTf)₂(mcp)] (75a, OTf = CF₃SO₃[−], mcp = *N,N'*-dimethyl-*N,N'*-bis(2-pyridylmethyl)-cyclohexane-1,2-diamine) [147]; [Fe(Cl)₂(mcp)] (75b, mcp = *N,N'*-dimethyl-*N,N'*-bis(2-pyridylmethyl)-cyclohexane-1,2-diamine) [147]; [Fe(OTf)₂(bpbp)] (76, OTf = CF₃SO₃[−], bpbp = *N,N'*-bis(2-pyridylmethyl)-2,2'-bipyridine) [147]; [Fe(OTf)₂(mep)] (77, OTf = CF₃SO₃[−], mep = *N,N'*-dimethyl-*N,N'*-bis(2-pyridylmethyl)-ethane-1,2-diamine) [147]; [Fe(OTf)₂(tpa)] (78, OTf = CF₃SO₃[−], tpa = tris(2-pyridylmethyl)amine) [147]; [Fe(OTf)₂(tmc)] (79, OTf = CF₃SO₃[−], tmc = 1,4,8,11-tetra-methyl-1,4,8,11-tetraazacyclotetradecane) [147]; [Fe(NCCH₃)(L))(OTf)₂ (80, L = 1-(di-pyridin-2-yl-methyl)-4,7-dimethyl-1,4,7-triazonane) [147]; [Fe(Me₃tacn)(Cl)₃] (81, Me₃tacn = 1,4,7-trimethyltriazacyclononane) [149]; [Fe(L-N₄Me₂)(CH₃CN)₂]²⁺ (82, L-N₄Me₂ = *N,N'*-dimethyl-2,11-diaza[3.3](2,6)pyridinophane) [149]; [Fe(OTf)₂(mcp)] (topological isomers 83 and 84, OTf = CF₃SO₃[−], mcp = *N,N'*-dimethyl-*N,N'*-bis(2-pyridylmethyl)-cyclohexane-1,2-diamine) [150]; [Fe(L)(OTf)₂] (85, L = *N,N'*-diisopropyl-*N,N'*-bis(2-pyridylmethyl)-1,2-diaminoethane) [151]; [Fe(L)(OTf)₂] (86, L = *N*-methyl-*N*-(2-pyridylmethyl)-2,2'-bipyridine-6-methanamine) [151]; [Cl-Fe(dpa)-Cl]⁺ (87, dpa = bis-phenanthroline amine) [152]; [Fe(Py5OH)Cl]⁺ (88, Py5OH = pyridine-2,6-diylbis[di(pyridin-2-yl)methanol]) [153]; [Fe(Py5OH)(CH₃OH)]⁺ (89, Py5OH = pyridine-2,6-diylbis[di(pyridin-2-yl)methanol]) [153]; cis-[Fe(cbc)Cl₂]⁺ (90, cbc = 4,11-dimethyl-1,4,8,11-tetraazabicyclo[6.6.2]hexadecane) [154]; [Fe(cyclen)Cl₂] (91, cyclen = 1,4,7,10-tetraazacyclododecane) [155,156]; [Fe(tpa)₂(H₂O)₂(μ-O)]⁴⁺ (92, tpa = tris(2-pyridylmethyl)amine) [158]; [(tpa)₂Fe₂(μ-O)(μ-OAc)]³⁺ (93, tpa = tris(2-pyridylmethyl)amine) [159]; [(H₂O)-Fe(ppq)-(μ-O)-(ppq)-Fe-Cl]³⁺ (94, ppq = 2-(pyridin-2'-yl)-8-(1'',10'')-phenanthrolin-2''-ylquinoline) [152]; [Fe₂(Hbbpya)₂(MeOH)₂(μ-O)]⁴⁺ (95, Hbbpya = *N,N*-bis(2,2'-bipyrid-6-yl)amine) [160].

The dinuclear cobalt complex [(TPA)Co(μ -OH)(μ -O₂)Co(TPA)](ClO₄)₃ (where, TPA = tris(2-pyridylmethyl)amine) (**98**), developed by Thapper and coworkers in 2014, was shown to catalyze water oxidation both photo- and electrochemically; the former used [Ru(bipy)₃]²⁺ as a photosensitizer and Na₂S₂O₈ as a sacrificial electron acceptor with a TON of 58 and a TOF of 1.75 s⁻¹ [162]. Dynamic light scattering experiments were conducted to interrogate the molecular integrity of the complex during photocatalysis and no CoO_x particles were detected after 1 min illumination of a solution of the complex. Inspired by the report of photo-/electrochemical catalytic water oxidation by [(TPA)Co(μ -OH)(μ -O₂)Co(TPA)](ClO₄)₃, a structurally similar complex, Co^{III}₂(μ -OH)(μ -O₂)(BPMEN)₂](ClO₄)₃ (**99**) (where, BPMEN = *N,N'*-dimethyl-*N,N'*-bis(pyridin-2-ylmethyl)ethane-1,2-diamine), was synthesized in 2016 by Lu et al. [164]. This latter complex was found to be catalytically inactive based on cyclic voltammetry (CV) [164]. This result spurred the group to reinvestigate the catalytic activity of (**98**) and multiple characterization techniques were employed due to the difficulty in probing CoO_x particle measurements by dynamic light scattering under photochemical conditions [164]. The study suggested that titration of a chelating bipyridine (or EDTA) ligand in conjunction with transmission electron microscopy (TEM) may confirm the presence of (nano)particulate CoO_x [164].

In 2016, Fukuzumi et al. reported a dinuclear cobalt complex, [Co^{III}(TPA)(μ -OH)₂Co^{III}(TPA)]⁴⁺ (**100**) (where, TPA = tris(2-pyridylmethyl)amine), as a molecular catalyst for light-driven water oxidation using [Ru(bipy)₃]²⁺ and Na₂S₂O₈ [171]. The complex achieved a high quantum yield (44%) and a TON of 742 without forming CoO_x particles; the study employed NMR and dynamic light scattering to rule out the formation of nanoparticles [171]. During the period of photocatalytic activity under the same condition in a deuterated borate buffer, ¹H NMR spectra of the solution showed that the catalyst remained intact over 2 h, and dynamic light scattering did not support the formation or presence of nanoparticles. Chemical water oxidation with [Ru(bipy)₃]³⁺ as an oxidant was also carried out and dioxygen evolved with a TON of 4.3.

Another dinuclear cobalt complex was published recently with bridging μ -OH and μ -O₂ structural features [172]. Under photochemical water oxidation conditions with [Ru(bipy)₃]²⁺ and Na₂S₂O₈, the complex afforded dioxygen yield of 46.7%, however, this value plummeted to 9.6% when bipy was added as a chelating agent, and complete deactivation was observed with an elevated bipy concentration [172]. Upon the addition the chelating agent, it was observed that these cobalt polypyridyl complexes possessing a μ -OH/ μ -O₂ structural motif (**98**, **99**, and **101** in Figure 8) do not catalyze water oxidation [172].

An unusual cobalt-based water oxidation catalyst, **102**, with oligopyridine ligands was developed by Lau and coworkers in 2014 [173]. The complex is highly distorted from octahedral geometry and exhibits a double helical type structure by X-ray crystallography [173]. It was found to be active in chemical water oxidation with [Ru(bipy)₃]³⁺ as an oxidant (TON of 56 and a TOF of 1.9 s⁻¹) and photochemically active catalyst using [Ru(bipy)₃]²⁺ photosensitizer and Na₂S₂O₈ as a sacrificial electron acceptor (TON of 442) [173]. Dynamic light scattering was used during photocatalysis and no (nano)particles were observed. In addition, inductively coupled plasma atomic emission spectroscopy (ICP-AES) was used to measure supernatant cobalt content of a solution that was centrifuged post-photocatalysis, and the result showed that 98.1% of the total cobalt remained in solution. The titration of terpy (to scavenge free Co²⁺ ions) reduced oxygen evolution by around 10%, which was ascribed to the oxidation of the free terpy ligand [173]. Nocera and coworkers reported a cobalt complex (**103**) with aqua ligands positioned on each cobalt so as to investigate the mechanism of oxygen evolution reaction (OER) at the edge sites of cobaltate clusters; ¹⁸O-labeling experiments demonstrated the mechanism of the water oxidation by the complex involved intra-molecular coupling between edge-site oxygen atoms [174].

Berlinguette and Thapper and coworkers reported similar mononuclear Co(II) polypyridyl complexes in 2011 and 2015, respectively [175,176]. The difference between these two complexes (**104** and **105**) is primarily the axial ligand, which is an aqua ligand in **104** (a dicationic species) and chloride in complex **105** (a monocationic complex). Complex **104**,

$[\text{Co}(\text{PY5})(\text{OH}_2)]^{2+}$ (where, PY5 = 2,6-(bis(bis-2-pyridyl)-methoxymethane)pyridine), was found to electrochemically catalyze water oxidation over the pH range of 7.6 to 10.3 [175]. The CV of **104** showed two oxidation processes at 0.75 V (pH 2.2) and 1.43 V over the pH range of 7.6–10.3, respectively. The first oxidation process was related to the $[\text{Co}^{\text{III}}\text{-OH}]^{2+}/[\text{Co}^{\text{II}}\text{-OH}_2]^{2+}$ redox couple, while the second oxidation proposed the formation of a $[\text{Co}^{\text{IV}}\text{-OH}]^{3+}$ intermediate [175]. The formation of an O–O bond was suggested through the nucleophilic water attack on a Co(IV)-oxo species, which purportedly formed upon the deprotonation of a $[\text{Co}^{\text{IV}}\text{-OH}]^{3+}$ species [175]. The mechanism of water oxidation involving complex **104** was studied by DFT and was suggested to involve a $[\text{Co}^{\text{IV}}\text{-}\ddot{\text{O}}]^{2+}$ species which can be interpreted as a cobalt–oxene moiety $[\text{Co}^{\text{II}}\text{-}(\cdot\text{O}\cdot)]^{2+}$ [177]. This cobalt–oxene moiety was thought to have enhanced the radical character of oxygen, thereby promoting nucleophilic attack of hydroxide substrate on oxygen to form the O–O bond [177]. In consideration of the ‘oxo wall’ concept, established for late-transition-metal oxo complexes (Groups 9–11), high-valent metal oxo species are rare, unstable, and require careful examination for Co, Ni, and Cu when these species are claimed as intermediates in catalytic reactions [178]. Complex **105**, $[\text{Co}(\text{PY5OH})(\text{Cl})]^+$, was inspired by studies of complex **104** and features free hydroxy groups (in lieu of methoxy), which allows for further functionalization [175,176]. It was found to be active in chemical water oxidation (with $[\text{Ru}(\text{bipy})_3]^{3+}$ as an oxidant) with a TON of 15 and photochemically active (using $[\text{Ru}(\text{bipy})_3]^{2+}$ and $\text{Na}_2\text{S}_2\text{O}_8$) exhibiting a TON of 51 and a TOF of 1.3 s^{-1} . Incorporation of a chloride ligand in complex **105** is important considering improved observed catalytic activity relative to $[\text{Co}(\text{PY5OH})(\text{OH}_2)]^{2+}$ (axial aqua ligand replacing axial chloro in **105**), which exhibited lower catalytic activity (TON of 6.5 using $[\text{Ru}^{\text{III}}(\text{bipy})_3]^{3+}$ as chemical oxidant).

Wang and coworkers synthesized mononuclear cobalt complex **106** with an ester-functionalized (–COOMe) TPA ligand (TPA = tris(2-pyridylmethyl)amine); photo-induced catalysis showed a TON of 127.7 and a TOF of 3.8 s^{-1} using $[\text{Ru}(\text{bipy})_3]^{2+}$ and $\text{Na}_2\text{S}_2\text{O}_8$ [179]. In comparison, complex **107** with non-functionalized TPA showed reduced activity by roughly an order of magnitude (TON of 12.6 and TOF 0.3 s^{-1}); the high efficiency of complex **106** was attributed to the moderately more electron-withdrawing nature of COOMe-functionalized TPA (or steric considerations), thought to increase the stability of **106** by precluding self-oxidation and dimerization [179]. Interestingly, both complexes **106** and **107** have chloride ligands, which enhanced the catalytic activity relative to complex **104**.

Lau and coworkers reported the cobalt complex, **108**, with a quaterpyridyl backbone and axial aqua ligands. This complex was shown to be both chemically and photochemically active for WO displaying a TON of 160 and initial TOF of 4 s^{-1} with $[\text{Ru}(\text{bipy})_3]^{3+}$ as the oxidant, and a TON of 335 after irradiation at 457 nm for 1.5 h in the presence of photosensitizer $[\text{Ru}(\text{bipy})_3]^{2+}$ and sacrificial electron acceptor $\text{Na}_2\text{S}_2\text{O}_8$ [180]. The study by Lau et al. suggested that the actual mechanism is likely dependent on the stability of ligand-metal-oxo species, LM=O, vs. metal oxide (MO), and that a strongly chelating and oxidation-resistant ligand is more likely to support molecular LM=O for water oxidation. In the absence of such a ligand, LM=O is unstable with respect to the decomposition to MO, which is active as the real catalyst for water oxidation [180]. In 2012, Fukuzumi and coworkers reported a series of polyamino-based mononuclear cobalt complexes (**109–111**) and one Cp*-based cobalt complex with bipyridine shown as complex **112** [181]. Evidence has been presented to indicate that both **109** and **112** converted to nanoparticles under photocatalytic water oxidation conditions and that $\text{Co}(\text{OH})_x$ nanoparticles were responsible for the activity [181]. The catalytic activity of $\text{Co}(\text{NO}_3)_2$ as pre-catalyst was examined as a reference material to demonstrate the catalytic ability of complexes **109** to **112** and the yield of dioxygen evolved from water oxidation with these complexes increases in the order of $111 < 112 < 110 < \text{Co}(\text{NO}_3)_2 < 109$ [181].

In 2013, Sakai and coworkers reported a series of water-soluble porphyrin-based cobalt complexes **113a–113c** that photochemically catalyzed water oxidation using the photosensitizer, $[\text{Ru}(\text{bipy})_3]^{2+}$, and sacrificial electron acceptor $\text{Na}_2\text{S}_2\text{O}_8$ [182]. The TOF of **113c** was found to be dependent on the pH and the highest activity was achieved at

pH 11 with a TOF of 0.17 s^{-1} [182], and the TOF of **113c** can reach up to 0.62 s^{-1} with pH 9 [183]. Due to the reported observation of a second order dependence on catalyst concentration, the mechanism for water oxidation catalyzed by complexes **113a–113c** was proposed to involve radical coupling of two Co(III) or Co(IV) oxyl species [182]. Oxyl radical involvement was supported via DFT calculations, however, a Co(IV) or oxyl radical species was not observed in the EPR spectroscopy studies [182]. Modification to the porphyrin ligand at the *meso* position of complex **113c** yielded a fluorinated Co-porphyrin. Moreover, **113d** not only exhibited enhanced catalytic activity for water oxidation with a TON of 571 and a TOF of 1.1 s^{-1} , but also fundamentally changed the mechanism for water oxidation from oxyl–oxyl coupling for **113c** [182] to nucleophilic attack by water on Co(IV)=O species due to the observed first-order dependence on catalyst concentration for **113d** [184]. A similar enhancement of catalytic activity was observed for **113e** by the replacement of fluoride atoms with larger (blocking) chloride atoms.

Groves and coworkers also investigated porphyrin-based cobalt complexes for water oxidation and a representative of the type is cationic complex **114**, which electrochemically catalyzed water oxidation to dioxygen under neutral conditions (pH 7). Complex **114** was confirmed as the active molecular catalyst with much evidence; EDTA titration showed that cobalt ions were not released from the porphyrin during catalysis, and the analysis of the working electrode surface by energy dispersive X-ray spectroscopy showed no evidence of deposition [185]. In 2018, Najafpour and coworkers reported Co^{II}(phthalocyanine) (**115**) and Co^{II}(salen) (**116**). These complexes were screened for electrochemical catalytic water oxidation, and it was found that **116** was active at pH 11, whereas no dioxygen was observed for complex **115** [186]. High resolution visible spectra showed peaks at 410–430 nm and 680–740 nm that are characteristic of nanoparticles, which is indicative of the nanoparticulate nature of the real catalyst. Gross and coworkers reported a cobalt corrole complex, **117**, as electrochemically active for water oxidation [187].

4.4. Copper Catalysts

In 2012, Mayer and coworkers reported the first copper-based homogenous catalyst, [Cu(bipy)(OH)₂] (**118**) (Figure 9), for electrochemical water oxidation and showed a TOF of $\sim 100 \text{ s}^{-1}$ calculated by foot-of-wave analysis (FOWA) [189] (Table 8). The catalysis occurred at a high pH (11.8–12.3) and overpotential (750 mV), and the mechanism for the reaction was not probed. Subsequently, Meyer and coworkers reported another copper-based electrocatalyst, **119**, using a triglycylglycine macrocyclic ligand which catalyzed water oxidation with a TOF of 33 s^{-1} in phosphate buffer at pH 11; a copper–peroxo complex was established as a key intermediate for O–O bond formation in this mechanistic study [190]. Meyer and coworkers also reported an electrocatalytic variant, [Cu^{II}(Py₃P)] (**120**) (where, Py₃P = *N,N*-bis(2-(2-pyridyl)ethyl)pyridine-2,6-dicarboxamidate), for water oxidation at pH 8. It was suggested that O–O bond formation was facilitated by PCET, with electron transfer to the cathode coupled to proton migration involving HPO₄²⁻ [191].

In 2014, Lin and coworkers reported a copper complex, [(dhbp)Cu(OH)₂]₂ (**121**) (where, dhbp = 6,6'-dihydroxy-2,2'-bipyridine) that mimicked the function of the redox-active tyrosine residue, Y_Z, of PSII as a mediator in the electron transfer process [192]. The electrocatalytic complex, **121**, leveraged a non-innocent redox active ligand with pendant hydroxyl groups that likely participated in PCET so that the overpotential was 510 to 560 mV. Due to difficulties in the characterization of intermediates, the proposed intramolecular PCET process could not be determined experimentally [192]. In 2015, Llobet and coworkers reported a new family of copper catalysts, **122a–122d**, using derivatives of a tetraanionic tetradentate amidate ligand that reduced the overpotential to 170 mV by the tuning of the electronic structure in this series of Cu complexes [193].

Wei et al. reported a new type of copper-azo catalyst, **124**, for chemical water oxidation driven by Ce^{IV} with an initial TOF of 4.0 kPa h^{-1} . The proposed mechanism for O–O bond formation was the coupling of two Cu^{III}=O units [194]. Najafpour and coworkers reinvestigated the catalytic performance of **124**, under both chemical and electrochemical

conditions for water oxidation, and found no oxygen evolution in the presence of Ce^{IV} at $\text{pH} \sim 1$. The EDX results of a film formed on a fluorine-doped tin oxide (FTO) electrode after bulk electrolysis indicated low amounts of Cu that suggested decomposition of the catalyst. Combined with cyclic voltammetry (CV), which displayed an oxidation peak comparable to water oxidation mediated by CuO , it suggested that the true catalyst was a copper oxide film that was formed during the measurements [195].

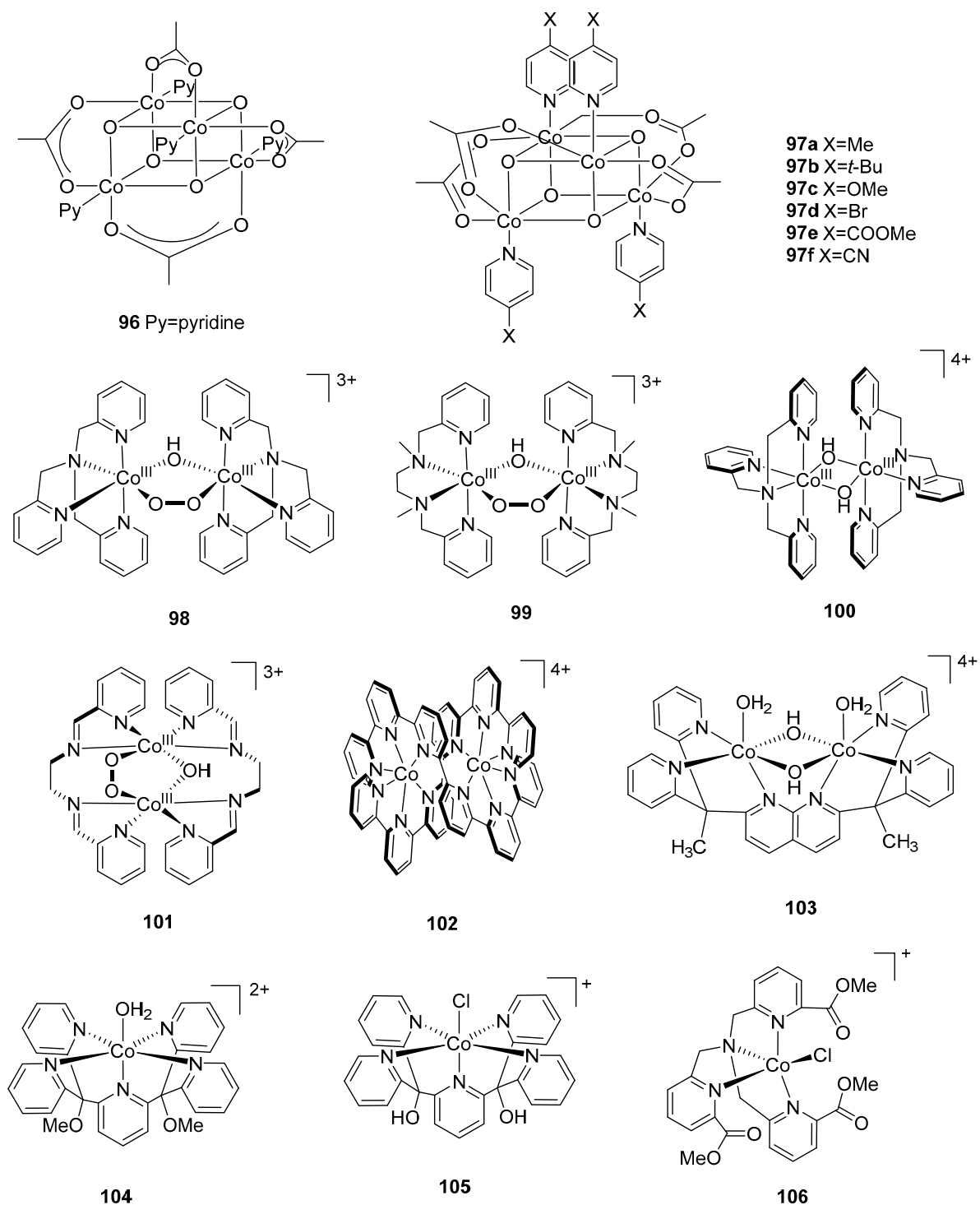


Figure 8. Cont.

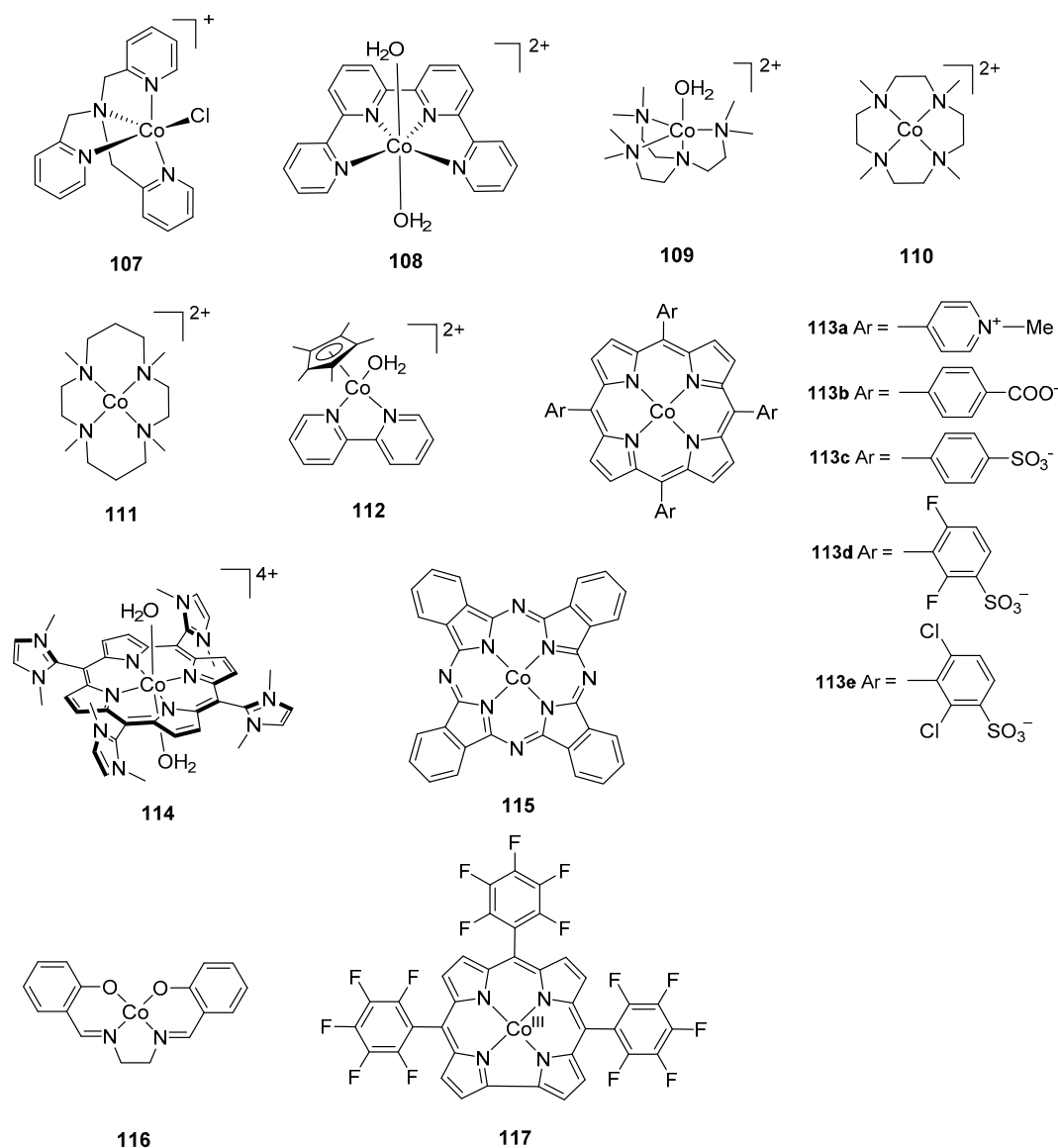


Figure 8. Selected cobalt complexes 96–117 for water oxidation: $[\text{Co}_4\text{O}_4(\mu\text{-OAc})_4(\text{py})_4]$ (96, py = pyridine) [143]; $[\text{Co}_4(\mu\text{-O})_4(\mu\text{-OAc})_4(p\text{-pyX})_4]$ (97a–97f, py = pyridine, X = Me, *t*-Bu, OMe, Br, COOMe, CN) [166]; $[(\text{TPA})\text{Co}(\mu\text{-OH})(\mu\text{-O}_2)\text{Co}(\text{TPA})]^{3+}$ (98, TPA = tris(2-pyridylmethyl)amine) [162]; $\text{Co}_2(\mu\text{-OH})(\mu\text{-O}_2)(\text{BPMEN})]^{3+}$ (99, BPMEN = *N,N'*-dimethyl-*N,N'*-bis(pyridin-2-ylmethyl)ethane-1,2-diamine) [164]; $[\text{Co}^{\text{III}}(\text{TPA})(\mu\text{-OH})_2\text{Co}^{\text{III}}(\text{TPA})]^{4+}$ (100, TPA = tris(2-pyridylmethyl)amine) [171]; $\mu\text{-OH}, \mu\text{-O}_2\text{-}\{(\text{enN}4)_2\text{Co}_2\}^{3+}$ (101, enN4 = 1,6-bis(2-pyridyl-2,5-diazaocta-2,6-diene) [172]; $[\text{Co}_2(\text{spy})_2]^{4+}$ (102, spy = 2,2':6',2'':6'',2''':6''',2''''':6''''',2''''':6''''',2''''''':6'''''''-sexipyridine) [173]; $[\text{Co}_2(\mu\text{-OH})_2(\text{H}_2\text{O})_2(\text{DPEN})]^{4+}$ (103, DPEN = dipyridylethane naphthyridine) [174]; $[\text{Co}(\text{PY}5)(\text{OH}_2)]^{2+}$ (104, PY5 = 2,6-bis(bis-2-pyridyl-methoxymethane)pyridine) [175]; $[\text{Co}(\text{Py}5\text{OH})\text{Cl}]^+$ (105, Py5OH = pyridine-2,6-diylbis(di-(pyridin-2-yl)methanol) [176]; $[\text{Co}(\text{COOMe-TPA})(\text{Cl})]^+$ (106, COOMe-TPA = tris[6-(methoxycarbonyl)-2-pyridylmethyl]amine) [179]; $[\text{Co}(\text{TPA})(\text{Cl})]^+$ (107, TPA = tris(2-pyridylmethyl)amine) [179]; $\text{trans-}[\text{Co}(\text{qpy})(\text{OH}_2)_2]^{2+}$ (108, qpy = 2,2':6',2'':6'',2''':6'''-quaterpyridine) [180]; $[\text{Co}(\text{Me}_6\text{tren})(\text{OH}_2)]^{2+}$ (109, Me₆tren = tris(*N,N,N'*-dimethylaminoethyl)amine) [181]; $[\text{Co}(12\text{-TMC})]^{2+}$ (110, 12-TMC = 1,4,7,10-tetramethyl-1,4,7,10-tetraazacyclododecane) [181]; $[\text{Co}(13\text{-TMC})]^{2+}$ (111, 13-TMC = 1,4,7,10-tetramethyl-1,4,7,10-tetraazacyclotridecane) [181]; $[\text{Co}(\text{Cp}^*)(\text{bipy})(\text{OH}_2)]^{2+}$ (112, Cp* = η^5 -pentamethylcyclopentadienyl, bipy = 2,2'-bipyridine) [181]; $[\text{CoTMPyP}]$ (113a, TMPyP = *meso*-tetra(4-*N*-methylpyridyl)porphyrinato) [182]; $[\text{CoTCPP}]$ (113b, TCPP = *meso*-tetra(4-carboxyphenyl)porphyrinato) [182]; $[\text{CoTPPS}]$ (113c, TPPS = *meso*-tetra(4-sulfonatophenyl)porphyrinato) [182]; $[\text{CoFPS}]$ (113d, FPS = 5,10,15,20-tetra(2,6-difluoro-3-sulfophenyl)porphyrin) [183,184]; $[\text{CoCIPS}]$ (113e, CIPS = 5,10,15,20-tetra(2,6-dichloro-3-sulfophenyl)porphyrin) [183]; $[\text{TMDImPCo}(\text{OH}_2)_2]^{4+}$ (114, TMDImP = 5,10,15,20-tetrakis-(1,3-dimethylimidazolium-2-yl)porphyrin) [185]; $[\text{CoP}]$ (115, P = phthalocyanine) [186]; $[\text{CoSALEN}]$ (116, SALEN = *N,N'*-bis(salicylidene)ethylenediamino) [186]; $[\text{Co}(\text{tpfc})]$ (117, tpfc = 5,10,15-tris(pentafluorophenyl)corrole) [187].

Table 7. Selected catalytic parameters and experimental conditions for Co catalysts **96–117** for water oxidation. Photochemical, electrochemical, and chemical water oxidation are abbreviated as ‘photochem WO’, ‘electrochem WO’, and ‘chem WO’, respectively. The TON or TOF values that are not listed in this table are unavailable in literature. Irradiation wavelength for photochemical WO is in parentheses.

Co Complex	TON	TOF (s ⁻¹)	Condition	References
Co-POM	1000	>5	chem WO w/[Ru(bipy) ₃] ³⁺	[161]
Co-POM	224	-	photochem WO (420–470 nm)	[165]
Co-POM	-	-	electrochem WO	[163]
[Co ₄ (H ₂ O) ₂ (VW ₉ O ₃₄) ₂] ¹⁰⁻	~35	>1000	photochem WO (455 nm)	[188]
96	>40	0.02	photochem WO (510 nm)	[143]
97	140	-	photochem WO (>400 nm)	[166]
98	58	1.75	photochem WO (470 ± 10 nm)	[162]
99	inactive	inactive	electrochem WO	[164]
100	742/4.3	-	photochem WO (420 nm), chem WO w/CAN/[Ru(bipy) ₃] ³⁺	[171]
101	inactive	inactive	photochem WO (≥420 nm)	[172]
102	56	1.9	chem WO w/[Ru(bipy) ₃] ³⁺	[173]
103	-	-	-	[174]
104	-	79	electrochem WO	[175]
105	51	1.3	photochem WO (470 ± 10 nm)	[176]
106	127.7	3.8	photochem WO (470 ± 10 nm)	[179]
107	12.6	0.3	photochem WO (470 ± 10 nm)	[179]
108	160	4	chem WO w/[Ru(bipy) ₃] ³⁺	[180]
109 *	54	-	photochem WO (>420 nm)	[181]
110	16	-	photochem WO (>420 nm)	[181]
111	41	-	photochem WO (>420 nm)	[181]
112 *	29	-	photochem WO (>420 nm)	[181]
113a	88.7	0.118	photochem WO (400–800 nm)	[182]
113b	103.4	0.138	photochem WO (400–800 nm)	[182]
113c	301	0.62	photochem WO (430–510 nm)	[182,183]
113d	571	1.1	photochem WO (430–510 nm)	[183,184]
113e	836	1.7	photochem WO (430–510 nm)	[183]
114	-	1400	electrochem WO	[185]
115	-	-	electrochem WO	[186]
116	-	-	electrochem WO	[186]
117	-	0.2	electrochem WO	[187]

* Co(OH)_x nanoparticles were responsible for activity.

In 2015, inspired by the amino acid ligands of the catalyst, **119**, Pap and Szyrwił and coworkers incorporated branched peptides in two copper-based catalysts, **125** and **126**, for electrocatalytic water oxidation with a TOF of 53 s⁻¹ and 24 s⁻¹, respectively, at pH 11 [196]. No deposition of Cu was observed by X-ray photoelectron spectroscopy (XPS) before and after controlled-potential electrolysis (CPE), and no dioxygen was evolved during CPE when the (rinsed) indium tin oxide (ITO) electrode was transferred to fresh phosphate buffer, which implied that the catalysts were molecular [196]. In 2017, Brudvig, Crabtree and coworkers reported a robust molecular copper-based electrocatalyst, [Cu(pyalk)₂] (**127**) (where, pyalk = 2-pyridyl-2-propanoate), for water oxidation with an overpotential of 520–580 mV under basic conditions at pH > 10.4 [197]. This catalyst incorporated an oxidation resistant and strongly electron donating alkoxide ligand, which allowed water oxidation at relatively low overpotential. In 2017, Warren and coworkers reported a copper catalyst, [Cu(pimH)(H₂O)₂]²⁺ (**128**) (where, pimH = 2-(2'-pyridyl)-imidazole), that was active at significantly reduced overpotential of ~300 mV, due in large part to the use of strongly basic conditions (pH 12) and deprotonation of the coordinated 2-(2'-pyridyl)-imidazole ligand. A TOF of 35 s⁻¹ was reported for this catalyst [198].

In 2017, Sun and coworkers investigated the difference in electrocatalytic performance of two similar copper complexes; the diamine–dipyridine (**129**) and the diimine–dipyridine (**130**) complexes [199]. Complex **130** showed a lower overpotential of 700 mV and a higher

TOF of 50.4 s^{-1} relative to complex **129**, with an overpotential of 1070 mV and a TOF of 13.5 s^{-1} [199]. Moreover, CPE results showed that **130** displayed better stability than **129**, which was possibly due to the fact that the degradation of the C=N bonds in the ligand of **130** was avoided [199]. The author attributed the difference of catalytic activity between **129** and **130** to the conjugate effect and the type of the coordinating N atom of the ligand in molecular catalysts [199]. The study highlighted a possibility of the simultaneous enhancement of the activity, decrease in the overpotential, and improvement of the stability of molecular catalysts through fine tuning the ligand structures. Sun and coworkers also reported two copper complexes (**131** and **132**) bearing amine-pyridine ligands for electrochemical water oxidation, which displayed TOFs of 13.1 s^{-1} and 18.7 s^{-1} with overpotentials of 440 mV and 570 mV, respectively, at pH 11.5 [200].

Cao and Lai et al. reported a copper catalyst, **133**, that incorporated a dianionic tridentate ligand, with a carbonate group in the equatorial plane, that electrochemically catalyzed water oxidation at pH 10 with an observed overpotential of 650 mV [201]. Computational studies indicated that the HCO_3^- group functioned as an intra-molecular base (assisted in proton removal from water) and facilitated O–O bond formation when the purported oxo radical intermediate $[\text{LCu}^{\text{III}}-\text{O}^{\bullet-}]$ experienced water nucleophilic attack [201]. In 2018, inspired by the cuboidal Mn_4CaO_5 cluster in the OEC of PSII, Wu and coworkers reported the first set of copper–cubane complexes (**134a**, **134b**) as effective electrocatalysts for water oxidation with TOFs of 267 s^{-1} and 105 s^{-1} at 1.70 V and 1.56 V, respectively. The EDX, XPS, and electrochemical studies excluded the formation of a film during catalysis and in situ EPR and Raman spectroscopy measurements indicated high-valent Cu^{III} and $\text{Cu}^{\text{III}}\text{O}^{\bullet}$ as intermediates in the catalytic cycle [202].

Catalyst **135** was reported by Sakai and coworkers and was found to follow second-order kinetics that suggested a bimolecular radical coupling mechanism was at play [203]. Meanwhile, Najafpour and coworkers reinvestigated stabilities and activities of copper complexes **135–138** comparing them to a copper(II) salt, i.e., copper(II) sulfate pentahydrate. The copper(II) salt was found to have the highest activity for water oxidation among **135–138** from linear sweep voltammetry (LSV) and CV [204]. Catalyst **135**, **136** and **138** are stable at pH 11, except catalyst **137**, which decomposed to form Cu^{2+} ions during long-term amperometry suggesting copper ions are the true catalyst for water oxidation [204]. This explained why catalyst **137** displayed better activity than the rest of molecular catalysts examined (**135**, **136**, **138**) [204]. In 2019, Cao and coworkers reported a copper-porphyrin complex, **139**, which catalyzed water oxidation electrochemically with a TOF of 30 s^{-1} and a low overpotential of 310 mV at neutral pH conditions [205]. Moreover, it can catalyze water oxidation to hydrogen peroxide in acidic conditions at pH 3 [205]. In 2020, Zhang, Verpoort and coworkers reported a copper-based electrocatalyst, $[\text{Cu}(\text{TCA})_2]$ (**140**) (where, HTCA = 1-mesityl-1H-1,2,3-triazole-4-carboxylic acid), that displayed first-order kinetics and a single-site mechanism was implied [206].

Catalyst **140** displayed activity at a low potential of 290 mV and good stability by maintenance of current density at 1.0 mAcm^{-2} for more than 15 h at 2.0 V under neutral pH conditions [206]. Interestingly, the tuning of the aryl ligands did not affect the onset potential for water oxidation, whereas modification of the triazole moiety significantly influenced the overpotential of the catalyst [206]. While mononuclear copper complexes are dominant, there is one example of a dinuclear copper complex for water oxidation. In 2015, Zhang and coworkers reported a dinuclear copper complex, **123**, as a catalyst for electrochemical water oxidation with an overpotential of 800 mV. DFT calculations of transition states and intermediates suggested that an intra-molecular direct coupling was most likely involved in O–O bond formation [207]. Meyerstein et al. reported a copper-based electrochemical catalyst with carbonate as a non-innocent ligand for water oxidation [208]. The study highlighted that carbonate can stabilize high-valent transition metal cations.

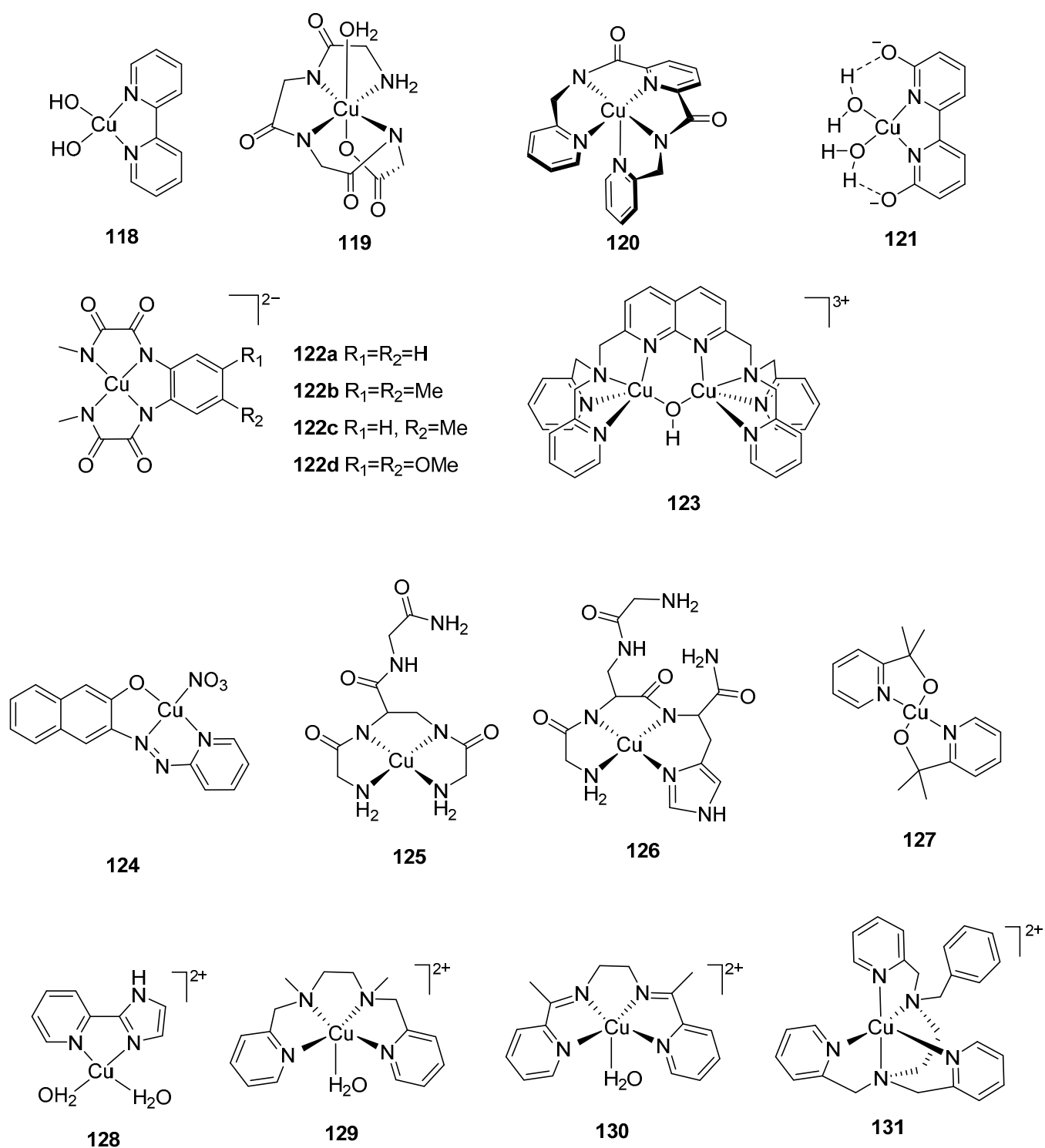


Figure 9. Cont.

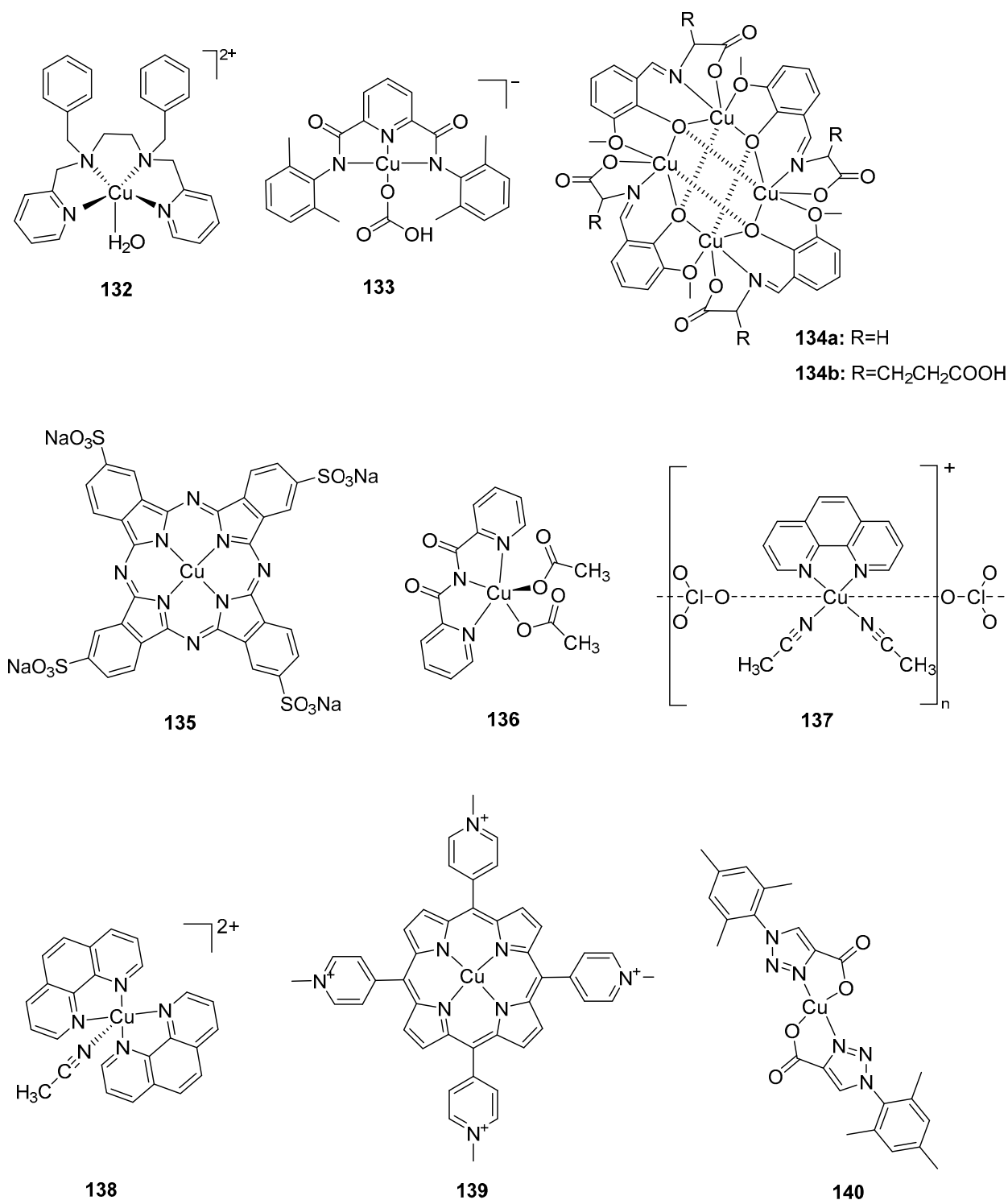


Figure 9. Selected copper complexes **118–140** for water oxidation: [Cu(bipy)(OH)₂] (**118**, bipy = 2,2'-bipyridine) [189]; [(TGG)Cu-OH₂]²⁻ (**119**, TGG = triglycylglycine macrocyclic ligand) [190]; [Cu(Py₃P)] (**120**, Py₃P = *N,N*-bis[2-(2-pyridyl)ethyl]pyridine-2,6-dicarboxamidate) [191]; [(dhbp)Cu(OH)₂] (**121**, dhbp = 6,6'-dihydroxy-2,2'-bipyridine) [192]; [CuL1]²⁻ (**122a**, L1 = *N*-methyl-*N'*-[2-(methylaminoxalyl-amino)-phenyl]-oxalamide) [193]; [CuL2]²⁻ (**122b**, L2 = *N*-[4,5-dimethyl-2-(methylaminoxalyl-amino)-phenyl]-*N'*-methyl-oxalamide) [193]; [CuL3]²⁻ (**122c**, L3 = *N*-[4,5-dimethoxy-2-(methylaminoxalyl-amino)-phenyl]-*N'*-methyl-oxalamide) [193]; [CuL4]²⁻ (**122d**, L4 = *N*-[4-methoxy-2-(methylaminoxalyl-amino)-phenyl]-*N'*-methyl-oxalamide) [193]; [Cu₂(BPMAN)(μ-OH)]³⁺ (**123**, BPMAN = 2,7-[bis(2-pyridylmethyl)aminomethyl]-1,8-naphthyridine) [207]; [(L)Cu(NO₃)] (**124**, L = (*E*)-3-(pyridin-2-yl-diazanyl)naphthalen-2-ol) [194]; [CuH₂3G(OH₂)] (**125**, 3G = H-Gly-Dap(H-Gly)-Gly-NH₂, Gly = glycine, Dap = L-2,3-diaminopropionic acid,

the axial aqua ligands in the chemical structure are omitted for clarity) [196]; [CuH₂G(OH₂)] (**126**, 2G = H-Gly-Dap(H-Gly)-His-NH₂, Gly = glycine, His = histine, Dap = L-2,3-diaminopropionic acid, the axial aqua ligands in the chemical structure are omitted for clarity) [196]; [Cu(pyalk)₂] (**127**, pyalk = 2-pyridyl-2-propanoate) [197]; [Cu(pimH)(H₂O)₂]²⁺ (**128**, pimH = 2-(2'-pyridyl)-imidazole) [198]; [(L1)Cu(OH₂)]²⁺ (**129**, L1 = *N,N'*-di-methyl-*N,N'*-bis(pyridin-2-ylmethyl)-1,2-diaminoethane) [199]; [(L2)Cu(OH₂)]²⁺ (**130**, L2 = 2,7-bis(2-pyridyl)-3,6-diaza-2,6-octadiene) [199]; [(bztpen)Cu]²⁺ (**131**, bztpen = *N*-benzyl-*N,N',N'*-tris(pyridin-2-ylmethyl)ethylenediamine) [200]; [(dbzbpn)Cu(OH₂)]²⁺ (**132**, dbzbpn = *N,N'*-dibenzyl-*N,N'*-bis(pyridin-2-ylmethyl)ethylenediamine) [200]; [L-Cu-CO₃H]⁻ (**133**, L = *N,N'*-2,6-dimethylphenyl-2,6-pyridinedicarboxamidate) [201]; [(L_{Gly}-Cu)₄] (**134a**, L_{Gly} = 3-methoxy-salicylidene-glycine) [202]; [(L_{Glu}-Cu)₄] (**134b**, L_{Glu} = 3-methoxy-salicylidene-glutamic acid) [202]; [CuP-(SO₃)₄] (**135**, P-(NaSO₃)₄ = phthalocyanine-3,4',4'',4'''-tetrasulfonic acid tetrasodium) [203,204]; [Cu(tptz)(H₂O)(CH₃COO)₂] (**136**, tptz = 2,4,6-tris(2-pyridyl)-s-triazine) [204]; Cu(phen)(CH₃CN)₂(ClO₄)₂ (**137**, phen = phenanthrene) [204]; Cu(phen)₂(CH₃CN)(ClO₄)₂ (**138**, phen = phenanthrene) [204]; [Cu(PorphPyMe)]⁴⁺ (**139**, PorphPyMe = *meso*-tetrakis(4-*N*-methylpyridyl)porphyrin) [205]; [Cu(TCA)₂] (**140**, TCA = 1-mesityl-1H-1,2,3-triazole-4-carboxylate) [206].

Table 8. Selected catalytic parameters and experimental conditions for Cu catalysts **118–140** for water oxidation. Electrochemical photochemical and chemical water oxidation are abbreviated as ‘electrochem WO’, ‘photochem WO’, and ‘chem WO’, respectively. The TOF values that are not listed in this table are unavailable in literature. Irradiation wavelength for photochemical WO is in parentheses.

Cu Complex	TON	TOF	Condition	References
118	-	100 s ⁻¹	electrochem WO	[189]
119	13	33 s ⁻¹	electrochem WO	[190]
120	19	38 s ⁻¹	electrochem WO	[191]
121	~400 *	0.4 s ⁻¹	electrochem WO	[192]
122a	-	3.56 s ⁻¹	electrochem WO	[193]
122b	-	3.58 s ⁻¹	electrochem WO	[193]
122c	-	0.43 s ⁻¹	electrochem WO	[193]
122d	-	0.16 s ⁻¹	electrochem WO	[193]
123	-	0.6 s ⁻¹	electrochem WO	[207]
124	-	4.0 kPa h ⁻¹	chem WO	[194]
125	-	53 s ⁻¹	electrochem WO	[196]
126	-	24 s ⁻¹	electrochem WO	[196]
127	30	0.6 s ⁻¹	electrochem WO	[197]
128	-	35 s ⁻¹	electrochem WO	[198]
129	-	13.5 s ⁻¹	electrochem WO	[199]
130	-	50.4 s ⁻¹	electrochem WO	[199]
131	-	13.1 s ⁻¹	electrochem WO	[200]
132	-	18.7 s ⁻¹	electrochem WO	[200]
133	-	20.1 s ⁻¹	electrochem WO	[201]
134a	-	267 s ⁻¹	electrochem WO	[202]
134b	-	105 s ⁻¹	electrochem WO	[202]
135	26	0.063 s ⁻¹	photochem (400–800 nm)	[203]
136	-	-	electrochem WO	[204]
137	-	-	electrochem WO	[204]
138	-	-	electrochem WO	[204]
139	-	30 s ⁻¹	electrochem WO	[205]
140	-	0.6 s ⁻¹	electrochem WO	[206]

* The turnover number is ~1 based on [CuL] in solution, however, the TON is estimated to be 400 based on the [CuL] involved in electrolysis.

4.5. Nickel Catalysts

The first homogenous nickel-based catalyst was not reported until 2014 when Ke, Lu and coworkers introduced a macrocyclic nickel(II) complex, [Ni(*meso*-L)](ClO₄)₂ (**141**) (where, L = 5,5,7,12,12,14-hexamethyl-1,4,8,11-tetraazacyclotetradecane), that electrochemically catalyzed water oxidation with a low overpotential of 170 mV at neutral pH. Interest-

ingly, complex **141** (Figure 10) also served as an electrocatalyst for hydrogen production by water reduction [209]. Multiple characterization techniques, such as, SEM, EDX and dynamic light scattering (DLS), were employed to verify that complex **141** was a stable active homogenous catalyst. Additionally, X-ray analysis indicated that the catalyst remained intact after being recovered from controlled electrolysis.

Complex **142** was said to be in an equilibrium with complex **141** in an aqueous solution and participated in PCET to form the intermediate, $[(\text{meso-L})(\text{H}_2\text{O})\text{Ni}^{\text{IV}}=\text{O}]^{2+}$ or $[(\text{meso-L})(\text{H}_2\text{O})\text{Ni}^{\text{III}}-\text{O}^\bullet]^{2+}$, to engender O–O bond formation. Kinetic studies showed first-order dependence on the concentration of the nickel complex, and three possible mechanisms were proposed for O–O bond formation, which included HO–OH coupling, water nucleophilic attack, and O–H insertion (Figure 11). However, DFT calculations suggested that among three possible Ni^{IV} isomeric intermediates, a triplet *cis* Ni intermediate, $[\text{Ni}^{\text{III}}-\text{OH}-\text{HO}^\bullet]^{2+}$, experienced the least energy Gibbs free energy ($\Delta G^\ddagger = 24.6 \text{ kcal mol}^{-1}$) for O–O bond formation via an HO–HO coupling mechanism [209]. Therefore, an HO–OH coupling mechanism from the triplet *cis* Ni intermediate was the preferred pathway for O–O bond formation.

Complex **141** displayed relatively low catalytic performance with a TON of 15 (Table 9), which may have been due to the conformational change during catalysis from an inactive *trans*-isomer to the active *cis*-isomer. Recall, in a study involving an iron-based molecular catalyst for water oxidation, Costa and coworkers indicated the importance of two *cis* labile coordination sites is a key structural feature for catalysis [147]. Thus, Lu et al. hypothesized that design of a six-coordinate Ni^{II} complex with two *cis* labile sites to facilitate the HO–OH coupling, would improve catalytic performance. In 2016, a Ni^{II} complex, **143**, possessing two *cis* labile sites for electrocatalytic water oxidation was reported by Lu et al., and the catalyst was found to be less efficient than complex **141**, which suggested that more Ni^{II} complexes need to be investigated to understand the structure-performance relationship [210]. This study also revealed that base (acetate buffer) played a role in facilitating the formation of a key intermediate and aided in atom-proton transfer (APT) for O–O bond formation. No catalytic activity was observed when complex **143** was in phosphate buffer due to occupation of two *cis* labile sites by bidentate HPO_4^{2-} , whereas complex **143** displayed catalytic activity in acetate buffer [210]. The acetate buffer not only aided in generation of a peroxide intermediate, $[\text{Ni}^{\text{II}} \text{L}(\text{OOH})]^{2+}$, formed through intramolecular O–O coupling, but it also acted as a proton acceptor to lower the barrier to O–O bond formation [210]. Meyer and coworkers had reported that the addition of base could enhance the rate in a catalytic water oxidation with a Ru complex, $[\text{Ru}(\text{bda})(\text{isq})_2]$ (where, bda = 2,2'-bipyridine-6,6'-dicarboxylate and isq = isoquinoline) [211]. Similar findings were observed with the complex, Co-porphyrin, where the base played multiple roles in the catalytic cycle [185]. In this case, the sodium phosphate buffer (Na-Pi) was reported to: (1) act as a proton acceptor for the conversion of $\text{Co}^{\text{III}}-\text{OH}$ to $\text{Co}^{\text{IV}}-\text{O}$ intermediate, (2) act as a base to deprotonate water coupled with the rate-limiting O–O bond formation step, and (3) inhibit catalytic water oxidation activity at high buffer concentrations [185]. In addition, Meyerstein et al. used carbonate and phosphate buffer to investigate their role in electrochemical water oxidation catalyzed by $\text{Ni}^{\text{IV}}(\text{meso-L})\text{X}_2$ (L = 1,4,8,11-tetraazacyclotetradecane; X = CO_3^{2-} or PO_4^{3-}) [212]. The study highlighted the role of carbonate in stabilizing $\text{Ni}^{\text{III}}\text{L}$ (L = 1,4,8,11-tetraazacyclotetradecane) and engaging in the redox process as a non-innocent ligand [212].

Lu and coworkers investigated the role of buffer in a homogeneous electrocatalytic system involving complex **144** that exhibited a moderate overpotential of ~480 mV in phosphate buffer at neutral pH. The electrocatalysis results indicated a dual role of HPO_4^{2-} as a proton acceptor to facilitate PCET and as an inhibitor for electrolysis by replacing *cis* labile sites with HPO_4^{2-} [213]. Based on the catalytic activity of copper complexes with polypeptide ligands [190,196], a nickel-glycine electrocatalyst was reported by Allen and coworkers with an overpotential of 475 mV in phosphate buffer at pH 11. However, further electrochemical studies suggested that the formation of nickel oxide was responsible for

catalysis, and XPS confirmed the presence of a nickel hydroxide film [214]. Ni-POM was reported as a homogeneous catalyst for photochemical water oxidation in 2012 by Hill and coworkers [215] and by Wang and coworkers in 2015 [216]. The pentanickel silicotungstate complex, $K_{10}H_2[Ni_5(OH)_6(OH_2)_3(Si_2W_{18}O_{66})] \cdot 34H_2O$, with photosensitizer $[Ru(bipy)_3]^{2+}$ and $Na_2S_2O_8$ as a sacrificial electron acceptor in sodium borate buffer at pH 8, revealed that the complex can catalyze photo-driven water oxidation with a TON of 60 and a TOF of $\sim 0.18 s^{-1}$. Various techniques, such as UV-Vis, infrared spectroscopy (IR), and DLS, were employed to demonstrate the stability of the complex in buffered solution; the integrity of the complex remained for one month [215].

The Ni-POMs, including $Na_{24}[Ni_{12}(OH)_9(CO_3)_3(PO_4)(SiW_9O_{34})_3] \cdot 56H_2O$, $Na_{25}[Ni_{13}(H_2O)_3(OH)_9(PO_4)_4(SiW_9O_{34})_3] \cdot 50H_2O$, and $Na_{50}[Ni_{25}(H_2O)_2(OH)_{18}(CO_3)_2(PO_4)_6(SiW_9O_{34})_6] \cdot 85H_2O$, that were reported by Wang and coworkers had much higher TONs of 128.2, 147.6, and 204.5, respectively, for photochemical water oxidation with the photosensitizer $[Ru(bipy)_3]^{2+}$ and $Na_2S_2O_8$ as a sacrificial electron acceptor in sodium borate buffer (pH 9). No Ni-POM has been reported as an electrocatalyst for water oxidation. In 2015, Cao and coworkers reported a nickel porphyrin complex, **145**, as a molecular electrocatalyst for water oxidation in phosphate buffer solution at pH 7 with a TOF of $0.67 s^{-1}$. Based on DFT calculations and electrochemical studies, WNA of $[Por-Ni^{III}-O^\bullet]^{4+}$ was proposed as the mechanism for O–O bond formation [217]. Careful examination excluded the possibility of NiO_x formation, which is highly active for water oxidation [217]. Sun and coworkers reported a homogenous pre-electrocatalyst, $[Ni^{II}PY5Cl](ClO_4)$ (**146**) (where, PY5 = 2,6-bis(1,1-bis(2-pyridyl)ethyl)pyridine), for water oxidation in phosphate buffer at pH 10.8 with a TON of 19 and a TOF of ~ 145 [218]. A crystallographic study on the complex after bulk electrolysis revealed that the bound chloride was substituted by water molecule, suggesting that the real catalyst was $[Ni^{II}PY5(H_2O)]^{2+}$. The phosphate in the buffer is thought to accept a proton from the water molecule that attacks the proposed $Ni^V=O$ intermediate, facilitating the atom-proton transfer (APT) for O–O bond formation.

In 2017, Lu, Ke and coworkers investigated the steric effect on nickel complexes with a macrocyclic ligand reminiscent of complex **141** by studying two nickel complexes, **147** and **148**, with four or six methyl groups, respectively [219]. The results showed that $[Ni(Me_8L)](ClO_4)_2$ (**148**) was more active in electrocatalysis than $[Ni(Me_6L)](ClO_4)_2$ (**141**) which outperformed $[Ni(Me_4L)](ClO_4)_2$ (**147**), suggesting that the steric repulsion between methyl groups and phosphate anions bound axially to the in situ formed Ni^{III} can affect catalytic activity. Bruner et al. reported that a nickel phenolate complex, **149**, can catalyze water oxidation electrochemically under neutral conditions with a TOF of $0.15 s^{-1}$ [220]. Ding and coworkers reported a homogeneous nickel complex (**150a**) bearing an *o*-phenylenebis(*N'*-methyloxamidate) ligand for electrochemical water oxidation with a TOF of $0.4 s^{-1}$ in phosphate buffer at pH 11 [221]. Two other complexes, investigated by Ding and coworkers, that share a similar structure to **150a** but have the functional groups with nitrogen atoms replaced by one or two carboxyl groups displayed instability and decomposed to form NiO_x [221]. This suggested that nitrogen functional groups are more beneficial than carboxyl groups to stabilize nickel-based homogeneous catalysts. Llobet and coworkers further investigated the electronic effects on the catalytic activity by modification of the *o*-phenylene moiety of complex **150a** to generate complexes **150b** and **150c**. The introduction of electro-donating groups on the phenyl ring in **150b** and **150c** decreased the overpotential to ~ 170 and 220 mV, respectively.

The study also demonstrated that **150b** shared similar reversible behavior in the first redox wave as complex **150a**, however, **150c** displayed a prominent decrease in the reduction wave, suggesting the presence of deactivation [222]. In 2019, Verpoort and coworkers reported the first Ni–NHC complex (**151**) for homogeneous electrochemical water oxidation catalysis in sodium acetate buffer (NaOAc) and sodium phosphate buffer (Na–Pi) at pH 7 and pH 9 [223]. The study also demonstrated improved catalyst activity in the phosphate buffer with an overpotential of 800 mV at pH 9, and the complete loss of activity in the acetate buffer, which highlighted the recent finding on the role

of phosphate ions as a proton acceptor to enhance catalytic activity in PCET [223]. In 2020, Sun and coworkers reported a homogeneous Ni-TAML complex (**152**) (where TAML is a redox-active ligand) for electrochemical water oxidation with a TOF of 0.32 s^{-1} in neutral phosphate buffer with an overpotential of 680 mV [224]. The mechanistic study proposed the generation of $[\text{Ni}^{\text{III}}(\text{TAML}^{2-})-\text{O}^\bullet]$ attacked by a water molecule for O-O bond formation indicating a base-assisted APT process [224].

Table 9. Selected catalytic parameters and experimental conditions for nickel catalysts **141**–**152** for water oxidation. Electrochemical and photochemical water oxidation are abbreviated as ‘electrochem WO’ and ‘photochem WO’, respectively. The TON or TOF values that are not listed in this table are unavailable in literature. Irradiation wavelength for photochemical WO is in parentheses.

Ni Complex	TON	TOF (s^{-1})	Condition	Reference
141	15	-	electrochem WO	[209]
142	15	-	electrochem WO	[209]
143	-	-	electrochem WO	[210]
144	-	0.19	electrochem WO	[213]
$\text{K}_{10}\text{H}_2[\text{Ni}_5(\text{OH})_6(\text{OH}_2)_3(\text{Si}_2\text{W}_{18}\text{O}_{66})] \cdot 34\text{H}_2\text{O}$	60	0.18	photochem WO (455 nm)	[215,216]
145	-	0.67	electrochem WO	[217]
146	19	~145	electrochem WO	[218]
147	3.6	-	electrochem WO	[219]
148	15.2	-	electrochem WO	[219]
149	-	0.15	electrochem WO	[220]
150a	3.81	0.4	electrochem WO	[221,222]
150b	-	-	electrochem WO	[222]
150c	-	-	electrochem WO	[222]
151	-	-	electrochem WO	[223]
152	-	0.32	electrochem WO	[224]

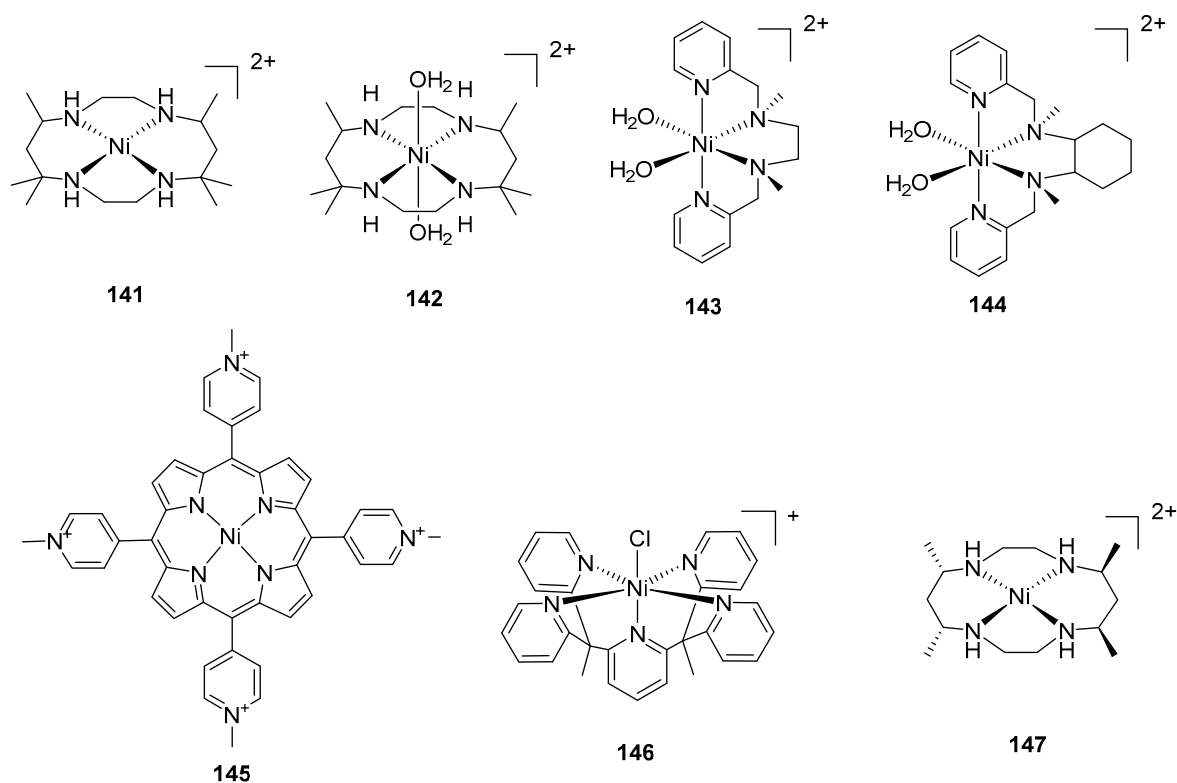


Figure 10. Cont.

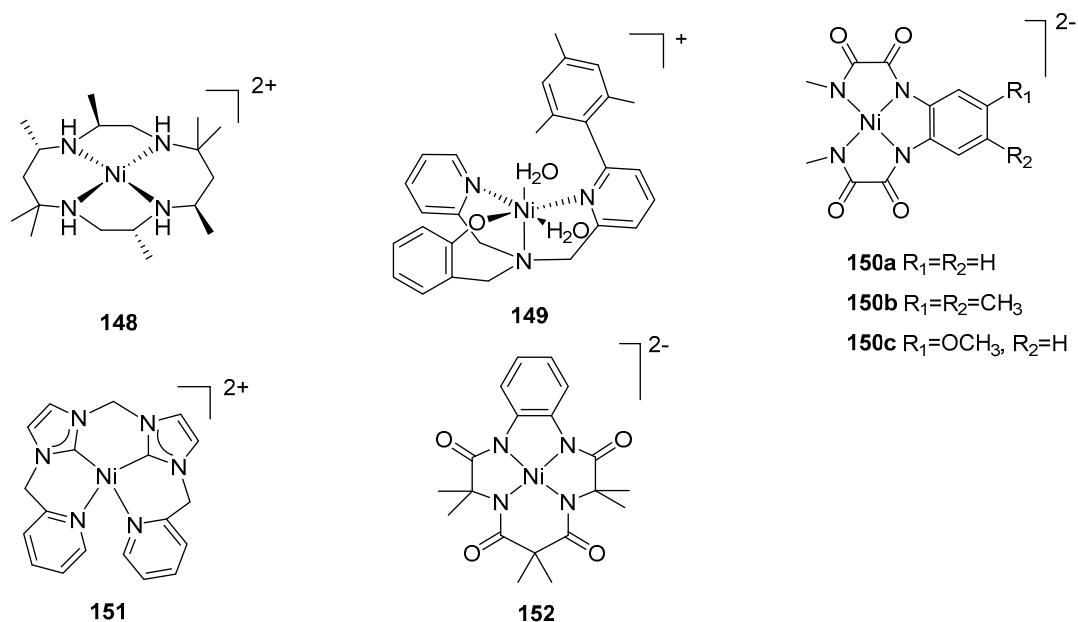


Figure 10. Selected cobalt complexes 141–152 for water oxidation: $[\text{Ni}(\text{meso-L})]^{2+}$ (141, L = 5,5,7,12,12,14 hexamethyl-1,4,8,11-tetraazacyclotetradecane) [209]; $[\text{Ni}(\text{meso-L})(\text{H}_2\text{O})_2]^{2+}$ (142, L = 5,5,7,12,12,14 hexamethyl-1,4,8,11-tetraazacyclotetradecane) [209]; $[\text{NiL}(\text{H}_2\text{O})_2]^{2+}$, (143, L = *N,N'*-dimethyl-*N,N'*-bis(pyridin-2-ylmethyl)-1,2-diaminoethane) [210]; $[\text{Ni}(\text{mcp})(\text{H}_2\text{O})_2]^{2+}$ (144, mcp = (1*R*,2*R*)-*N*¹,*N*²-dimethyl-*N*¹,*N*²-bis(pyridin-2-ylmethyl)cyclohexane) [213]; $[\text{Ni}(\text{PorphPyMe})]^{4+}$ (145, PorphPyMe = *meso*-tetrakis(4-*N*-methylpyridyl)porphyrin) [217]; $[\text{Ni}(\text{PY5})\text{Cl}]^+$ (146, PY5 = 2,6-bis(1,1-bis(2-pyridyl)ethyl)pyridine) [218]; $[\text{Ni}(\text{Me}_4\text{L})]^{2+}$ (147, Me₄L = (5*S*,7*R*,12*R*,14*S*)-5,7,12,14-tetramethyl-1,4,8,11-tetraazacyclotetradecane) [219]; $[\text{Ni}(\text{Me}_8\text{L})]^{2+}$ (148, Me₈L = (2*S*,7*R*,9*R*,14*S*)-2,5,5,7,9,12,12,14-octamethyl-1,4,8,11-tetraazacyclotetradecane) [219]; $[\text{NiL}(\text{H}_2\text{O})]^+$ (149, L = {2-[(6-mesitylpyridin-2-yl)(pyridin-2-ylmethyl)amino]methyl}phenol)) [220]; $[\text{NiL}]^{2-}$ (150a, L = *o*-phenylenebis(oxamidate)) [222]; $[\text{NiL}]^{2-}$ (150b, L = 4,5-dimethyl-1,2-phenylenebis(oxamidate)) [222]; $[\text{NiL}]^{2-}$ (150c, L = 4-methoxy-1,2-phenylenebis(oxamidate)) [222]; $[\text{NiL}]^{2+}$ (151, L = bis(2-pyridyl)-methylimidazolylidene)methane) [223]; $[\text{Ni}(\text{TAML})]^{2-}$ (152, TAML = tetraanionic tetradentate amidate) [224].

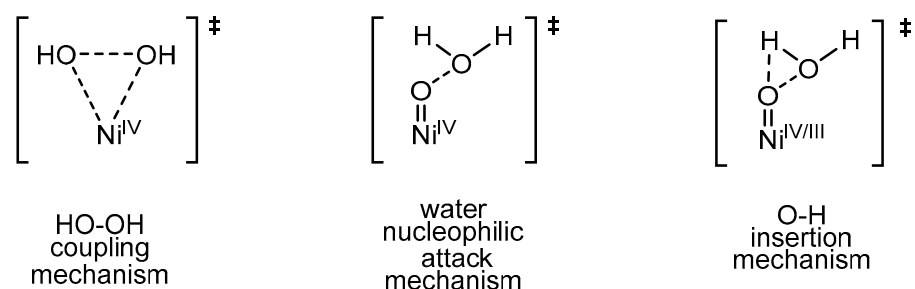


Figure 11. Three proposed transition states for O–O bond formation.

5. Conclusions

The development of molecular catalysts for water oxidation has experienced rapid progress over the past two decades, especially ruthenium (4d metal-based) catalysts. The design principles that were employed for ruthenium-based catalysts are being applied in the development of molecular catalysts based on first-row (3d) metals, including Mn, Fe, Co, Cu, and Ni, as well as iridium (a 5d) metal. The development of efficient and robust molecular catalysts based on the first-row metals is challenging. This is due, in part, to the fact that 4d metals (ruthenium) can bind a ligand backbone better as compared to first-row (3d) metals due to larger atomic radii, which allows for a stronger interaction (overlap) between the central metal ion and its ligands and a reduction in the repulsion between all coordinated ligands. In contrast, the first-row metals, Mn, Fe, Co, Cu, and

Ni, are generally substitutionally labile, which indicates that the ligands coordinated to the metals can undergo ligand exchange (with solvent), thus limiting the development of water oxidation catalysts based on these metals. Additionally, an added complication is the decomposition of the first-row metal catalysts to corresponding oxides and/or hydroxides that are also catalytically active for water oxidation. This can interfere with quantitative measurements of the catalytic activity of molecular catalysts of the first-row transition metals. Although the current catalytic performance of molecular catalysts based on the first-row transition metals is moderate, it remains promising and is a worthwhile endeavor given their abundance and economic feasibility.

Author Contributions: Conceptualization, P.J.B.J. and K.V.L.; investigation, D.X. and J.G.; resources, P.J.B.J. and K.V.L.; writing—original draft preparation, D.X. and J.G.; writing—review and editing, P.J.B.J. and K.V.L.; supervision, P.J.B.J. and K.V.L.; project administration, P.J.B.J. and K.V.L. All authors have read and agreed to the published version of the manuscript.

Funding: This research received no external funding.

Data Availability Statement: No original data available from authors.

Conflicts of Interest: The authors declare no conflict of interest.

Abbreviations

WO	water oxidation
OEC	oxygen-evolving complex
PSII	photosystem II
XFEL	femtosecond X-ray free electron lasers
PCET	proton-coupled electron transfer
NHE	normal hydrogen electrode
TON	turnover number
TOF	turnover frequency
WOC	water oxidation complex
CAN or Ce ^{IV}	cerium ammonium nitrate [Ce(NO ₃) ₆][(NH ₄) ₂]
WNA	water nucleophilic attack
ITO	indium tin oxide
I2M	interaction between two metal units or intermolecular bimolecular mechanism
EDG	electron-donating group
EWG	electron-withdrawing group
DFT	density functional theory
FOWA	foot-of-wave analysis
FAME ligands	flexible, adaptive, multidentate and equatorial
Nano ITO	tin-doped indium oxide nanoparticles
CSI-HRMS	cryospray high-resolution mass spectrometry
ESI-MS	electrospray ionization mass spectrometry
NHC	N-heterocyclic carbene
m-CPBA	m-chloroperbenzoic acid
POM	polyoxometalate
UV-Vis	ultraviolet–visible spectroscopy
SEM	scanning electron microscopy
EDX	energy-dispersive X-ray
EPR	electron paramagnetic resonance
NMR	nuclear magnetic resonance
CV	cyclic voltammetry
EDTA	ethylenediaminetetraacetic acid
TEM	transmission electron microscopy
ICP-AES	inductively coupled plasma atomic emission spectroscopy
XRD	X-ray diffraction
MO	metal oxide

DLS	dynamic light scattering
OER	oxygen evolution reaction
Yz	tyrosine
EDX	energy-dispersive X-ray
FTO	fluorine-doped tin oxide
XPS	X-ray photoelectron spectroscopy
CPE	controlled-potential electrolysis
IR	infrared spectroscopy
Na-Pi	sodium phosphate buffer
APT	atom-proton transfer

References

- Barber, J. Photosynthetic energy conversion: Natural and artificial. *Chem. Soc. Rev.* **2009**, *38*, 185–196. [[CrossRef](#)]
- Junge, W. Oxygenic photosynthesis: History, status and perspective. *Q. Rev. Biophys.* **2019**, *52*, 35. [[CrossRef](#)]
- Lubitz, W.; Chrysina, M.; Cox, N. Water oxidation in photosystem II. *Photosynth. Res.* **2019**, *142*, 105–125. [[CrossRef](#)]
- Matheu, R.; Garrido-Barros, P.; Gil-Sepulcre, M.; Ertem, M.Z.; Sala, X.; Gimbert-Suriñach, C.; Llobet, A. The development of molecular water oxidation catalysts. *Nat. Rev. Chem.* **2019**, *3*, 331–341. [[CrossRef](#)]
- Barber, J. Photosystem II: An enzyme of global significance. *Biochem. Soc. Trans.* **2006**, *34*, 619–631. [[CrossRef](#)]
- Vinyard, D.J.; Ananyev, G.M.; Charles Dismukes, G. Photosystem II: The reaction center of oxygenic photosynthesis. *Annu. Rev. Biochem.* **2013**, *82*, 577–606. [[CrossRef](#)]
- Blakemore, J.D.; Crabtree, R.H.; Brudvig, G.W. Molecular catalysts for water oxidation. *Chem. Rev.* **2015**, *115*, 12974–13005. [[CrossRef](#)]
- McEvoy, J.P.; Brudvig, G.W. Water-Splitting chemistry of photosystem II. *Chem. Rev.* **2006**, *106*, 4455–4483. [[CrossRef](#)]
- Sproviero, E.M.; Gascón, J.A.; McEvoy, J.P.; Brudvig, G.W.; Batista, V.S. Computational studies of the O₂-evolving complex of photosystem II and biomimetic oxomanganese complexes. *Coord. Chem. Rev.* **2008**, *252*, 395–415. [[CrossRef](#)]
- Umena, Y.; Kawakami, K.; Shen, J.-R.; Kamiya, N. Crystal structure of oxygen-evolving photosystem II at a resolution of 1.9 Å. *Nature* **2011**, *473*, 55–60. [[CrossRef](#)]
- Kawakami, K.; Umena, Y.; Kamiya, N.; Shen, J.-R. Structure of the catalytic, inorganic core of oxygen-evolving photosystem II at 1.9 Å resolution. *J. Photochem. Photobiol. B Biol.* **2011**, *104*, 9–18. [[CrossRef](#)]
- Shen, J.-R. The structure of photosystem II and the mechanism of water oxidation in photosynthesis. *Annu. Rev. Plant Biol.* **2015**, *66*, 23–48. [[CrossRef](#)] [[PubMed](#)]
- Najafpour, M.M.; Zaharieva, I.; Zand, Z.; Maedeh Hosseini, S.; Kouzmanova, M.; Holyńska, M.; Tranca, I.; Larkum, A.W.; Shen, J.-R.; Allakhverdiev, S.I. Water-oxidizing complex in photosystem II: Its structure and relation to manganese-oxide based catalysts. *Coord. Chem. Rev.* **2020**, *409*, 213183. [[CrossRef](#)]
- Suga, M.; Akita, F.; Hirata, K.; Ueno, G.; Murakami, H.; Nakajima, Y.; Shimizu, T.; Yamashita, K.; Yamamoto, M.; Ago, H.; et al. Native structure of photosystem II at 1.95 Å resolution viewed by femtosecond X-ray pulses. *Nature* **2015**, *517*, 99–103. [[CrossRef](#)]
- Kern, J.; Alonso-Mori, R.; Tran, R.; Hattne, J.; Gildea, R.J.; Echols, N.; Glockner, C.; Hellmich, J.; Laksmono, H.; Sierra, R.G.; et al. Simultaneous femtosecond x-ray spectroscopy and diffraction of photosystem II at room temperature. *Science* **2013**, *340*, 491–495. [[CrossRef](#)]
- Kern, J.; Tran, R.; Alonso-Mori, R.; Koroidov, S.; Echols, N.; Hattne, J.; Ibrahim, M.; Gul, S.; Laksmono, H.; Sierra, R.G.; et al. Taking snapshots of photosynthetic water oxidation using femtosecond x-ray diffraction and spectroscopy. *Nat. Commun.* **2014**, *5*, 1–11. [[CrossRef](#)]
- Suga, M.; Shimada, A.; Akita, F.; Shen, J.-R.; Tosha, T.; Sugimoto, H. Time-resolved studies of metalloproteins using x-ray free electron laser radiation at SACLA. *Biochim. Biophys. Acta-Gen. Subj.* **2020**, *1864*, 129466. [[CrossRef](#)]
- Milikisiyants, S.; Chatterjee, R.; Coates, C.S.; Koua, F.H.M.; Shen, J.-R.; Lakshmi, K.V. The structure and activation of substrate water molecules in the S₂ state of photosystem II studied by hyperfine sublevel correlation spectroscopy. *Energy Environ. Sci.* **2012**, *5*, 7747. [[CrossRef](#)]
- Yang, K.R.; Lakshmi, K.V.; Brudvig, G.W.; Batista, V.S. Is deprotonation of the oxygen-evolving complex of photosystem II during the S₁ → S₂ transition suppressed by proton quantum delocalization? *J. Am. Chem. Soc.* **2021**, *143*, 8324–8332. [[CrossRef](#)]
- Askerka, M.; Brudvig, G.W.; Batista, V.S. The O₂-evolving complex of photosystem II: Recent insights from quantum mechanics/molecular mechanics (QM/MM), extended x-ray absorption fine structure (EXAFS), and femtosecond x-ray crystallography data. *Acc. Chem. Res.* **2017**, *50*, 41–48. [[CrossRef](#)]
- Kok, B.; Forbush, B.; McGloin, M. Cooperation of charges in photosynthetic O₂ evolution-I. A linear four step mechanism. *Photochem. Photobiol.* **1970**, *11*, 457–475. [[CrossRef](#)] [[PubMed](#)]
- Dau, H.; Haumann, M. Eight steps preceding O–O bond formation in oxygenic photosynthesis—A basic reaction cycle of the Photosystem II manganese complex. *Biochim. Biophys. Acta-Bioenerg.* **2007**, *1767*, 472–483. [[CrossRef](#)]
- Dau, H.; Haumann, M. The manganese complex of photosystem II in its reaction cycle—Basic framework and possible realization at the atomic level. *Coord. Chem. Rev.* **2008**, *252*, 273–295. [[CrossRef](#)]

24. Klauss, A.; Haumann, M.; Dau, H. Alternating electron and proton transfer steps in photosynthetic water oxidation. *Proc. Natl. Acad. Sci. USA* **2012**, *109*, 16035–16040. [[CrossRef](#)]
25. Huynh, M.H.V.; Meyer, T.J. Proton-Coupled Electron Transfer. *Chem. Rev.* **2007**, *107*, 5004–5064. [[CrossRef](#)]
26. Reece, S.Y.; Nocera, D.G. Proton-Coupled electron transfer in biology: Results from synergistic studies in natural and model systems. *Annu. Rev. Biochem.* **2009**, *78*, 673–699. [[CrossRef](#)]
27. Cukier, R.I.; Nocera, D.G. Proton-Coupled electron transfer. *Annu. Rev. Phys. Chem.* **1998**, *49*, 337–369. [[CrossRef](#)]
28. Weinberg, D.R.; Gagliardi, C.J.; Hull, J.F.; Murphy, C.F.; Kent, C.A.; Westlake, B.C.; Paul, A.; Ess, D.H.; McCafferty, D.G.; Meyer, T.J. Proton-Coupled electron transfer. *Chem. Rev.* **2012**, *112*, 4016–4093. [[CrossRef](#)]
29. Gagliardi, C.J.; Vannucci, A.K.; Concepcion, J.J.; Chen, Z.; Meyer, T.J. The role of proton coupled electron transfer in water oxidation. *Energy Environ. Sci.* **2012**, *5*, 7704. [[CrossRef](#)]
30. Suzuki, H.; Sugiura, M.; Noguchi, T. Monitoring proton release during photosynthetic water oxidation in photosystem II by means of isotope-edited infrared spectroscopy. *J. Am. Chem. Soc.* **2009**, *131*, 7849–7857. [[CrossRef](#)] [[PubMed](#)]
31. Dismukes, G.C.; Brimblecombe, R.; Felton, G.A.N.; Pryadun, R.S.; Sheats, J.E.; Spiccia, L.; Swiegers, G.F. Development of bioinspired Mn₄O₄-cubane water oxidation catalysts: Lessons from photosynthesis. *Acc. Chem. Res.* **2009**, *42*, 1935–1943. [[CrossRef](#)] [[PubMed](#)]
32. Young, K.J.; Martini, L.A.; Milot, R.L.; Snoeberger, R.C.; Batista, V.S.; Schmuttenmaer, C.A.; Crabtree, R.H.; Brudvig, G.W. Light-driven water oxidation for solar fuels. *Coord. Chem. Rev.* **2012**, *256*, 2503–2520. [[CrossRef](#)]
33. Messinger, J.; Lubitz, W.; Shen, J.-R. Photosynthesis: From natural to artificial. *Phys. Chem. Chem. Phys.* **2014**, *16*, 11810. [[CrossRef](#)]
34. Styring, S. Artificial photosynthesis for solar fuels. *Faraday Discuss.* **2012**, *155*, 357–376. [[CrossRef](#)]
35. Hammarström, L.; Sun, L.; Åkermark, B.; Styring, S. Artificial photosynthesis: Towards functional mimics of photosystem II? *Biochim. Biophys. Acta-Bioenerg.* **1998**, *1365*, 193–199. [[CrossRef](#)]
36. Duan, L. Artificial water splitting: Ruthenium complexes for water oxidation. Ph.D. Thesis, KTH Royal Institute of Technology, Stockholm, Sweden, 2011.
37. Tong, L.; Thummel, R.P. Mononuclear ruthenium polypyridine complexes that catalyze water oxidation. *Chem. Sci.* **2016**, *7*, 6591–6603. [[CrossRef](#)]
38. Shaffer, D.W.; Xie, Y.; Concepcion, J.J. O–O bond formation in ruthenium-catalyzed water oxidation: Single-site nucleophilic attack vs. O–O radical coupling. *Chem. Soc. Rev.* **2017**, *46*, 6170–6193. [[CrossRef](#)]
39. Schilling, M.; Lubner, S. Insights into artificial water oxidation—A computational perspective. In *Advances in Inorganic Chemistry*; van Eldik, R., Hubbard, C.D., Eds.; Academic Press: Cambridge, MA, USA, 2019; Volume 74, pp. 61–114, ISBN 9780128160824.
40. Zhang, B.; Sun, L. Artificial photosynthesis: Opportunities and challenges of molecular catalysts. *Chem. Soc. Rev.* **2019**, *48*, 2216–2264. [[CrossRef](#)]
41. Li, Y.; Yao, R.; Chen, Y.; Xu, B.; Chen, C.; Zhang, C. Mimicking the catalytic center for the water-splitting reaction in photosystem II. *Catalysts* **2020**, *10*, 185. [[CrossRef](#)]
42. Young, K.J.; Brennan, B.J.; Tagore, R.; Brudvig, G.W. Photosynthetic water oxidation: Insights from manganese model Chemistry. *Acc. Chem. Res.* **2015**, *48*, 567–574. [[CrossRef](#)] [[PubMed](#)]
43. Barber, J.; Tran, P.D. From natural to artificial photosynthesis. *J. R. Soc. Interface* **2013**, *10*, 857–870. [[CrossRef](#)] [[PubMed](#)]
44. Barber, J. Solar-driven water-splitting provides a solution to the energy problem underpinning climate change. *Biochem. Soc. Trans.* **2020**, *48*, 2865–2874. [[CrossRef](#)]
45. Najafpour, M.M.; Renger, G.; Hołyńska, M.; Moghaddam, A.N.; Aro, E.-M.; Carpentier, R.; Nishihara, H.; Eaton-Rye, J.J.; Shen, J.-R.; Allakhverdiev, S.I. Manganese compounds as water-oxidizing catalysts: From the natural water-oxidizing complex to nanosized manganese oxide structures. *Chem. Rev.* **2016**, *116*, 2886–2936. [[CrossRef](#)]
46. McCrory, C.C.L.; Jung, S.; Peters, J.C.; Jaramillo, T.F. Benchmarking heterogeneous electrocatalysts for the oxygen evolution reaction. *J. Am. Chem. Soc.* **2013**, *135*, 16977–16987. [[CrossRef](#)]
47. McCrory, C.C.L.; Jung, S.; Ferrer, I.M.; Chatman, S.M.; Peters, J.C.; Jaramillo, T.F. Benchmarking hydrogen evolving reaction and oxygen evolving reaction electrocatalysts for solar water splitting devices. *J. Am. Chem. Soc.* **2015**, *137*, 4347–4357. [[CrossRef](#)] [[PubMed](#)]
48. Daniel, Q. Water Oxidation: From Molecular Systems to Functional Devices. Ph.D. Thesis, KTH Royal Institute of Technology, Stockholm, Sweden, 2017.
49. Gersten, S.W.; Samuels, G.J.; Meyer, T.J. Catalytic oxidation of water by an oxo-bridged ruthenium dimer. *J. Am. Chem. Soc.* **1982**, *104*, 4029–4030. [[CrossRef](#)]
50. Zhang, B.; Sun, L. Ru-bda: Unique molecular water-oxidation catalysts with distortion induced open site and negatively charged ligands. *J. Am. Chem. Soc.* **2019**, *141*, 5565–5580. [[CrossRef](#)] [[PubMed](#)]
51. Matheu, R.; Ertem, M.Z.; Gimbert-Suriñach, C.; Sala, X.; Llobet, A. Seven coordinated molecular ruthenium–water oxidation catalysts: A coordination chemistry journey. *Chem. Rev.* **2019**, *119*, 3453–3471. [[CrossRef](#)] [[PubMed](#)]
52. Kamdar, J.; Grotjahn, D. An overview of significant achievements in ruthenium-based molecular water oxidation catalysis. *Molecules* **2019**, *24*, 494. [[CrossRef](#)]
53. Duan, L.; Bozoglian, F.; Mandal, S.; Stewart, B.; Privalov, T.; Llobet, A.; Sun, L. A molecular ruthenium catalyst with water-oxidation activity comparable to that of photosystem II. *Nat. Chem.* **2012**, *4*, 418–423. [[CrossRef](#)]

54. Matheu, R.; Ertem, M.Z.; Benet-Buchholz, J.; Coronado, E.; Batista, V.S.; Sala, X.; Llobet, A. Intramolecular proton transfer boosts water oxidation catalyzed by a Ru complex. *J. Am. Chem. Soc.* **2015**, *137*, 10786–10795. [CrossRef]
55. Matheu, R.; Benet-Buchholz, J.; Sala, X.; Llobet, A. Synthesis, structure, and redox properties of a *trans*-iaqua Ru complex that reaches seven-coordination at high oxidation states. *Inorg. Chem.* **2018**, *57*, 1757–1765. [CrossRef]
56. Yagi, M.; Kaneko, M. Molecular catalysts for water oxidation. *Chem. Rev.* **2001**, *101*, 21–36. [CrossRef] [PubMed]
57. Romain, S.; Vigara, L.; Llobet, A. Oxygen–Oxygen bond formation pathways promoted by ruthenium complexes. *Acc. Chem. Res.* **2009**, *42*, 1944–1953. [CrossRef] [PubMed]
58. Sala, X.; Romero, I.; Rodríguez, M.; Escriche, L.; Llobet, A. Molecular catalysts that oxidize water to dioxygen. *Angew. Chem. Int. Ed.* **2009**, *48*, 2842–2852. [CrossRef]
59. Liu, X.; Wang, F. Transition metal complexes that catalyze oxygen formation from water: 1979–2010. *Coord. Chem. Rev.* **2012**, *256*, 1115–1136. [CrossRef]
60. Kärkäs, M.D.; Verho, O.; Johnston, E.V.; Åkermark, B. Artificial photosynthesis: Molecular systems for catalytic water oxidation. *Chem. Rev.* **2014**, *114*, 11863–12001. [CrossRef]
61. Collin, J.P.; Sauvage, J.P. Synthesis and study of mononuclear ruthenium(II) complexes of sterically hindering diimine chelates. Implications for the catalytic oxidation of water to molecular oxygen. *Inorg. Chem.* **1986**, *25*, 135–141. [CrossRef]
62. Nagoshi, K.; Yamashita, S.; Yagi, M.; Kaneko, M. Catalytic activity of $[(bpy)_2(H_2O)Ru-O-Ru(H_2O)(bpy)_2]^{4+}$ for four-electron water oxidation. *J. Mol. Catal. A Chem.* **1999**, *144*, 71–76. [CrossRef]
63. Parent, A.R.; Crabtree, R.H.; Brudvig, G.W. Comparison of primary oxidants for water-oxidation catalysis. *Chem. Soc. Rev.* **2013**, *42*, 2247–2252. [CrossRef]
64. Geselowitz, D.; Meyer, T.J. Water oxidation by $[(bpy)_2(O)Ru^VORu^V(O)(bpy)_2]^{4+}$. An oxygen-labeling study. *Inorg. Chem.* **1990**, *29*, 3894–3896. [CrossRef]
65. Yamada, H.; Siems, W.F.; Koike, T.; Hurst, J.K. Mechanisms of water oxidation catalyzed by the *cis*, *cis*- $[(bpy)_2Ru(OH)_2]_2O^{4+}$ Ion. *J. Am. Chem. Soc.* **2004**, *126*, 9786–9795. [CrossRef] [PubMed]
66. Liu, F.; Concepcion, J.J.; Jurss, J.W.; Cardolaccia, T.; Templeton, J.L.; Meyer, T.J. Mechanisms of water oxidation from the blue dimer to photosystem II. *Inorg. Chem.* **2008**, *47*, 1727–1752. [CrossRef] [PubMed]
67. Hurst, J.K. Water oxidation catalyzed by dimeric μ -oxo bridged ruthenium diimine complexes. *Coord. Chem. Rev.* **2005**, *249*, 313–328. [CrossRef]
68. Binstead, R.A.; Chronister, C.W.; Ni, J.; Hartshorn, C.M.; Meyer, T.J. Mechanism of water oxidation by the μ -oxo dimer $[(bpy)_2(H_2O)Ru^{III}ORu^{III}(OH_2)(bpy)_2]^{4+}$. *J. Am. Chem. Soc.* **2000**, *122*, 8464–8473. [CrossRef]
69. Sens, C.; Romero, I.; Rodríguez, M.; Llobet, A.; Parella, T.; Benet-Buchholz, J. A new Ru complex capable of catalytically oxidizing water to molecular dioxygen. *J. Am. Chem. Soc.* **2004**, *126*, 7798–7799. [CrossRef]
70. Neudeck, S.; Maji, S.; López, I.; Meyer, S.; Meyer, F.; Llobet, A. New powerful and oxidatively rugged dinuclear Ru water oxidation catalyst: Control of mechanistic pathways by tailored ligand design. *J. Am. Chem. Soc.* **2014**, *136*, 24–27. [CrossRef]
71. Zong, R.; Thummel, R.P. A new family of Ru complexes for water oxidation. *J. Am. Chem. Soc.* **2005**, *127*, 12802–12803. [CrossRef]
72. Xu, Y.; Åkermark, T.; Gyollai, V.; Zou, D.; Eriksson, L.; Duan, L.; Zhang, R.; Åkermark, B.; Sun, L. A new dinuclear ruthenium complex as an efficient water oxidation catalyst. *Inorg. Chem.* **2009**, *48*, 2717–2719. [CrossRef]
73. Xu, Y.; Fischer, A.; Duan, L.; Tong, L.; Gabrielsson, E.; Åkermark, B.; Sun, L. Chemical and light-driven oxidation of water catalyzed by an efficient dinuclear ruthenium complex. *Angew. Chem. Int. Ed.* **2010**, *49*, 8934–8937. [CrossRef]
74. Wada, T.; Tsuge, K.; Tanaka, K. Syntheses and redox properties of bis(hydroxoruthenium) complexes with quinone and bipyridine ligands. water-oxidation catalysis. *Inorg. Chem.* **2001**, *40*, 329–337. [CrossRef]
75. Masaoka, S.; Sakai, K. Clear evidence showing the robustness of a highly active oxygen-evolving mononuclear ruthenium complex with an aqua ligand. *Chem. Lett.* **2009**, *38*, 182–183. [CrossRef]
76. Bozoglian, F.; Romain, S.; Ertem, M.Z.; Todorova, T.K.; Sens, C.; Mola, J.; Rodríguez, M.; Romero, I.; Benet-Buchholz, J.; Fontrodona, X.; et al. The Ru–hbpp water oxidation catalyst. *J. Am. Chem. Soc.* **2009**, *131*, 15176–15187. [CrossRef] [PubMed]
77. Romain, S.; Bozoglian, F.; Sala, X.; Llobet, A. Oxygen–Oxygen bond formation by the Ru–hbpp water oxidation catalyst occurs solely via an intramolecular reaction pathway. *J. Am. Chem. Soc.* **2009**, *131*, 2768–2769. [CrossRef] [PubMed]
78. Hoque, M.A.; Gil-Sepulcre, M.; Benet-Buchholz, J.; Llobet, A.; Gimbert-Suriñach, C. Synthesis, electrochemical characterization, and water oxidation chemistry of Ru complexes containing the 2,6-pyridinedicarboxylato ligand. *Inorg. Chem.* **2020**, *59*, 11432–11441. [CrossRef]
79. Deng, Z.; Tseng, H.-W.; Zong, R.; Wang, D.; Thummel, R. Preparation and study of a family of dinuclear Ru(II) complexes that catalyze the decomposition of water. *Inorg. Chem.* **2008**, *47*, 1835–1848. [CrossRef]
80. Lomoth, R.; Huang, P.; Zheng, J.; Sun, L.; Hammarström, L.; Åkermark, B.; Styring, S. Synthesis and characterization of a dinuclear manganese(III,II) complex with three phenolate ligands. *Eur. J. Inorg. Chem.* **2002**, *2002*, 2965–2974. [CrossRef]
81. Patra, S.G.; Mondal, T.; Sathiyam, K.; Mizrahi, A.; Kornweitz, H.; Meyerstein, D. $Na_3[Ru_2(\mu-CO_3)_4]$ as a homogeneous catalyst for water oxidation; HCO_3^- as a co-catalyst. *Catalysts* **2021**, *11*, 281. [CrossRef]
82. Concepcion, J.J.; Jurss, J.W.; Templeton, J.L.; Meyer, T.J. One site is enough. Catalytic water oxidation by $[Ru(tpy)(bpm)(OH_2)]^{2+}$ and $[Ru(tpy)(bpz)(OH_2)]^{2+}$. *J. Am. Chem. Soc.* **2008**, *130*, 16462–16463. [CrossRef]
83. Concepcion, J.J.; Jurss, J.W.; Brennaman, M.K.; Hoertz, P.G.; Patrocínio, A.O.T.; Murakami, I.N.Y.; Templeton, J.L.; Meyer, T.J. Making oxygen with ruthenium complexes. *Acc. Chem. Res.* **2009**, *42*, 1954–1965. [CrossRef]

84. Asaduzzaman, A.M.; Wasylenko, D.; Berlinguette, C.P.; Schreckenbach, G. Substitution effects on the water oxidation of ruthenium catalysts: A quantum-chemical look. *J. Phys. Chem. C* **2015**, *119*, 242–250. [[CrossRef](#)]
85. Wasylenko, D.J.; Ganesamoorthy, C.; Koivisto, B.D.; Henderson, M.A.; Berlinguette, C.P. Insight into water oxidation by mononuclear polypyridyl Ru catalysts. *Inorg. Chem.* **2010**, *49*, 2202–2209. [[CrossRef](#)]
86. Tseng, H.-W.; Zong, R.; Muckerman, J.T.; Thummel, R. Mononuclear ruthenium(II) complexes that catalyze water oxidation. *Inorg. Chem.* **2008**, *47*, 11763–11773. [[CrossRef](#)]
87. Wasylenko, D.J.; Ganesamoorthy, C.; Henderson, M.A.; Berlinguette, C.P. Unraveling the roles of the acid medium, experimental probes, and terminal oxidant, $(\text{NH}_4)_2[\text{Ce}(\text{NO}_3)_6]$, in the study of a homogeneous water oxidation catalyst. *Inorg. Chem.* **2011**, *50*, 3662–3672. [[CrossRef](#)] [[PubMed](#)]
88. Wasylenko, D.J.; Ganesamoorthy, C.; Henderson, M.A.; Koivisto, B.D.; Osthoff, H.D.; Berlinguette, C.P. Electronic modification of the $[\text{Ru}^{\text{II}}(\text{tpy})(\text{bpy})(\text{OH}_2)]^{2+}$ scaffold: Effects on catalytic water oxidation. *J. Am. Chem. Soc.* **2010**, *132*, 16094–16106. [[CrossRef](#)]
89. Concepcion, J.J.; Tsai, M.-K.; Muckerman, J.T.; Meyer, T.J. Mechanism of water oxidation by single-site ruthenium complex catalysts. *J. Am. Chem. Soc.* **2010**, *132*, 1545–1557. [[CrossRef](#)] [[PubMed](#)]
90. Duan, L.; Fischer, A.; Xu, Y.; Sun, L. Isolated seven-coordinate Ru(IV) dimer complex with $[\text{HOHOH}]^-$ bridging ligand as an intermediate for catalytic water oxidation. *J. Am. Chem. Soc.* **2009**, *131*, 10397–10399. [[CrossRef](#)] [[PubMed](#)]
91. Duan, L.; Xu, Y.; Gorlov, M.; Tong, L.; Andersson, S.; Sun, L. Chemical and photochemical water oxidation catalyzed by mononuclear ruthenium complexes with a negatively charged tridentate ligand. *Chem. Eur. J.* **2010**, *16*, 4659–4668. [[CrossRef](#)]
92. Kärkäs, M.D.; Åkermark, T.; Johnston, E.V.; Karim, S.R.; Laine, T.M.; Lee, B.-L.; Åkermark, T.; Privalov, T.; Åkermark, B. Water oxidation by single-site ruthenium complexes: Using ligands as redox and proton transfer mediators. *Angew. Chem. Int. Ed.* **2012**, *51*, 11589–11593. [[CrossRef](#)] [[PubMed](#)]
93. Duan, L.; Xu, Y.; Zhang, P.; Wang, M.; Sun, L. Visible light-driven water oxidation by a molecular ruthenium catalyst in homogeneous system. *Inorg. Chem.* **2010**, *49*, 209–215. [[CrossRef](#)] [[PubMed](#)]
94. Rabten, W.; Kärkäs, M.D.; Åkermark, T.; Chen, H.; Liao, R.-Z.; Tinnis, F.; Sun, J.; Siegbahn, P.E.M.; Andersson, P.G.; Åkermark, B. Catalytic water oxidation by a molecular ruthenium complex: Unexpected generation of a single-site water oxidation catalyst. *Inorg. Chem.* **2015**, *54*, 4611–4620. [[CrossRef](#)] [[PubMed](#)]
95. Rabten, W.; Åkermark, T.; Kärkäs, M.D.; Chen, H.; Sun, J.; Andersson, P.G.; Åkermark, B. A ruthenium water oxidation catalyst based on a carboxamide ligand. *Dalton Trans.* **2016**, *45*, 3272–3276. [[CrossRef](#)] [[PubMed](#)]
96. Matheu, R.; Ertem, M.Z.; Pipelier, M.; Lebreton, J.; Dubreuil, D.; Benet-Buchholz, J.; Sala, X.; Tessier, A.; Llobet, A. The role of seven-coordination in Ru-catalyzed water oxidation. *ACS Catal.* **2018**, *8*, 2039–2048. [[CrossRef](#)]
97. Shatskiy, A.; Bardin, A.A.; Oschmann, M.; Matheu, R.; Benet-Buchholz, J.; Eriksson, L.; Kärkäs, M.D.; Johnston, E.V.; Gimbert-Suriñach, C.; Llobet, A.; et al. Electrochemically driven water oxidation by a highly active ruthenium-based catalyst. *ChemSusChem* **2019**, *12*, 2251–2262. [[CrossRef](#)]
98. Ghaderian, A.; Holub, J.; Benet-Buchholz, J.; Llobet, A.; Gimbert-Suriñach, C. A Ru-bda complex with a dangling carboxylate group: Synthesis and electrochemical properties. *Inorg. Chem.* **2020**, *59*, 4443–4452. [[CrossRef](#)]
99. Xie, Y.; Shaffer, D.W.; Lewandowska-Andralojc, A.; Szalda, D.J.; Concepcion, J.J. Water oxidation by ruthenium complexes incorporating multifunctional bipyridyl diphosphonate ligands. *Angew. Chem. Int. Ed.* **2016**, *55*, 8067–8071. [[CrossRef](#)]
100. Shaffer, D.W.; Xie, Y.; Szalda, D.J.; Concepcion, J.J. Lability and basicity of bipyridine-carboxylate-phosphonate ligand accelerate single-site water oxidation by ruthenium-based molecular catalysts. *J. Am. Chem. Soc.* **2017**, *139*, 15347–15355. [[CrossRef](#)]
101. Vereshchuk, N.; Matheu, R.; Benet-Buchholz, J.; Pipelier, M.; Lebreton, J.; Dubreuil, D.; Tessier, A.; Gimbert-Suriñach, C.; Ertem, M.Z.; Llobet, A. Second coordination sphere effects in an evolved Ru complex based on highly adaptable ligand results in rapid water oxidation catalysis. *J. Am. Chem. Soc.* **2020**, *142*, 5068–5077. [[CrossRef](#)]
102. Shi, J.; Guo, Y.; Xie, F.; Chen, Q.; Zhang, M. Redox-Active ligand assisted catalytic water oxidation by a $\text{Ru}^{\text{IV}}=\text{O}$ intermediate. *Angew. Chem. Int. Ed.* **2020**, *59*, 4000–4008. [[CrossRef](#)]
103. Hoque, M.A.; Benet-Buchholz, J.; Llobet, A.; Gimbert-Suriñach, C. Catalytic oxidation of water to dioxygen by mononuclear Ru complexes bearing a 2,6-pyridinedicarboxylate ligand. *ChemSusChem* **2019**, *12*, 1949–1957. [[CrossRef](#)] [[PubMed](#)]
104. Zhang, B.; Zhan, S.; Liu, T.; Wang, L.; Ken, I.A.; Duan, L.; Timmer, B.J.J.; Kravchenko, O.; Li, F.; Ahlquist, M.S.G.; et al. Switching O–O bond formation mechanism between WNA and I2M pathways by modifying the Ru-bda backbone ligands of water-oxidation catalysts. *J. Energy Chem.* **2021**, *54*, 815–821. [[CrossRef](#)]
105. Wang, L.; Duan, L.; Stewart, B.; Pu, M.; Liu, J.; Privalov, T.; Sun, L. Toward controlling water oxidation catalysis: Tunable activity of ruthenium complexes with axial imidazole/DMSO ligands. *J. Am. Chem. Soc.* **2012**, *134*, 18868–18880. [[CrossRef](#)] [[PubMed](#)]
106. Daniel, Q.; Wang, L.; Duan, L.; Li, F.; Sun, L. Tailored design of ruthenium molecular catalysts with 2,2'-bipyridine-6,6'-dicarboxylate and pyrazole based ligands for water oxidation. *Dalton Trans.* **2016**, *45*, 14689–14696. [[CrossRef](#)] [[PubMed](#)]
107. Tong, L.; Duan, L.; Xu, Y.; Privalov, T.; Sun, L. Structural modifications of mononuclear ruthenium complexes: A combined experimental and theoretical study on the kinetics of ruthenium-catalyzed water oxidation. *Angew. Chem. Int. Ed.* **2011**, *50*, 445–449. [[CrossRef](#)]
108. Scherrer, D.; Schilling, M.; Lubert, S.; Fox, T.; Spingler, B.; Alberto, R.; Richmond, C.J. Ruthenium water oxidation catalysts containing the non-planar tetradentate ligand, bisoquinoline dicarboxylic acid (biquaH_2). *Dalton Trans.* **2016**, *45*, 19361–19367. [[CrossRef](#)]

109. McDaniel, N.D.; Coughlin, F.J.; Tinker, L.L.; Bernhard, S. Cyclometalated iridium(III) aquo complexes: Efficient and tunable catalysts for the homogeneous oxidation of water. *J. Am. Chem. Soc.* **2008**, *130*, 210–217. [[CrossRef](#)]
110. Hull, J.F.; Balcells, D.; Blakemore, J.D.; Incarvito, C.D.; Eisenstein, O.; Brudvig, G.W.; Crabtree, R.H. Highly active and robust Cp* iridium complexes for catalytic water oxidation. *J. Am. Chem. Soc.* **2009**, *131*, 8730–8731. [[CrossRef](#)]
111. Blakemore, J.D.; Schley, N.D.; Balcells, D.; Hull, J.F.; Olack, G.W.; Incarvito, C.D.; Eisenstein, O.; Brudvig, G.W.; Crabtree, R.H. Half-Sandwich iridium complexes for homogeneous water-oxidation catalysis. *J. Am. Chem. Soc.* **2010**, *132*, 16017–16029. [[CrossRef](#)]
112. Savini, A.; Bellachioma, G.; Ciancaleoni, G.; Zuccaccia, C.; Zuccaccia, D.; Macchioni, A. Iridium(III) molecular catalysts for water oxidation: The simpler the faster. *Chem. Commun.* **2010**, *46*, 9218. [[CrossRef](#)]
113. Savini, A.; Belanzoni, P.; Bellachioma, G.; Zuccaccia, C.; Zuccaccia, D.; Macchioni, A. Activity and degradation pathways of pentamethyl-cyclopentadienyl-iridium catalysts for water oxidation. *Green Chem.* **2011**, *13*, 3360. [[CrossRef](#)]
114. Bucci, A.; Savini, A.; Rocchigiani, L.; Zuccaccia, C.; Rizzato, S.; Albinati, A.; Llobet, A.; Macchioni, A. Organometallic iridium catalysts based on pyridinecarboxylate ligands for the oxidative splitting of water. *Organometallics* **2012**, *31*, 8071–8074. [[CrossRef](#)]
115. Lalrempuia, R.; McDaniel, N.D.; Müller-Bunz, H.; Bernhard, S.; Albrecht, M. Water oxidation catalyzed by strong carbene-type donor-ligand complexes of iridium. *Angew. Chem. Int. Ed.* **2010**, *49*, 9765–9768. [[CrossRef](#)]
116. Brewster, T.P.; Blakemore, J.D.; Schley, N.D.; Incarvito, C.D.; Hazari, N.; Brudvig, G.W.; Crabtree, R.H. An iridium(IV) species, [Cp*Ir(NHC)Cl]⁺, related to a water-oxidation catalyst. *Organometallics* **2011**, *30*, 965–973. [[CrossRef](#)]
117. Savini, A.; Bellachioma, G.; Bolaño, S.; Rocchigiani, L.; Zuccaccia, C.; Zuccaccia, D.; Macchioni, A. Iridium-EDTA as an efficient and readily available catalyst for water oxidation. *ChemSusChem* **2012**, *5*, 1415–1419. [[CrossRef](#)]
118. Savini, A.; Bucci, A.; Bellachioma, G.; Giancola, S.; Palomba, F.; Rocchigiani, L.; Rossi, A.; Suriani, M.; Zuccaccia, C.; Macchioni, A. New iridium(III) organometallic complexes bearing strong electron donating bidentate ligands as catalysts for water oxidation. *J. Organomet. Chem.* **2014**, *771*, 24–32. [[CrossRef](#)]
119. Sheehan, S.W.; Thomsen, J.M.; Hintermair, U.; Crabtree, R.H.; Brudvig, G.W.; Schmuttenmaer, C.A. A molecular catalyst for water oxidation that binds to metal oxide surfaces. *Nat. Commun.* **2015**, *6*, 6469. [[CrossRef](#)] [[PubMed](#)]
120. Li, M.; Takada, K.; Goldsmith, J.I.; Bernhard, S. Iridium(III) bis-pyridine-2-sulfonamide complexes as efficient and durable catalysts for homogeneous water oxidation. *Inorg. Chem.* **2016**, *55*, 518–526. [[CrossRef](#)]
121. Li, M.; Bernhard, S. Synthetically tunable iridium(III) bis-pyridine-2-sulfonamide complexes as efficient and durable water oxidation catalysts. *Catal. Today* **2017**, *290*, 19–27. [[CrossRef](#)]
122. Volpe, A.; Tubaro, C.; Natali, M.; Sartorel, A.; Brudvig, G.W.; Bonchio, M. Light-Driven water oxidation with the Ir-blue catalyst and the Ru(bpy)₃²⁺/S₂O₈²⁻ cycle: Photogeneration of active dimers, electron-transfer kinetics, and light synchronization for oxygen evolution with high quantum efficiency. *Inorg. Chem.* **2019**, *58*, 16537–16545. [[CrossRef](#)]
123. Thomsen, J.M.; Sheehan, S.W.; Hashmi, S.M.; Campos, J.; Hintermair, U.; Crabtree, R.H.; Brudvig, G.W. Electrochemical activation of Cp* iridium complexes for electrode-driven water-oxidation catalysis. *J. Am. Chem. Soc.* **2014**, *136*, 13826–13834. [[CrossRef](#)] [[PubMed](#)]
124. Calvin, M. Solar energy by photosynthesis. *Science* **1974**, *184*, 375–381. [[CrossRef](#)]
125. Cooper, S.R.; Calvin, M. Solar energy by photosynthesis: Manganese complex photolysis complex. *Science* **1974**, *185*, 376. [[CrossRef](#)]
126. Mukhopadhyay, S.; Mandal, S.K.; Bhaduri, S.; Armstrong, W.H. Manganese clusters with relevance to photosystem II. *Chem. Rev.* **2004**, *104*, 3981–4026. [[CrossRef](#)]
127. Ashmawy, F.M.; McAuliffe, C.A.; Parish, R.V.; Tames, J. The photolysis of co-ordinated water in [Mn(saltm)(H₂O)]₂(ClO₄)₂ [saltm = N,N'-propylenebis(salicylideneaminato)]. *J. Chem. Soc., Chem. Commun.* **1984**, *1*, 14–16. [[CrossRef](#)]
128. Ashmawy, F.M.; McAuliffe, C.A.; Parish, R.V.D.; Tames, J. Water photolysis. Part 1. The photolysis of co-ordinated water in [MnL(H₂O)]₂[ClO₄]₂ (L = dianion of tetradentate O₂N₂-donor Schiff bases). A model for the manganese site in photosystem II of green plant photosynthesis. *J. Chem. Soc. Dalton Trans.* **1985**, *7*, 1391. [[CrossRef](#)]
129. Ruettinger, W.F.; Campana, C.; Dismukes, G.C. Synthesis and characterization of Mn₄O₄L₆ complexes with cubane-like core structure: A new class of models of the active site of the photosynthetic water oxidase. *J. Am. Chem. Soc.* **1997**, *119*, 6670–6671. [[CrossRef](#)]
130. Ruettinger, W.; Yagi, M.; Wolf, K.; Bernasek, S.; Dismukes, G.C. O₂ evolution from the manganese–oxo cubane core Mn₄O₄⁶⁺: A molecular mimic of the photosynthetic water oxidation enzyme? *J. Am. Chem. Soc.* **2000**, *122*, 10353–10357. [[CrossRef](#)]
131. Yagi, M.; Wolf, K.V.; Baesjou, P.J.; Bernasek, S.L.; Dismukes, G.C. Selective photoproduction of O₂ from the Mn₄O₄ cubane core: A structural and functional model for the photosynthetic water-oxidizing complex. *Angew. Chem. Int. Ed.* **2001**, *40*, 2925–2928. [[CrossRef](#)]
132. Zhang, C.; Chen, C.; Dong, H.; Shen, J.-R.; Dau, H.; Zhao, J. A synthetic Mn₄Ca-cluster mimicking the oxygen-evolving center of photosynthesis. *Science* **2015**, *348*, 690–693. [[CrossRef](#)] [[PubMed](#)]
133. Naruta, Y.; Sasayama, M.; Sasaki, T. Oxygen Evolution by Oxidation of Water with Manganese Porphyrin Dimers. *Angew. Chem. Int. Ed. Engl.* **1994**, *33*, 1839–1841. [[CrossRef](#)]
134. Shimazaki, Y.; Nagano, T.; Takesue, H.; Ye, B.-H.; Tani, F.; Naruta, Y. Characterization of a dinuclear Mn^V=O complex and its efficient evolution of O₂ in the presence of water. *Angew. Chem. Int. Ed.* **2004**, *43*, 98–100. [[CrossRef](#)]

135. Watkinson, M.; Whiting, A.; McAuliffe, C.A. Synthesis of a bis-manganese water splitting complex. *J. Chem. Soc. Chem. Commun.* **1994**, *44*, 2141. [[CrossRef](#)]
136. Aurangzeb, N.; Hulme, C.E.; McAuliffe, C.A.; Pritchard, R.G.; Watkinson, M.; Bermejo, M.R.; Garcia-Deibe, A.; Rey, M.; Sanmartin, J.; Sousa, A. Crystallographic characterisation of a possible model for photosystem II. *J. Chem. Soc. Chem. Commun.* **1994**, *2*, 1153. [[CrossRef](#)]
137. Poulsen, A.K.; Rompel, A.; McKenzie, C.J. Water oxidation catalyzed by a dinuclear Mn complex: A functional model for the oxygen-evolving center of photosystem II. *Angew. Chem. Int. Ed.* **2005**, *44*, 6916–6920. [[CrossRef](#)] [[PubMed](#)]
138. Limburg, J.; Vrettos, J.S.; Liable-sands, L.M.; Rheingold, A.L.; Crabtree, R.H.; Brudvig, G.W. A functional model for O-O bond formation by the O₂-evolving complex in photosystem II. *Science* **1999**, *283*, 1524–1527. [[CrossRef](#)]
139. Limburg, J.; Vrettos, J.S.; Chen, H.; de Paula, J.C.; Crabtree, R.H.; Brudvig, G.W. Characterization of the O₂-evolving reaction catalyzed by [(terpy)(H₂O)Mn^{III}(O)₂Mn^{IV}(OH₂)(terpy)](NO₃)₃ (terpy = 2,2':6,2''-Terpyridine). *J. Am. Chem. Soc.* **2001**, *123*, 423–430. [[CrossRef](#)]
140. Chen, H.; Tagore, R.; Das, S.; Incarvito, C.; Faller, J.W.; Crabtree, R.H.; Brudvig, G.W. General synthesis of di-μ-oxo dimanganese complexes as functional models for the oxygen evolving complex of photosystem II. *Inorg. Chem.* **2005**, *44*, 7661–7670. [[CrossRef](#)]
141. Young, K.J.; Takase, M.K.; Brudvig, G.W. An anionic N-donor ligand promotes manganese-catalyzed water oxidation. *Inorg. Chem.* **2013**, *52*, 7615–7622. [[CrossRef](#)]
142. Lant, H.M.C.C.; Michaelos, T.K.; Sharninghausen, L.S.; Mercado, B.Q.; Crabtree, R.H.; Brudvig, G.W. N,N,O Pincer ligand with a deprotonatable site that promotes redox-leveling, high Mn oxidation states, and a Mn₂O₂ dimer competent for catalytic oxygen evolution. *Eur. J. Inorg. Chem.* **2019**, *2019*, 2115–2123. [[CrossRef](#)]
143. McCool, N.S.; Robinson, D.M.; Sheats, J.E.; Dismukes, G.C. A Co₄O₄ “cubane” water oxidation catalyst inspired by photosynthesis. *J. Am. Chem. Soc.* **2011**, *133*, 11446–11449. [[CrossRef](#)]
144. Lloret-Fillol, J.; Costas, M. Water oxidation at base metal molecular catalysts. In *Advances in Organometallic Chemistry*; Pérez, P.J., Ed.; Academic Press: Cambridge, MA, USA, 2019; Volume 71, pp. 1–52, ISBN 9780128171158.
145. Ellis, W.C.; McDaniel, N.D.; Bernhard, S.; Collins, T.J. Fast water oxidation using iron. *J. Am. Chem. Soc.* **2010**, *132*, 10990–10991. [[CrossRef](#)] [[PubMed](#)]
146. Panda, C.; Debgupta, J.; Díaz, D.D.; Singh, K.K.; Sen Gupta, S.; Dhar, B.B. Homogeneous photochemical water oxidation by biuret-modified Fe-TAML: Evidence of Fe^V(O) intermediate. *J. Am. Chem. Soc.* **2014**, *136*, 12273–12282. [[CrossRef](#)]
147. Fillol, J.L.; Codolà, Z.; Garcia-Bosch, I.; Gómez, L.; Pla, J.J.; Costas, M. Efficient water oxidation catalysts based on readily available iron coordination complexes. *Nat. Chem.* **2011**, *3*, 807–813. [[CrossRef](#)]
148. Kasapbasi, E.E.; Whangbo, M.-H. Density Functional investigation of the water oxidation by iron complexes based on tetradentate nitrogen ligands. *Inorg. Chem.* **2012**, *51*, 10850–10855. [[CrossRef](#)]
149. Zhang, B.; Li, F.; Yu, F.; Cui, H.; Zhou, X.; Li, H.; Wang, Y.; Sun, L. Homogeneous oxidation of water by iron complexes with macrocyclic ligands. *Chem. Asian J.* **2014**, *9*, 1515–1518. [[CrossRef](#)] [[PubMed](#)]
150. Codolà, Z.; Gómez, L.; Kleespies, S.T.; Que, L., Jr.; Costas, M.; Lloret-Fillol, J. Evidence for an oxygen evolving iron-oxo-cerium intermediate in iron-catalysed water oxidation. *Nat. Commun.* **2015**, *6*, 5865. [[CrossRef](#)] [[PubMed](#)]
151. Panchbhai, G.; Singh, W.M.; Das, B.; Jane, R.T.; Thapper, A. Mononuclear iron complexes with tetraazadentate ligands as water oxidation catalysts. *Eur. J. Inorg. Chem.* **2016**, *2016*, 3262–3268. [[CrossRef](#)]
152. Wickramasinghe, L.D.; Zhou, R.; Zong, R.; Vo, P.; Gagnon, K.J.; Thummel, R.P. Iron complexes of square planar tetradentate polypyridyl-type ligands as catalysts for water oxidation. *J. Am. Chem. Soc.* **2015**, *137*, 13260–13263. [[CrossRef](#)]
153. Das, B.; Orthaber, A.; Ott, S.; Thapper, A. Iron pentapyridyl complexes as molecular water oxidation catalysts: Strong influence of a chloride ligand and pH in altering the mechanism. *ChemSusChem* **2016**, *9*, 1178–1186. [[CrossRef](#)]
154. Tan, P.; Kwong, H.-K.; Lau, T.-C. Catalytic oxidation of water and alcohols by a robust iron(III) complex bearing a cross-bridged cyclam ligand. *Chem. Commun.* **2015**, *51*, 12189–12192. [[CrossRef](#)]
155. Wang, Z.-Q.; Wang, Z.-C.; Zhan, S.; Ye, J.-S. A water-soluble iron electrocatalyst for water oxidation with high TOF. *Appl. Catal. A Gen.* **2015**, *490*, 128–132. [[CrossRef](#)]
156. Najafpour, M.M.; Safdari, R.; Ebrahimi, F.; Rafiqhi, P.; Bagheri, R. Water oxidation by a soluble iron(III)–cyclen complex: New findings. *Dalton Trans.* **2016**, *45*, 2618–2623. [[CrossRef](#)]
157. Okamura, M.; Kondo, M.; Kuga, R.; Kurashige, Y.; Yanai, T.; Hayami, S.; Praneeth, V.K.K.; Yoshida, M.; Yoneda, K.; Kawata, S.; et al. A pentanuclear iron catalyst designed for water oxidation. *Nature* **2016**, *530*, 465–468. [[CrossRef](#)]
158. Najafpour, M.M.; Moghaddam, A.N.; Sedigh, D.J.; Holyńska, M. A dinuclear iron complex with a single oxo bridge as an efficient water-oxidizing catalyst in the presence of cerium(IV) ammonium nitrate: New findings and current controversies. *Catal. Sci. Technol.* **2014**, *4*, 30–33. [[CrossRef](#)]
159. Liu, Y.; Xiang, R.; Du, X.; Ding, Y.; Ma, B. An efficient oxygen evolving catalyst based on a μ-O diiron coordination complex. *Chem. Commun.* **2014**, *50*, 12779–12782. [[CrossRef](#)]
160. Kottrup, K.G.; D’Agostini, S.; van Langevelde, P.H.; Siegler, M.A.; Hettterscheid, D.G.H. Catalytic activity of an iron-based water oxidation catalyst: Substrate effects of graphitic electrodes. *ACS Catal.* **2018**, *8*, 1052–1061. [[CrossRef](#)]
161. Yin, Q.; Tan, J.M.; Besson, C.; Geletii, Y.V.; Musaev, D.G.; Kuznetsov, A.E.; Luo, Z.; Hardcastle, K.I.; Hill, C.L. A fast soluble carbon-free molecular water oxidation catalyst based on abundant metals. *Science* **2010**, *328*, 342–345. [[CrossRef](#)] [[PubMed](#)]

162. Wang, H.-Y.; Mijangos, E.; Ott, S.; Thapper, A. Water oxidation catalyzed by a dinuclear cobalt-polypyridine complex. *Angew. Chem. Int. Ed.* **2014**, *53*, 14499–14502. [[CrossRef](#)] [[PubMed](#)]
163. Stracke, J.J.; Finke, R.G. Electrocatalytic water oxidation beginning with the cobalt polyoxometalate $[\text{Co}_4(\text{H}_2\text{O})_2(\text{PW}_9\text{O}_{34})_2]^{10-}$: Identification of heterogeneous CoOx as the dominant catalyst. *J. Am. Chem. Soc.* **2011**, *133*, 14872–14875. [[CrossRef](#)] [[PubMed](#)]
164. Wang, J.-W.; Sahoo, P.; Lu, T.-B. Reinvestigation of water oxidation catalyzed by a dinuclear cobalt polypyridine complex: Identification of CoOx as a real heterogeneous catalyst. *ACS Catal.* **2016**, *6*, 5062–5068. [[CrossRef](#)]
165. Huang, Z.; Luo, Z.; Geletii, Y.V.; Vickers, J.W.; Yin, Q.; Wu, D.; Hou, Y.; Ding, Y.; Song, J.; Musaev, D.G.; et al. Efficient light-driven carbon-free cobalt-based molecular catalyst for water oxidation. *J. Am. Chem. Soc.* **2011**, *133*, 2068–2071. [[CrossRef](#)] [[PubMed](#)]
166. Berardi, S.; La Ganga, G.; Natali, M.; Bazzan, I.; Puntoriero, F.; Sartorel, A.; Scandola, F.; Campagna, S.; Bonchio, M. Photocatalytic water oxidation: Tuning light-induced electron transfer by molecular Co_4O_4 cores. *J. Am. Chem. Soc.* **2012**, *134*, 11104–11107. [[CrossRef](#)]
167. La Ganga, G.; Puntoriero, F.; Campagna, S.; Bazzan, I.; Berardi, S.; Bonchio, M.; Sartorel, A.; Natali, M.; Scandola, F. Light-driven water oxidation with a molecular tetra-cobalt(III) cubane cluster. *Faraday Discuss.* **2012**, *155*, 177–190. [[CrossRef](#)] [[PubMed](#)]
168. Zhang, B.; Li, F.; Yu, F.; Wang, X.; Zhou, X.; Li, H.; Jiang, Y.; Sun, L. Electrochemical and photoelectrochemical water oxidation by supported cobalt-oxo cubanes. *ACS Catal.* **2014**, *4*, 804–809. [[CrossRef](#)]
169. Ullman, A.M.; Liu, Y.; Huynh, M.; Bediako, D.K.; Wang, H.; Anderson, B.L.; Powers, D.C.; Breen, J.J.; Abruña, H.D.; Nocera, D.G. Water oxidation catalysis by Co(II) impurities in $\text{Co(III)}_4\text{O}_4$ cubanes. *J. Am. Chem. Soc.* **2014**, *136*, 17681–17688. [[CrossRef](#)]
170. McAlpin, J.G.; Surendranath, Y.; Dincă, M.; Stich, T.A.; Stoian, S.A.; Casey, W.H.; Nocera, D.G.; Britt, R.D. EPR evidence for Co(IV) species produced during water oxidation at neutral pH. *J. Am. Chem. Soc.* **2010**, *132*, 6882–6883. [[CrossRef](#)]
171. Ishizuka, T.; Watanabe, A.; Kotani, H.; Hong, D.; Satonaka, K.; Wada, T.; Shiota, Y.; Yoshizawa, K.; Ohara, K.; Yamaguchi, K.; et al. Homogeneous photocatalytic water oxidation with a dinuclear Co^{III} -pyridylmethylamine complex. *Inorg. Chem.* **2016**, *55*, 1154–1164. [[CrossRef](#)] [[PubMed](#)]
172. Lin, J.; Ma, B.; Chen, M.; Ding, Y. Water oxidation catalytic ability of polypyridine complex containing a $\mu\text{-OH}$, $\mu\text{-O}_2$ dicobalt(III) core. *Chin. J. Catal.* **2018**, *39*, 463–471. [[CrossRef](#)]
173. Chen, M.; Ng, S.-M.; Yiu, S.-M.; Lau, K.-C.; Zeng, R.J.; Lau, T.-C. Photoinduced water oxidation catalyzed by a double-helical dicobalt(II) sexipyridine complex. *Chem. Commun.* **2014**, *50*, 14956–14959. [[CrossRef](#)]
174. Ullman, A.M.; Brodsky, C.N.; Li, N.; Zheng, S.-L.; Nocera, D.G. Probing edge site reactivity of oxidic cobalt water oxidation catalysts. *J. Am. Chem. Soc.* **2016**, *138*, 4229–4236. [[CrossRef](#)]
175. Wasylenko, D.J.; Ganesamoorthy, C.; Borau-Garcia, J.; Berlinguette, C.P. Electrochemical evidence for catalytic water oxidation mediated by a high-valent cobalt complex. *Chem. Commun.* **2011**, *47*, 4249. [[CrossRef](#)]
176. Das, B.; Orthaber, A.; Ott, S.; Thapper, A. Water oxidation catalysed by a mononuclear Co(II) polypyridine complex; possible reaction intermediates and the role of the chloride ligand. *Chem. Commun.* **2015**, *51*, 13074–13077. [[CrossRef](#)]
177. Crandell, D.W.; Ghosh, S.; Berlinguette, C.P.; Baik, M.-H. How a $[\text{Co}^{\text{IV}}\text{O}]^{2+}$ fragment oxidizes water: Involvement of a biradicaloid $[\text{Co}^{\text{II}}(\cdot\text{O})]^{2+}$ species in forming the O-O bond. *ChemSusChem* **2015**, *8*, 844–852. [[CrossRef](#)]
178. Larson, V.A.; Battistella, B.; Ray, K.; Lehnert, N.; Nam, W. Iron and manganese oxo complexes, oxo wall and beyond. *Nat. Rev. Chem.* **2020**, *4*, 404–419. [[CrossRef](#)]
179. Wang, H.; Xin, Z.; Xiang, R.; Liu, S.; Gao, X.; Li, C. Functional polypyridine Co complex as an efficient catalyst for photo-induced water oxidation. *Chin. J. Chem.* **2016**, *34*, 757–762. [[CrossRef](#)]
180. Leung, C.-F.; Ng, S.-M.; Ko, C.-C.; Man, W.-L.; Wu, J.; Chen, L.; Lau, T.-C. A cobalt(II) quaterpyridine complex as a visible light-driven catalyst for both water oxidation and reduction. *Energy Environ. Sci.* **2012**, *5*, 7903. [[CrossRef](#)]
181. Hong, D.; Jung, J.; Park, J.; Yamada, Y.; Suenobu, T.; Lee, Y.-M.; Nam, W.; Fukuzumi, S. Water-soluble mononuclear cobalt complexes with organic ligands acting as precatalysts for efficient photocatalytic water oxidation. *Energy Environ. Sci.* **2012**, *5*, 7606. [[CrossRef](#)]
182. Nakazono, T.; Parent, A.R.; Sakai, K. Cobalt porphyrins as homogeneous catalysts for water oxidation. *Chem. Commun.* **2013**, *49*, 6325. [[CrossRef](#)]
183. Nakazono, T.; Sakai, K. Improving the robustness of cobalt porphyrin water oxidation catalysts by chlorination of aryl groups. *Dalton Trans.* **2016**, *45*, 12649–12652. [[CrossRef](#)]
184. Nakazono, T.; Parent, A.R.; Sakai, K. Improving singlet oxygen resistance during photochemical water oxidation by cobalt porphyrin catalysts. *Chem. Eur. J.* **2015**, *21*, 6723–6726. [[CrossRef](#)]
185. Wang, D.; Groves, J.T. Efficient water oxidation catalyzed by homogeneous cationic cobalt porphyrins with critical roles for the buffer base. *Proc. Natl. Acad. Sci. USA* **2013**, *110*, 15579–15584. [[CrossRef](#)] [[PubMed](#)]
186. Najafpour, M.M.; Feizi, H. Water oxidation catalyzed by two cobalt complexes: New challenges and questions. *Catal. Sci. Technol.* **2018**, *8*, 1840–1848. [[CrossRef](#)]
187. Sinha, W.; Mizrahi, A.; Mahammed, A.; Tumanskii, B.; Gross, Z. Reactive intermediates involved in cobalt corrole catalyzed water oxidation (and oxygen reduction). *Inorg. Chem.* **2018**, *57*, 478–485. [[CrossRef](#)] [[PubMed](#)]
188. Lv, H.; Song, J.; Geletii, Y.V.; Vickers, J.W.; Sumliner, J.M.; Musaev, D.G.; Kögerler, P.; Zhuk, P.F.; Bacsá, J.; Zhu, G.; et al. An exceptionally fast homogeneous carbon-free cobalt-based water oxidation catalyst. *J. Am. Chem. Soc.* **2014**, *136*, 9268–9271. [[CrossRef](#)] [[PubMed](#)]

189. Barnett, S.M.; Goldberg, K.I.; Mayer, J.M. A soluble copper-bipyridine water-oxidation electrocatalyst. *Nat. Chem.* **2012**, *4*, 498–502. [[CrossRef](#)]
190. Zhang, M.-T.; Chen, Z.; Kang, P.; Meyer, T.J. Electrocatalytic water oxidation with a copper(II) polypeptide complex. *J. Am. Chem. Soc.* **2013**, *135*, 2048–2051. [[CrossRef](#)]
191. Coggins, M.K.; Zhang, M.-T.; Chen, Z.; Song, N.; Meyer, T.J. Single-Site copper(II) water oxidation electrocatalysis: Rate enhancements with HPO_4^{2-} as a proton acceptor at pH 8. *Angew. Chem.* **2014**, *126*, 12422–12426. [[CrossRef](#)]
192. Zhang, T.; Wang, C.; Liu, S.; Wang, J.-L.; Lin, W. A Biomimetic copper water oxidation catalyst with low overpotential. *J. Am. Chem. Soc.* **2014**, *136*, 273–281. [[CrossRef](#)]
193. Garrido-Barros, P.; Funes-Ardoiz, I.; Drouet, S.; Benet-Buchholz, J.; Maseras, F.; Llobet, A. Redox non-innocent ligand controls water oxidation overpotential in a new family of mononuclear Cu-based efficient catalysts. *J. Am. Chem. Soc.* **2015**, *137*, 6758–6761. [[CrossRef](#)]
194. Yu, W.-B.; He, Q.-Y.; Ma, X.-F.; Shi, H.-T.; Wei, X. A new copper species based on an azo-compound utilized as a homogeneous catalyst for water oxidation. *Dalton Trans.* **2015**, *44*, 351–358. [[CrossRef](#)]
195. Najafpour, M.M.; Ebrahimi, F.; Safdari, R.; Ghobadi, M.Z.; Tavahodi, M.; Rafiqhi, P. New findings and the current controversies for water oxidation by a copper(II)-azo complex: Homogeneous or heterogeneous? *Dalton Trans.* **2015**, *44*, 15435–15440. [[CrossRef](#)]
196. Pap, J.S.; Szyrwił, Ł.; Srankó, D.; Kerner, Z.; Setner, B.; Szewczuk, Z.; Malinka, W. Electrocatalytic water oxidation by Cu^{II} complexes with branched peptides. *Chem. Commun.* **2015**, *51*, 6322–6324. [[CrossRef](#)]
197. Fisher, K.J.; Materna, K.L.; Mercado, B.Q.; Crabtree, R.H.; Brudvig, G.W. Electrocatalytic water oxidation by a copper(II) complex of an oxidation-resistant ligand. *ACS Catal.* **2017**, *7*, 3384–3387. [[CrossRef](#)]
198. Stott, L.A.; Prosser, K.E.; Berdichevsky, E.K.; Walsby, C.J.; Warren, J.J. Lowering water oxidation overpotentials using the ionisable imidazole of copper(2-(2'-pyridyl)imidazole). *Chem. Commun.* **2017**, *53*, 651–654. [[CrossRef](#)]
199. Shen, J.; Wang, M.; Gao, J.; Han, H.; Liu, H.; Sun, L. Improvement of electrochemical water oxidation by fine-tuning the structure of tetradentate N_4 ligands of molecular copper catalysts. *ChemSusChem* **2017**, *10*, 4581–4588. [[CrossRef](#)] [[PubMed](#)]
200. Shen, J.; Wang, M.; Zhang, P.; Jiang, J.; Sun, L. Electrocatalytic water oxidation by copper(II) complexes containing a tetra- or pentadentate amine-pyridine ligand. *Chem. Commun.* **2017**, *53*, 4374–4377. [[CrossRef](#)] [[PubMed](#)]
201. Chen, F.; Wang, N.; Lei, H.; Guo, D.; Liu, H.; Zhang, Z.; Zhang, W.; Lai, W.; Cao, R. Electrocatalytic water oxidation by a water-soluble copper(II) complex with a copper-bound carbonate group acting as a potential proton shuttle. *Inorg. Chem.* **2017**, *56*, 13368–13375. [[CrossRef](#)] [[PubMed](#)]
202. Jiang, X.; Li, J.; Yang, B.; Wei, X.-Z.; Dong, B.-W.; Kao, Y.; Huang, M.-Y.; Tung, C.-H.; Wu, L.-Z. A Bio-inspired Cu_4O_4 cubane: Effective molecular catalysts for electrocatalytic water oxidation in aqueous solution. *Angew. Chem. Int. Ed.* **2018**, *57*, 7850–7854. [[CrossRef](#)] [[PubMed](#)]
203. Terao, R.; Nakazono, T.; Parent, A.R.; Sakai, K. Photochemical water oxidation catalyzed by a water-soluble copper phthalocyanine complex. *Chempluschem* **2016**, *81*, 1064–1067. [[CrossRef](#)] [[PubMed](#)]
204. Najafpour, M.M.; Mehrabani, S.; Mousazade, Y.; Holyńska, M. Water oxidation by a copper(II) new findings, questions, challenges and a new hypothesis. *Dalton Trans.* **2018**, *47*, 9021–9029. [[CrossRef](#)]
205. Liu, Y.; Han, Y.; Zhang, Z.; Zhang, W.; Lai, W.; Wang, Y.; Cao, R. Low overpotential water oxidation at neutral pH catalyzed by a copper(II) porphyrin. *Chem. Sci.* **2019**, *10*, 2613–2622. [[CrossRef](#)]
206. Younus, H.A.; Zhang, Y.; Vandichel, M.; Ahmad, N.; Laasonen, K.; Verpoort, F.; Zhang, C.; Zhang, S. Water oxidation at neutral pH using a highly active copper-based electrocatalyst. *ChemSusChem* **2020**, *13*, 5088–5099. [[CrossRef](#)] [[PubMed](#)]
207. Su, X.-J.; Gao, M.; Jiao, L.; Liao, R.-Z.; Siegbahn, P.E.M.; Cheng, J.-P.; Zhang, M.-T. Electrocatalytic water oxidation by a dinuclear copper complex in a neutral aqueous solution. *Angew. Chem. Int. Ed.* **2015**, *54*, 4909–4914. [[CrossRef](#)] [[PubMed](#)]
208. Mizrahi, A.; Maimon, E.; Cohen, H.; Kornweitz, H.; Zilbermann, I.; Meyerstein, D. Mechanistic studies on the role of $[\text{Cu}^{\text{II}}(\text{CO}_3)_n]^{2-2n}$ as a water oxidation catalyst: Carbonate as a non-innocent ligand. *Chem. Eur. J.* **2018**, *24*, 1088–1096. [[CrossRef](#)]
209. Zhang, M.; Zhang, M.-T.; Hou, C.; Ke, Z.-F.; Lu, T.-B. Homogeneous electrocatalytic water oxidation at neutral pH by a robust macrocyclic nickel(II) Complex. *Angew. Chem.* **2014**, *126*, 13258–13264. [[CrossRef](#)]
210. Luo, G.-Y.; Huang, H.-H.; Wang, J.-W.; Lu, T.-B. Further investigation of a nickel-based homogeneous water oxidation catalyst with two cis labile sites. *ChemSusChem* **2016**, *9*, 485–491. [[CrossRef](#)]
211. Song, N.; Concepcion, J.J.; Binstead, R.A.; Rudd, J.A.; Vannucci, A.K.; Dares, C.J.; Coggins, M.K.; Meyer, T.J. Base-enhanced catalytic water oxidation by a carboxylate-bipyridine Ru(II) complex. *Proc. Natl. Acad. Sci. USA* **2015**, *112*, 4935–4940. [[CrossRef](#)]
212. Ariela, B.; Yaniv, W.; Dror, S.; Haya, K.; Yael, A.; Eric, M.; Dan, M. The role of carbonate in electro-catalytic water oxidation by using $\text{Ni}(1,4,8,11\text{-tetraazacyclotetradecane})^{2+}$. *Dalton Trans.* **2017**, *46*, 10774–10779. [[CrossRef](#)]
213. Wang, J.-W.; Zhang, X.-Q.; Huang, H.-H.; Lu, T.-B. A Nickel(II) Complex as a homogeneous electrocatalyst for water oxidation at neutral pH: Dual role of HPO_4^{2-} in catalysis. *ChemCatChem* **2016**, *8*, 3287–3293. [[CrossRef](#)]
214. Wang, D.; Ghirlanda, G.; Allen, J.P. Water oxidation by a nickel-glycine catalyst. *J. Am. Chem. Soc.* **2014**, *136*, 10198–10201. [[CrossRef](#)] [[PubMed](#)]
215. Zhu, G.; Glass, E.N.; Zhao, C.; Lv, H.; Vickers, J.W.; Geletii, Y.V.; Musaev, D.G.; Song, J.; Hill, C.L. A nickel containing polyoxometalate water oxidation catalyst. *Dalton Trans.* **2012**, *41*, 13043. [[CrossRef](#)]
216. Han, X.-B.; Li, Y.-G.; Zhang, Z.-M.; Tan, H.-Q.; Lu, Y.; Wang, E.-B. Polyoxometalate-Based nickel clusters as visible light-driven water oxidation catalysts. *J. Am. Chem. Soc.* **2015**, *137*, 5486–5493. [[CrossRef](#)]

217. Han, Y.; Wu, Y.; Lai, W.; Cao, R. Electrocatalytic water oxidation by a water-soluble nickel porphyrin complex at neutral pH with low overpotential. *Inorg. Chem.* **2015**, *54*, 5604–5613. [[CrossRef](#)] [[PubMed](#)]
218. Wang, L.; Duan, L.; Ambre, R.B.; Daniel, Q.; Chen, H.; Sun, J.; Das, B.; Thapper, A.; Uhlig, J.; Dinér, P.; et al. A nickel (II) PY5 complex as an electrocatalyst for water oxidation. *J. Catal.* **2016**, *335*, 72–78. [[CrossRef](#)]
219. Wang, J.-W.; Hou, C.; Huang, H.-H.; Liu, W.-J.; Ke, Z.-F.; Lu, T.-B. Further insight into the electrocatalytic water oxidation by macrocyclic nickel(II) complexes: The influence of steric effect on catalytic activity. *Catal. Sci. Technol.* **2017**, *7*, 5585–5593. [[CrossRef](#)]
220. Wang, D.; Bruner, C.O. Catalytic water oxidation by a bio-inspired nickel complex with a redox-active ligand. *Inorg. Chem.* **2017**, *56*, 13638–13641. [[CrossRef](#)] [[PubMed](#)]
221. Lin, J.; Kang, P.; Liang, X.; Ma, B.; Ding, Y. Homogeneous electrocatalytic water oxidation catalyzed by a mononuclear nickel complex. *Electrochim. Acta* **2017**, *258*, 353–359. [[CrossRef](#)]
222. Garrido-Barros, P.; Grau, S.; Drouet, S.; Benet-Buchholz, J.; Gimbert-Suriñach, C.; Llobet, A. Can Ni complexes behave as molecular water oxidation catalysts? *ACS Catal.* **2019**, *9*, 3936–3945. [[CrossRef](#)]
223. Shahadat, H.M.; Younus, H.A.; Ahmad, N.; Rahaman, M.A.; Khattak, Z.A.K.; Zhuiykov, S.; Verpoort, F. Homogenous electrochemical water oxidation by a nickel(II) complex based on a macrocyclic N-heterocyclic carbene/pyridine hybrid ligand. *Catal. Sci. Technol.* **2019**, *9*, 5651–5659. [[CrossRef](#)]
224. Lee, H.; Wu, X.; Sun, L. Homogeneous electrochemical water oxidation at neutral pH by water-soluble Ni^{II} complexes bearing redox non-innocent tetraamido macrocyclic ligands. *ChemSusChem* **2020**, *13*, 3277–3282. [[CrossRef](#)]